ISTANBUL TECHNICAL UNIVERSITY ★ GRADUATE SCHOOL OF SCIENCE ENGINEERING AND TECHNOLOGY

COMPUTER SIMULATION OF BONE REMODELING

M.Sc. THESIS

Meral TUNA

Department of Mechanical Engineering

Solid Mechanics Programme

JANUARY 2013

ISTANBUL TECHNICAL UNIVERSITY ★ GRADUATE SCHOOL OF SCIENCE ENGINEERING AND TECHNOLOGY

COMPUTER SIMULATION OF BONE REMODELING

M.Sc. THESIS

Meral TUNA
(503101503)

Department of Mechanical Engineering

Solid Mechanics Programme

Thesis Advisor: Ergün BOZDAĞ, Ph. D.
Emin SÜNBÜLOĞLU, Ph. D.

JANUARY 2013

İSTANBUL TEKNİK ÜNİVERSİTESİ ★ FEN BİLİMLERİ ENSTİTÜSÜ

KEMİK ADAPTASYONUNUN BİLGİSAYAR ORTAMINDA SİMÜLE EDİLMESİ

YÜKSEK LİSANS TEZİ

Meral TUNA
(50310503)

Makina Mühendisliği Anabilim Dalı

Katı Cisimlerin Mekaniği Programı

Tez Danışmanı: Dr. Ergün BOZDAĞ
Dr. Emin SÜNBÜLOĞLU

OCAK 2013

Meral Tuna, a **M.Sc.** student of ITU **Graduate School of Science Engineering and Technology** student ID **503101503**, successfully defended the **thesis** entitled **"COMPUTER SIMULATION OF BONE REMODELING"**, which she prepared after fulfilling the requirements specified in the associated legislations, before the jury whose signatures are below.

Thesis Advisor :	**Öğr. Gör. Dr. Ergün BOZDAĞ** İstanbul Technical University	.....
Co-advisor :	**Öğr. Gör. Dr. Emin SÜNBÜLOĞLU** İstanbul Technical University	.....
Jury Members :	**Prof. Dr. Tuncer TOPRAK** İstanbul Technical University	.....
	Prof. Dr. Murat Hancı İstanbul University	.....
	Yar. Doç. Dr. Hakan HANIMOĞLU Bezmialem Vakıf University	.....

Date of Submission : 17 December 2012
Date of Defense : 24 January 2013

To my family,

FOREWORD

This thesis would not have been possible without a great deal of support.

I would especially like to thank Dr. Emin SÜNBÜLOĞLU and Dr. Ergün BOZDAĞ for being supervisors of this study, their suggestions, scientific and moral supports. I am grateful to assist them.

I would also like to thank Prof. Dr. Murat HANCI and Yar. Doç. Dr. Hakan HANIMOĞLU for their medical support.

Finally, infinite thanks to my family for their understanding and encouragement through my life.

December 2012

Meral TUNA
Research Assistant

TABLE OF CONTENTS

Page

ABBREVIATIONS

MIL **:** Mean Interception Length
SED **:** Strain Energy Density

LIST OF TABLES

Page

LIST OF FIGURES

Page

COMPUTER SIMULATION OF BONE REMODELING

SUMMARY

Beside the well known functions such as; support, protection, assist movement, and deposit important minerals, bones have the ability of growing, repairing itself in a case of fracture and changing its internal structure and external shape constantly to adapt the environment.

Bones are classified based on their macroscopic shapes and microscopic structures. According to their shapes there are four type of bone; long, short, flat and irregular. And according to their microscopic structure bones can be classified as; cortical and trabecular. Cortical bone has very compact structure with little porosity while trabecular bone has a very porous structure and not as rigid as cortical bone. The change in internal structure as other words remodeling process generally occurs in trabecular rather than cortical bone.

This lifelong remodeling process modified by a lot of parameter such as; sex, age, race, hormonal, physilogical conditions and mechanical activities. The most influental one is mechanical activities and developing an algorithm based on mechanical activities is sufficient enough for most of the cases. The response of bone to mechanical loading conditions is also known as Wolff's Law which indicates that by the self-regularity character, bone provide the required strength by changing the distribution of trabeculea.

The investigation of bone remodeling parameters help us for detecting the best shape of implant according to the region that is going to be applied and the actions patient can or can not do after an operation.

To be able to understand the evolution and results of bone remodeling, mechanical behaviour of bone have to be clarified. Bone is a porous, heterogenous, nonlinear, viscoelastic and anisotropic material with different properties in tension and compression. However to be able to build a model in computer and follow the principle of continuum mechanics some assumptions have to be made. First of all, properties in trabecular bone are averaged in a volume due to the discontinuous structure of trabeculea. Secondly; on the contrary of soft tissues, the deformation of bone is small enough to ignore geometric nonlinearity and as a result of that the strain-displacement relation remains linear. Although bone is a viscoelastic material due to the flow network, the contribution of marrows and water to the mechanical strength is inefficient which allows us to neglect the viscoelastic behaviour. Additionaly, the behaviour of bone remain almost linear in physiological strain. According to the informations above bone can be taken as linear elastic and isotropic material.

There are a lot of different theories and models that investigate remodeling process both in macroscopic and microscopic level but they have a common point that many

apply a mechanical stimulus as s feedback system. Mechanical stimulus is taken as stress, strain, strain energy density, strain energy density rate, strain energy per mass or damage. In this work mechanical stimulus is taken as strain energy per mass and a model that based on adaptive elasticity theory is proposed which claims that when a change of load or abnormal strain state occurs, bone is stimulated to adapt its mass to regain the equilibrium state. So driving force of remodeling is the difference between homeostatic state and actual state. It is assumed that between the error and remodeling process linear or parabolic relation is exists. As a result the formation due to loading and resoprtion due to overloading and underloading is occured during remodeling process which is coincidence with the clinical data.

An algorithm is developed based on mechanical activities and is implements to finite element program (ABAQUS) by writing FORTRAN codes to subroutines (UMAT, USDFLD, URDFIL, SDVINI). The most important advantage of algorithm is investigation of loading and remodeling processes into two different phases. First an analysis is performed within seconds and then the remodeling process is performed within days according to the value of mechanical stimulus which is calculated by taking into account the frequency, period and importance of different load cases.

For validation of code; different analysis with different load, boundary conditions, interactions and meshes are performed both with and without code. Same results are observed. The validation of remodeling algorithm have been validated against density distribution of proximal femur during gait cycle and density distribution of implant induced mandibula during mastication. Good agreement has been observed with the results available in the literature.

After validations, new method is applied to investigate bone remodeling around lumbar pedicle screw and results are found to be consistent with clinical observations. In future studies the lumbar model has to be improved by adding other vertebrae segments and complementary disk and facets. Beside that the existing model is going to be improved by adding the fabtic tensor to simulate the anisotropic behaviour of bone. Additionaly; by writing a new multifield element model the diminishing rate of remodeling signal due to the distance between sensing and forming-resorbing cells can be taking into account.

KEMİK ADAPTASYONUNUN BİLGİSAYAR ORTAMINDA SİMÜLE EDİLMESİ

ÖZET

Kemikler; destek, koruma, harekete yardımcı olma, mineralleri depolama gibi herkesçe bilinen özelliklerinin yanı sıra büyüyen, gelişen, hasar durumunda kendini onaran ve bulunduğu ortama iç yapısını ve dış şeklini değiştirerek adapte olabilme özelliğine sahip canlı dokulardır.

Kemikler şekillerine göre uzun, kısa, yassı kemik, mikroskopik yapılarına göre de trabeküler ve kortikal kemik olarak sınıflandırılırlar. Kortikal kemik iskeletin yüzde seksenini oluşturur. Uzun kemiklerin şaft bölgesinde, kısa ve yassı kemiklerinde dış çevresinde bulunur. Sert ve boşluksuz bir yapıya sahiptir. Diğer yandan; trabeküler kemik ise iskeletin yüzde yirmisini oluşturur. Uzun kemiklerin uçlarında ve kısa ve yassı kemiklerde bulunur. Oldukça düzensiz ve boşluklu bir yapıya sahiptir. Kemiğin kendini ortama adapte etmesinde en büyük pay kortikal kemikten çok bu mineral içerikli trabeküler yapıdaki kemiğe aittir. Kimyasal yapısında bulunan organik ve inorganik (mineral) bileşenlerin oranlarını değiştirerek kendi iç yapısını sürekli bir şekilde düzenlemektedir. Adaptasyon süreci tek bir hücre tarafından değil, aksine "basic multicellular unit" denilen ve kemik yapımında görev alan "osteoblast" ile kemik yıkımında görev alan "osteoclast" adına sahip hücrelerin belli bir döngü içerisinde beraber çalışmasıyla mümkün olmaktadır.

Yaşam boyunca devam eden bir süreç olan iç yapının adaptasyonu; yaş, cinsiyet, ırk, hormonal ve fizyolojik durum gibi kişinin bünyesel özelliklerine ve çevreden gelen mekanik etkilere bağlıdır. Bu parametrelerden kemik adaptasyonunu en çok etkileyeni şüphesiz mekanik etkilerdir. Wolff Yasaları olarakta bilinen, kemiğinin mekanik yükleme koşullarına karşı davranışı şu şekilde açıklanabilir: Mekanik uyaranlara karşı kemik kendi kendini adapte etme özelliğine sahiptir ve trabeküler hatlarla asal gerilme doğrultularını çakıştırarak gereken dayanım ile ağırlık arasındaki optimum noktaya ulaşabilmektedir.

Kemiğin iç yapısını ortama adapte etmesini etkileyen parametlerin incelenmesi, hem gerektiğinde kemiğe uygulanacak en uygun implant şekillerinin belirlenmesi için hem de yapılan operasyon sonrasında, hastanın rehabilitasyon süresince yapması uygun olan ve olmayan hareketlerin tespiti için oldukça büyük önem arz etmektedir.

Kemik adaptasyonunun tam olarak anlaşılabilmesi için öncelikle kemiğin mekanik özelliklerinin açığa kavuşturulması gerekmektedir. Her ne kadar kortikal kemiğin malzeme özellikleri klasik mekanik ve ultrason testler ile tespit edilebilsede, düzensiz ve boşluklu yapısından ötürü aynı durum trabeküler kemik için geçerli değildir. Genel anlamda incelendiğinde kemik dokusunun; nonlineer, anizotropik, heterojen, viskoelastik bir yapıda olduğu gözlemlenmiştir. Ancak bilgisayar ortamında modellenmesini mümkün kılmak ve sürekli ortamlar mekaniğinin

prensiplerini uygulayabilmek için bir takım kabullerin yapılması şarttır. Bunlardan ilki süreksiz bir yapıya sahip olan trabeküler kemiğin malzeme özelliklerin belli bir hacimde ortalamalarının alınarak sürekli ortamlar mekaniği prensiplerinin uygulanmasına olanak sağlanmasıdır. Kemikler küçük deformasyonlara maruz kaldığından şekil değiştirme ve deplasman arasındaki ilişki nonlineer terimler ihmal edilerek lineer olarak alınabilir, ayrıca kemiğin maruz kaldığı şekil değiştirme değerlerinde gerilme ile birim şekil değişimi arasındaki ilişkinin de lineer olduğu gözlemlenmiştir. Her ne kadar kemikteki boşluklar kemik iliği ve su gibi yapılarla dolu olsada bu yapılar mekanik dayanıma herhangi bir katkı sağlamadığından kemiğin viskoelastik özelliği de elastik olarak alınabilmektedir ve son olarak kemik her ne kadar anizotropik bir yapıya sahip olsa da bu çalışma kapsamında izotropik olarak ele alınmıştır. Sonuçta yapılan bütün kabuller gözönüne alınınca kemik, sürekli bir yapıya sahip olan, izotropik, lineer elastik bir malzeme olarak ele alınabilmektedir.

Şu ana kadar bu konu ile ilgili birçok teori geliştirilmiş ve bu teorilerden yola çıkılarak gerek makroskopik gerekse mikroskopik ölçeklerde çeşitli modeller oluşturulmuştur. Yapılan çalışmalar incelendiğinde bütün modellerde adaptasyonu tetikleyen ve sistemde geri beslemeyi sağlayan mekanik bir uyaran olduğu saptanmıştır. Bu uyaran çalışmadan çalışmaya değişmekle beraber, genelde gerilme, birim şekil değişimi, şekil değiştirme enerjisi yoğunluğu, birim kütle başına düşen şekil değiştirme enerjisi veya hasar olarak seçilmiştir.

Bu çalışma kapsamında mekanik uyaran olarak kütle başına düşen şekil değiştirme enerjisi seçilmiş ve adaptif elastisite teorisi esas alınmıştır. Bu teoriye göre kemiğin adaptasyonunu, denge durumundaki ve şu andaki mekanik uyaran değerleri arasındaki fark tetiklemektedir. Mekanik uyaranlar arasındaki farka bağlı olarak trabeküler ve azda olsa kortikal kemikteki yoğunluk dağılımı değişmektedir. Mekanik uyaran ile kemikte oluşan yapım ve yıkım arasındaki ilişki bazı çalışmalarda parabolik, bazı çalışmalarda ise lineer olarak kabul edilmiştir ve sonuç olarak; kemikte yüklenmeden ötürü yapımın, hem az hem de aşırı yüklenmeden ötürü ise yıkımın olduğu gözlemlenmiştir. Elde edilen sonuçlar ile klinikteki veriler karşılaştırıldığında tatmin edici derecede bir uyuşmanın olduğu görülmüştür.

Bahsedildiği gibi mekanik etkiler neticesinde gerçekleşen kemik adaptasyonunu yansıtan bir algoritma oluşturulmuştur. Bu algoritma sonlu elemanlar programının (ABAQUS), gerekli altprogramlarına (UMAT, USDFLD, URDFIL, SDVINI) kodlar yazılarak monte edilmiştir. Oluşturulan algoritmanın şu ana kadar incelenenlere göre en büyük avantajı yükleme gibi saniyeler bazında gerçekleşen bir olay ile adaptasyon gibi günler bazında gerçekleşen bir sürecin iki ayrı fazda ele alınmasını sağlayan yapısıdır. Bu şekilde, basit sistemlerin yanı sıra daha karmaşık sistemlerde de gün içinde maruz kalınan bütün mekanik yükler hesaba katılarak kemiğin adaptasyonu incelenebilmektedir. Bunun için ise herşeyden önce uygulanan yüklerin karakteristiği saptanmalıdır. Yapılan çalışmalar neticesinde görülmüştür ki yükleme ve adaptasyonun farklı zaman skalalarında gerçekleşmesinden ötürü yüklerin uygulanma sırasının değiştirilmesi adaptasyonu etkilememektedir. Ayrıca yüksek frekanslı yüklerin etkisinde daha fazla adaptasyon olduğu görülmüştür. Başka bir önemli nokta ise yükün uygulanış süresine bağlı olarak adaptasyonun artmayışı, aksine kemiğin bir süre sonra sürekli uygulanan yüke karşı duyarsız hale gelişidir. Sonuç olarak yüklerin uygulanma sıklıkları, frekansları ve periyodları gözönüne alınarak kemiğin adaptasyonu incelebilmektedir. Öncelikle incelenen kemiğe gün içerisinde gelen bütün yükler tespit edilir. Ardından bu yüklerin ağırlıkları;

önemlerine ve yukarıda bahsedilen özelliklere bağlı olarak tespit edilir ve çeşitli katsayılar ile her yükün etkisi yansıtılmış olur. Daha sonra uygun sınır ve yükleme koşulları uygulanarak analiz yapılır. Saniyeler bazında gerçekleşen analizden elde edilen mekanik uyaran değerleri yukarıda bahsedilen yükleme koşullarının etkilerini yansıtmak için tespit edilen katsayılar ile çarpılarak manipüle edilir. Ardından analizin ikinci kısmı olan ve günler mertebesinde gerçekleşen süreci yansıtan adaptasyon fazı başlamış olur. Elde edilen mekanik uyaran değerleri ile denge durumu arasındaki farktan yola çıkılarak her bir integrasyon noktasındaki yeni yoğunluk değeri tespit edilir ve yoğunluk ile elastisite modulu arasındaki ilişkiden yararlanılarak her integrasyon noktasındaki yeni elastisite modülleri hesaplanmış olur. Adaptasyonu sürecinden sonra sistemin yakınsayıp yakınsamadığına bakılır ve sistem yakınsayana kadar yukarıdaki döngü devamlı olarak gerçekleştirilir. Sistemin yakınsaması zamana bağlı olarak her bir integrasyon noktasında gerçekleşen yoğunluk değişiminin belli bir töleransın altına düşmesiyle gerçeklenmektedir.

Uygun algoritma oluşturulduktan sonra kodun validasyonu için farklı yükleme koşulları, sınır koşulları, etkileşim ve eleman tipine sahip küplerin tek başına sonlu elemanlar programında ve adaptasyon özelliği aktif olmayan kod monte edilen sonlu elemanlar programında aynı sonuçları verip vermediği kontrol edilmiştir. Ardından kemikte gözlenen yoğunluk dağılımının, aynı yükleme ve sınır koşulları uygulanmış ve adaptasyon kodu monte edilmiş model ile örtüşüp örtüşmediğine bakılmıştır. Bunun için de femur kemiğinin yürüme, diş implantının çevresindeki çene kemiğinin de çiğneme yüklerine maruz kalması neticesinde kemiğin zamanla yoğunluk dağılımının ne duruma geldiğine bakılmış ve sonuçta literatür ve klinik ile örtüşen sonuçlar gözlemlenmiştir.

Gerekli validasyonlardan sonra, L3 segmentini ve altında ve üstünde bulunan disklerini içeren ve segmente monte edilmiş vidayı içeren lumbar modeli oluşturulmuştur. Günlük hareketleri simüle edecek şekilde uygun kuvvetler ve sınır koşulları verilmiştir. Vida çevresinde bulunan kortikal ve trabeküler kemikteki yapım ve yıkım ya da başka bir değişle yoğunluk değişimi incelenmiştir. Klinikle örtüşen sonuçlara ulaşılmıştır. Ancak ileride yapılacak çalışmada lumbar modeli diğer segmentler ve onlara bağlı diskler, ligamentler ve gereken vida konstrüksiyonu eklenerek geliştirilecektir. Bu şekilde fizyolojik durumu daha gerçekçi bir şekilde yansıtan bir model oluşturulmuş olacaktır. Ayrıca sistemi sadeleştirmek adına kemiğin mekanik davranışları için yapılan izotropik kabulu yerine algoritmaya kemiğin anizotropik özelliğini yansıtan "fabric tenson" denilen ikinci derece bir tensor konulacaktır. Ve son olarak sonlu elemanlar programına uygun eleman modeli yazılarak adaptasyon olması gerektiğini algılayan hücreler ile bunu gerçekleştiren hücreler arasındaki mesafenin adaptasyona etkiside ilave edilebilecektir.

1. INTRODUCTION

Bones are one of the most significant organs in the human body which exhibits the ability of repairing itself in a case of a fracture and adjusting its internal structure and external shape due to metabolic and mechanical activities. The adaptation of internal structure is called remodeling.

The remodeling of bone is a very complex process and is influenced from various parameters such as; sex, age, hormonal conditions, physiological conditions and mechanical activities. Consequently building a computational model that connects bone remodeling with the entire parameters considered above is almost impossible. However; it is believed that since bone adapt its (internal) structure to serve a specific function, mechanical activities can be taken as the most dominant contribution to remodeling. Thus; a mechanical activity based bone remodeling algorithm can be regarded as a sufficient enough model for most of the cases. Although there are a lot of phenomenological models that investigate remodeling process by using different theories either in macroscopic or microscopic levels, all agree on the "mechanical stimulus" concept according to which, material properties are updated.

The purpose of this study is to understand the bone remodeling concept, to investigate theories as well as computational models and to generate an algorithm with introduction of some original concepts. In the study, a model that based on adaptive elasticity theory is proposed which claims that when a change of load or abnormal strain state occurs, bone is stimulated to adapt its mass to regain the equilibrium state. As a result, the main idea in the work is the adaptation of internal structure in macroscopic level based on the distribution of strain energy density (SED) per mass which is arranged by the characteristics of daily mechanical loads.

During the study bone is assumed to be an isotropic, linear elastic material and analysis are performed with finite element software package ABAQUS/Standard. For

a proper implementation of remodeling algorithm; various user-defined subroutines are used simultaneously; which include UMAT, SDIVINI, USDFLD and URDFIL.

2. BONE STRUCTURE

In this chapter, the main characteristic of bone is mentioned. After describing functions of bones in 1.1 and types of bone in 1.2, detailed information about architecture and composition of bone and bone cells are outlined respectively in 1.3, 1.4, 1.5 which improve our knowledge about bone structure and help us to understand and study it as an living dynamic tissue.

2.1 Function of Bones

Bone is generally mentioned as a protective and supportive part of the body. Beside these functions, bone is a very dynamic organ which has the ability of adapting its internal body and external shape as a response to the mechanical loads and hormonal activities. The reason of that is bone has to be light enough to perform its functions properly while at the same time it has to be as strong as cast iron to secure required strength.

The five main purposes of bone is support, protection, movement, mineral storage and blood cell production. These functions can be explained as follow.

- Support: Bones provide a framework to muscles and tissues for attachment. Without bones, tissues and organs will collapse.
- Protection: Bones protect internal organs. For example, skull protects brain, while rib cage protects both heart and lungs, and spinal nerves are protected by vertebrae.
- Assisting in Movement: Bones provide surfaces or points for muscles, tendons and ligaments to attached. The movement of muscles, ligaments and tendons move the bones.
- Stroage of Minerals: Bones store minerals like phosphorus (P) and calcium (Ca) for various cellular activities. When mineral level in blood increases too

much, some of minerals are removed or stored in bones. As a contrary if mineral level in blood decreases too much, minerals are taken from the bones.

- Production of Blood Cells: Many bones contains cavities that are filled with bone marrow and most of the blood cell formation occurs in those marrows.

2.2 Classification of Bones

Human skeleton which consist of 206 bones is divided in two groups: axial and appendicular. The bones of the skull, vertebral column and rib cage are included in axial skeleton whose main function is protecting, supporting and carrying other part of bodies. On the other hand, the bones of the upper and lower limbs and the girdles are included in appendicular bones. Bones of limbs help us to move from place to place and manage our environment.

There are four different types of bones which are mainly classified by their shapes named as long, short, flat and irregular bones. Limbs can be given as an example of long bones while carpals and tarsals are classified as a short bone, ribs, skull, scapulea, sternum are flat bones, and vertebraes are irregular bones.

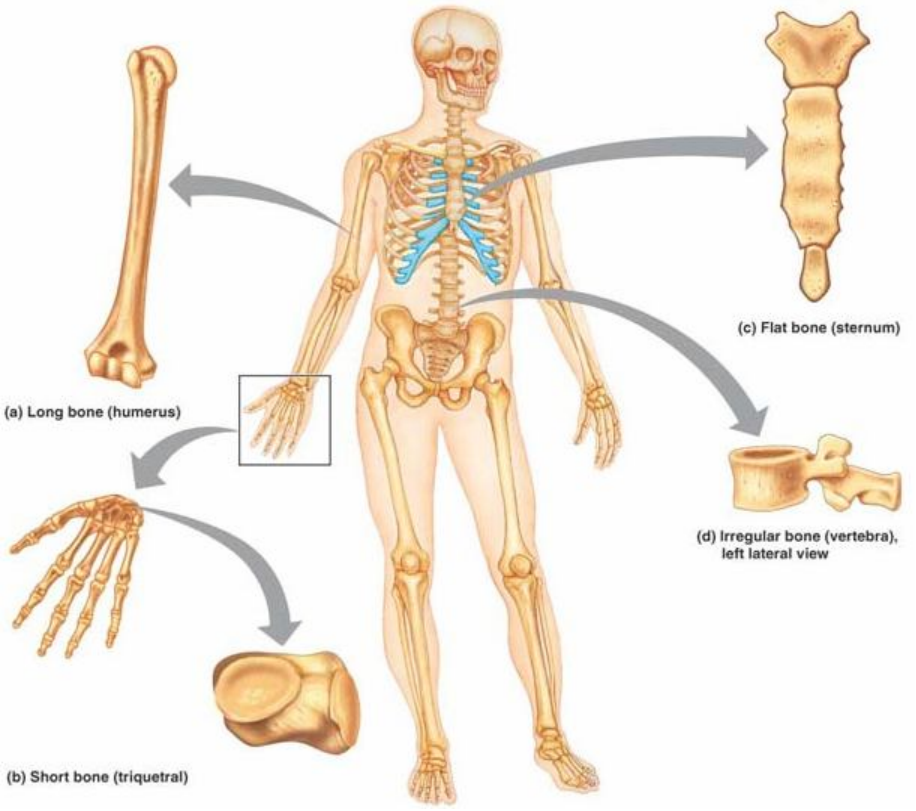

Figure 2.1 : Classification of bones [1].

2.2.1 Long bones

Long bones are considerably longer that computed to cross section dimensions, and have three major components; a diaphysis, an epiphysis and a metaphysis. The main part of long bone is called diaphysis which forms the axis with tubular shaft. It is basically composed by compact bone with few pores surrounding the medullary cavity. The pores of cancellous bone and the medullary cavity are filled with red and yellow marrow.

Shaft is covered with periosteom which is a membrane that contains osteoblasts (bone forming cells), osteoclasts (bone destroying cells), nerve fibers and lymphatic vessels. The medullary cavity is lined with endosteum, which is a thin layer of connective tissue and lines on the surface of tissue bone.

The expanded ends of the bone is called epiphysis. The epiphysis primarly consist of spongeous bone. At joint surfaces epiphysis covered with articular cartilage.

The thickest part of trabecula is located between epiphysis and diaphysis is called as metaphsis. Metaphsis includes epiphyseal line which seperates diaphysis and epiphysis. Epiphyseal line formed by ossification of epiphyseal plate, where growth of bone occurs.

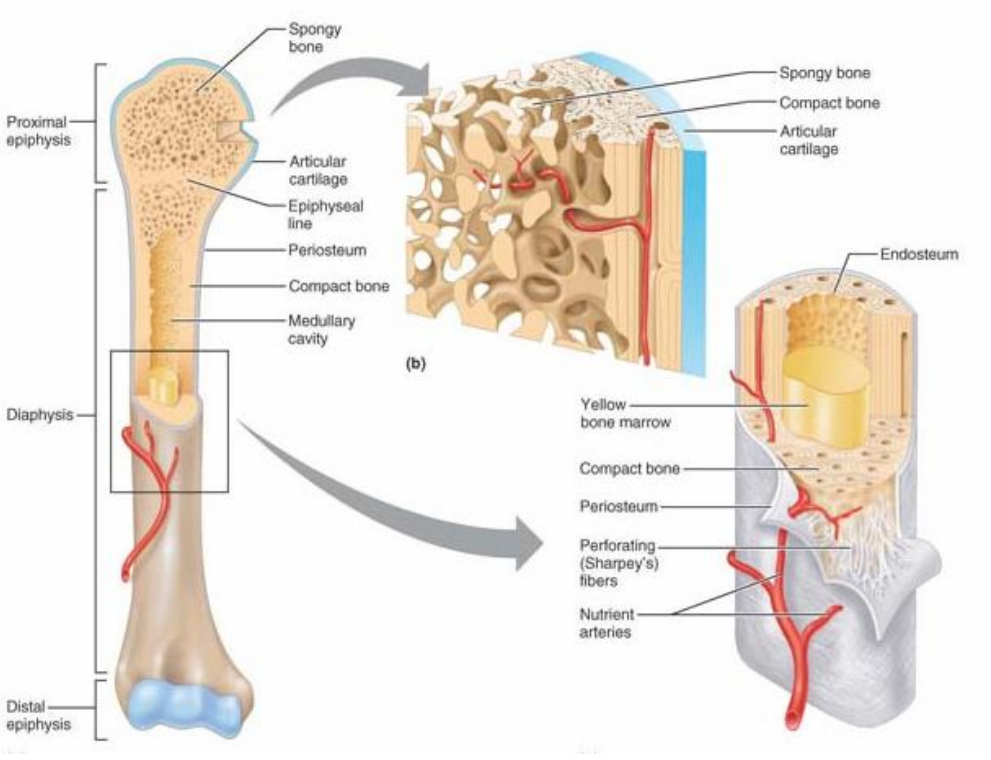

Figure 2.2 : Structure of long bone [1].

2.2.2 Short, flat and irregular bones

Short bones are shaped similar to cubes, while flat bones are thin with a little curvature. Irregular bones have complicated shapes as it can be inferred from the name.

These type of bones have neither diaphysis nor epihysis. In short and irregular bones, spongeous is surrounded by a thin layer of cortical bone while in flat bones the spongeous part is sandwiched between two layer of cortical bone tissue. Like long bones the outer surface of short and flat bones are covered by periosteom while inner surface is covered by endosteum. In some bones such as vertebrae, ribs, sternum the pores between trabeculea contain red marrow.

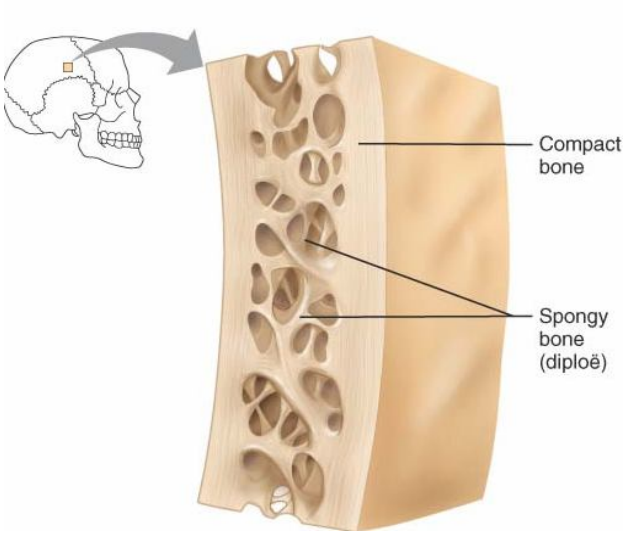

Figure 2.3 : Structure of flat bone [1].

2.3 Architecture of Bones

There are two major type of bone architecture; cortical (compact) and spongeous (cancellous) bone. Generally, bones have both cortical and spongeous tissue, but the composition of them changes through bones. Compact bones forms the outer part of bones and most of the structure of long bones while spongeous bones are generally found in the center of bones and at the inner end of long bones.

2.3.1 Compact bone

Compact bones consists of cylindrical units called osteons which are the basic structural unit. Osteons contain cylindirical lamellea (layers) of hard, calcified matrix around Haversian (central) canals. Osteocyctes (bone cells) are placed in spaces

(lacunae) between the layers. There are smaller canals called as canaliculi, which radiate outward from the central canal, containing blood vessels and nerve fibers. Osteocyctes connected to each other and to the central canal by fine cellular extensions passing through canaculis. By these cellular extensions, nutrients and waste are exchanged between osteocyctes and blood vessels. Also there is an other type of canal called as Volkmann's (perforating) canal which provides channels to connect central canals to each other with blood vessels and also to connect those blood vessels to the ones in the periosteom which surrounds the outer layer of bone.

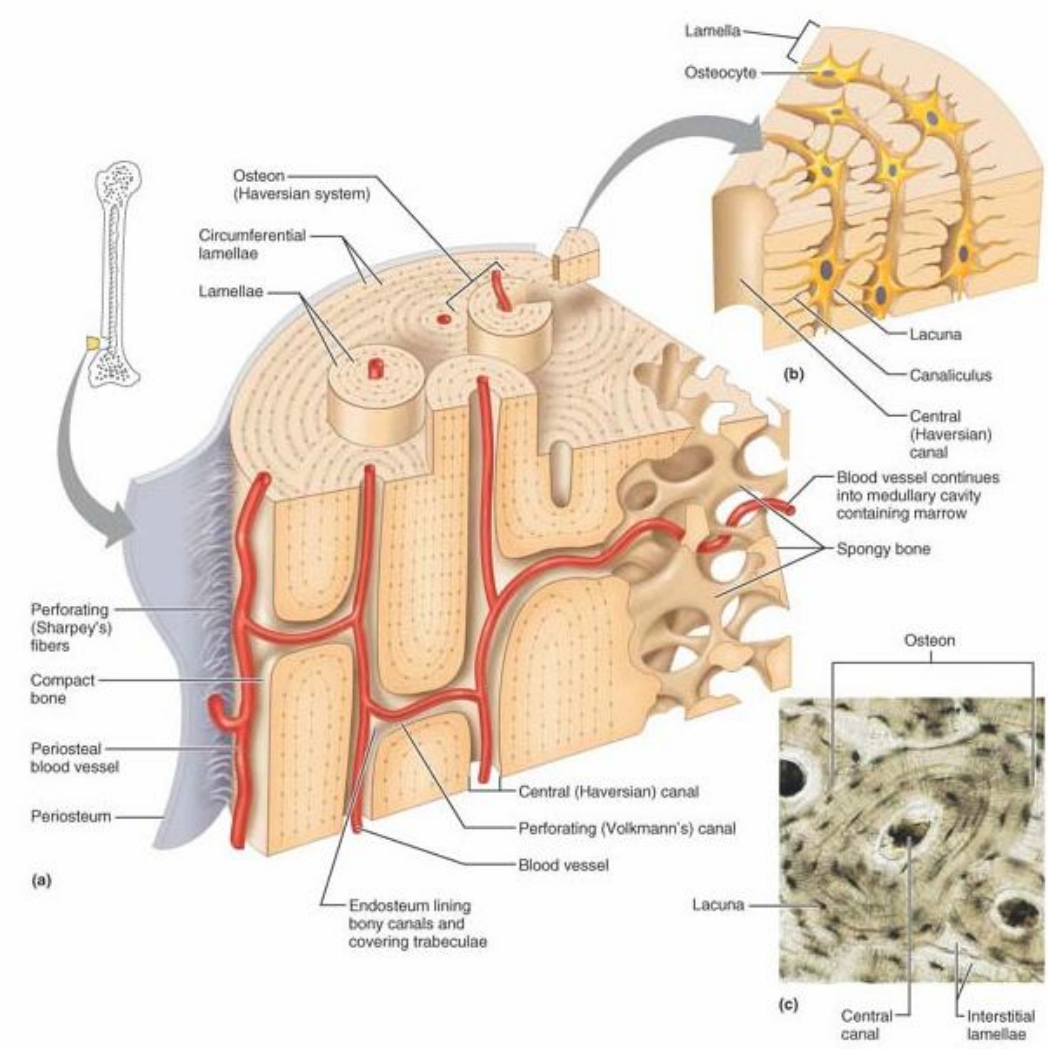

Figure 2.4 : Architecture of compact bone [1].

2.3.2 Spongious bone

Spongious bone does not contain any osteons (basic structural units), but consists of thin, irregularly shaped plates, rods or beams called trabeculae which also contains lamellae, osteocyctes, lacunea and canaliculi. Due to the shape of trabeculea, spongeous bone can be classified as a porous cellular solid and these pores are filled with bone marrow. As a result of that each osteocyctes is able to exchange nutrients with nearby blood vessels. Thus; a central canal is not needed, contrary to a cortical bone.

Because all the free bone surfaces are covered with bone cells (osteocyctes), trabeculea has the ability to change its morphology in response to changes in its mechanical environment. This process is called as bone remodeling.

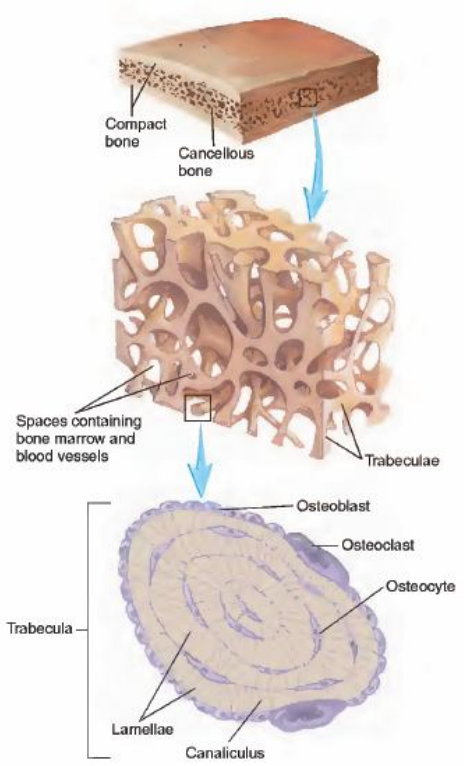

Figure 2.5 : Architecture of spongeous bone [2].

2.3.3 Comparison between cortical and spongious bone

Trabecular bone generally exist in the center of bones and is the porous part of bone. Because of its structure, trabecular bone has higher surface area but it is much weaker, softer and less stiff while cortical bone is the outer part of bones being much stronger, more stiff and less porous than trabecular bone. The porosity of trabecular bone is about 50-90 % while the porosity of cortical bone is only 5-10 %. Even

though cortical bone is seen as the protective covering of trabecular bone, trabecular bone has major tasks such as, mineral storage, blood cell regeneration and bone remodeling. By bone remodeling trabecular bone orient its internal structure along the stress lines. As a result of that spongious bone provide required strength with optimum weight.

2.4 Chemical Composition of Bone

Bone has both organic and inorganic components. Approximately 35% of total mass consists of organic components while 65% of it is inorganic.

Organic components include bone cells, such as osteoblasts, osteocyctes, osteoclasts, osteogenic cells, and osteoid. Osteoid includes basic substance and collagen fibers which are made and secreted by osteoblasts and form one third of the matrix. These basic substance and collagen also contribute to the flexibility of bones. For example; if collagen is removed, mineral component becomes the primary constituent and bone transforms into a over fragile organ.

Inorganic component is composed by calcium phosphate, calcium carbonate and other minerals such as flouride, potassium, magnesium that form 85%, 10%, 5% of it respectively. Calcium phosphate is in the form of small tightly packed crystals which are around or in the collagen fibers in the matrix. This form enables bone to resist compression and give the most to its stiffness. If mineral is removed, collagen becomes the primary constituent, then bone may transforms into a very bendable organ.

In short, it can be said that with proper combination of organic and inorganic components, the bone becomes exceedingly durable and strong due to minerals and collagen that respectively resist to compression and tension.

2.5 Bone Cells

There are three type of bone cells, osteoblasts, osteocyctes and osteoclasts. Osteoblasts (bone forming cells) produce collagen and proteoglycans. Collagen and proteoglycans are packaged into vesicles by Golgi apparatus until released from the cell by exocytosis which is a durable process. These vesicles are used to form

hydroxyapatite crystals which is also named as calcium phosphate crystlas. As a result of these processes, mineralized bone matrix is formed.

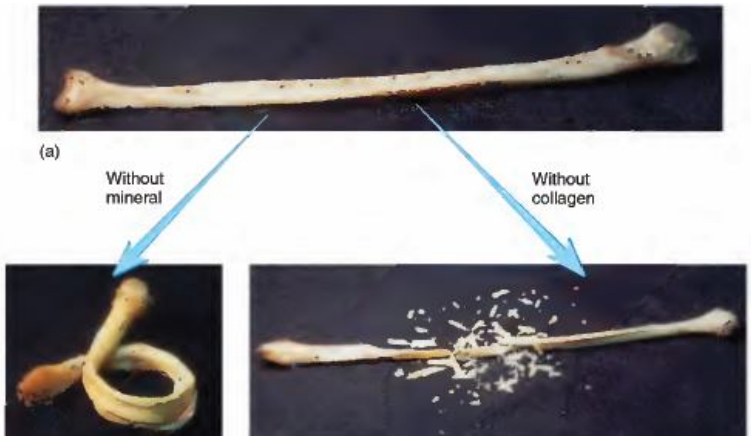

Figure 2.6 : Results of changes in bone matrix composition [2].

Ossificication and osteogenesis is the formation of bone by osteoblasts. Elongated cell processes from osteoblasts connect to cell processes of the other osteoblasts through the gap junction and then osteoblasts form an extracellular bony matrix that surronds the cells and their processes.

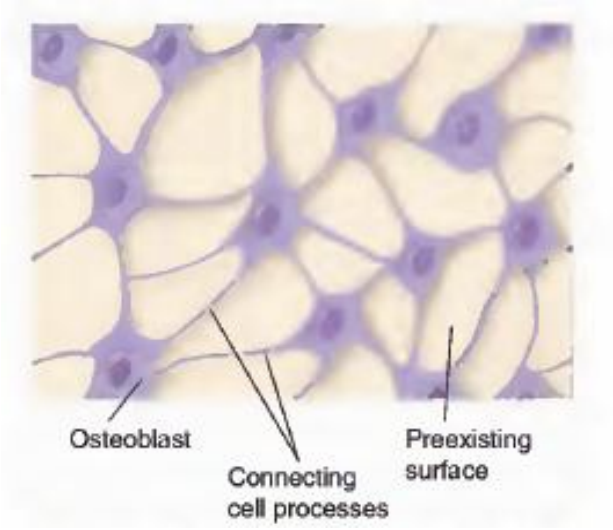

Figure 2.7 : Osteoblasts connect to eachother by cell processes [2].

Once osteblasts are surrounded by bone matrix, they are transformed to a mature bone cell called an osteocycte. Although osteocyctes are passive compared to the osteoblasts, they produce components which are required to preserve the bone matrix.

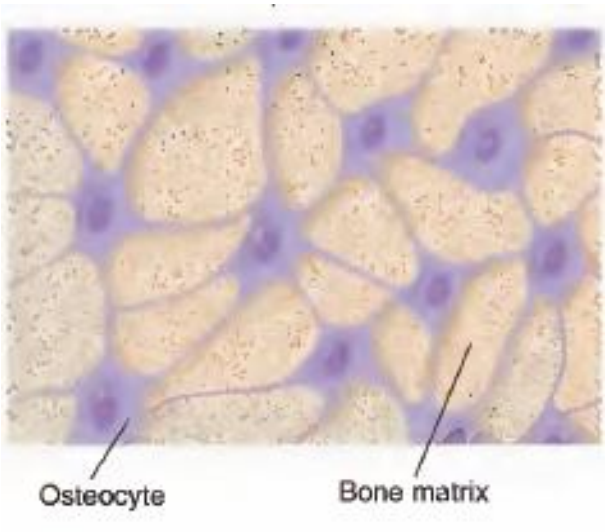

Figure 2.8 : Surrounded osteoblasts transform into osteocyctes [2].

Lacunae is a space which is occupied by osteoctcyes while canaculi is a space which is occupied by osteocycte cell processes. As a result of that the cells and their processes made up a mold space around which bone matrix is formed.

Osteoclasts are responsible for the resorption of bone. When the membrane of osteoclasts contact to bone matrix, it forms many projection called a ruffled border. Hydrogen ions are pumped across the ruffled border and produce an acid environment that causes decalcification of the bone matrix. Osteoclasts also release enzymes that digest the protein components of bone matrix.

Bone lining cells are inactive osteoblasts that are not buried in new bone. They remain in surface when bone formation stops and can be reactivated in response to chemical and mechanical stimuli [3].

3. BONE REMODELING

In this chapter, firstly bone remodeling concept is introduced by explaining two major loops; hormonal mechanicsm and mechanical effects. And then mechanical induced bone remodeling theories and models is decribed in a detailed way.

3.1 Bone Remodeling Concept

Bone can grow, change its shape**,** repair itself in a case of a fracture and adjust its internal structure constinuously due to metabolic and mechanical activities. Although bone grows only in the childhood stage and fracture heals in a case of fracture, the adaptation of internal structure is a life long process and takes place in the internal surfaces of the bone matrix such as trabecular surfaces of spongeous bone and Haversian system of cortical bone [4].

In bone remodeling concept, sometimes the terms “external remodeling” and “internal remodeling” is misplaced. The alterations in shape are results of modeling, whereas turnover, not influencing shape, is termed as remodeling (as cited in Buckwalter et al., 1995). For example; widening the cross section of medullary cavity or age related concavity of vertebrae or loose of bone around an implant application known as modeling which is a temporary activity. On the other hand, changes in trabeculea orientation and porosity known as remodeling which is a lifelong process.

This lifelong remodeling process modified by two major control loops, a negative feedback of the hormonal mechanism and the mechanical and gravitational forces that are acting on the skeleton.

3.1.1 Hormonal mechanicsm

The hormonal mechanism primarily involves parathyroid hormone (PTH), released when the level of ionic calcium in blood declines. The increased PTH level stimulates osteoclasts which resorb both old and new bone when activated. During the resorption, the level of calcium rises while the stimulus for PTH release

decreases. The increased level of calcium lead to secrete of calcitonin which discourage bone resorption and encourage calcium salt to deposit in bone matrix and as a result of that blood calcium level decreases. When blood calcium levels fall, calcitonin released decreases. So, it can be said that hormonal activities which regulate calcium level in the blood to maintain homeostasis also affect strength of bones. For example; if calcium level are low for a long time, bones become so demineralized and consequently the leakage of mineral decreases strength of bone.

Lastly, it should be mentioned that hormonal activities depend on not only the level of nutrition but also on age, gender and a variety of other factors.

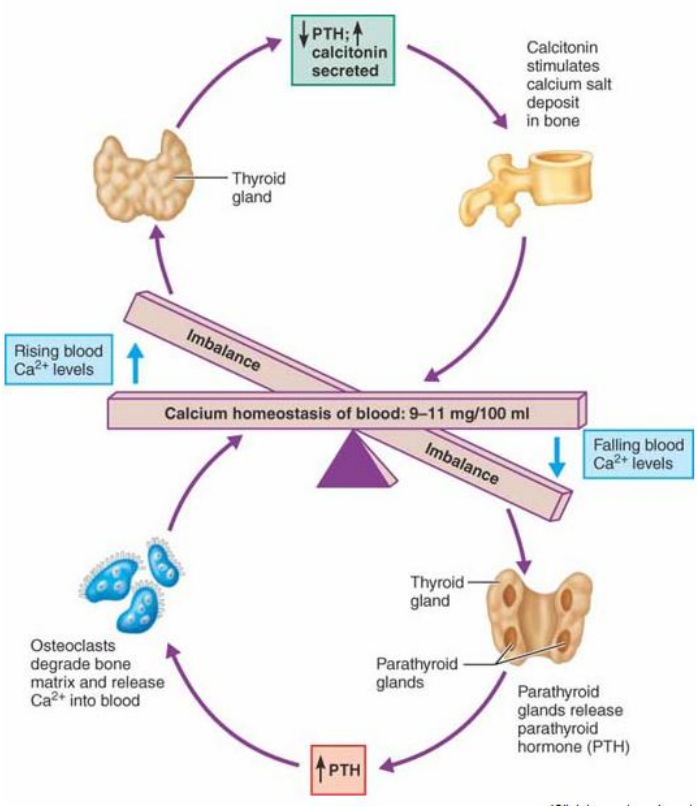

Figure 3.1 : Hormonal control blood calcium [1]**.**

3.1.2 Mechanical effects

The other control loop which regulate remoling process is the response of bone to mechanical loading conditions. To understand this concept, first we have to mention Wolff's Law, which is named after Julius Wolff. He is the first one publishing his ideas about adaptive process of bone and wrote his famous book, *Das Gesetz der Transformation der Knochen* in 1892 [5]. Based on the ideas of Roux (1881), Wolff assumed bone as a material with self-optimizing capabilities and a material that is

able to control its mass and structure in direct relationship to its mechanical demands [6]**.** As a result of that, three key concepts are given as a representation of Wolff's Law; the optimization of strength with respect to weight, the alignment of trabeculea in principle stress directions, and the self-regularity character in response to mechanical stimulus (Martin et al, 1998). Also, it can be said that bone in the first place, is an optimal structure relative to its mechanical requirements and able to maintain an optimal configuration relative to alternative mechanical requirements [7].

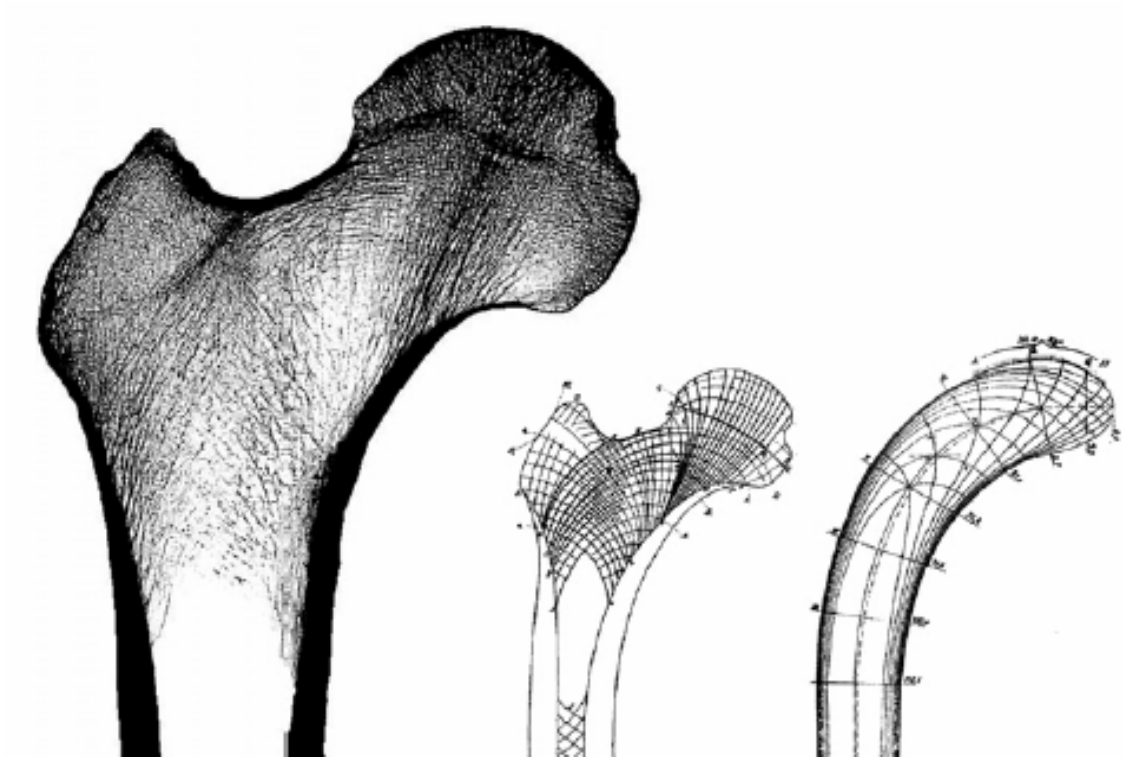

Figure 3.2 : The alignment of trabeculea in proximal femur [8]**.**

3.1.3 Basic multicellular units

Before explaining remodeling process, first we have to clarify the woven and lamellar bone concepts. Bone tissue is classified as either woven or lamellar bone. In wowen bone, the collogen fibers are oriented randomly and in many directions. We observe woven bone during fetal development and fracture repairment. After its formation, osteoclasts break down woven bone and osteoblasts build new bone matrix. Woven bone is remodeled to form lamellar bone which is the mature bone that organized into thin sheets or layers called lamallae. Collagen fibers of one lamallea is paralel to the one in the same lamallae but with an angle to the collogen

fibers in the adjacent lamallae. Osteocyctes, within their lacunae, are arranged in layers sandwiched between lamallae.

The remodeling process is not performed by a single cell, but by a group of cells which named as “basic multicellular units” by Frost. Basic multicellular units (BMU) consist of osteoblasts (bone-forming cells) and osteoclasts (bone-resorbing cells) which were mentioned in previous chapter. BMUs operate on Haversian and Volksmann canals, periosteom, endosteom and trabecular surfaces by replacing old bone with new one.

The sequence of remodeling process performed by BMUs known as A-R-F sequence; activation, resorption, formation and the sum of each sequence period refer to BMU life span. In the Figure 3.3 A-R-F sequence in cortical and trabecular bone is shown.

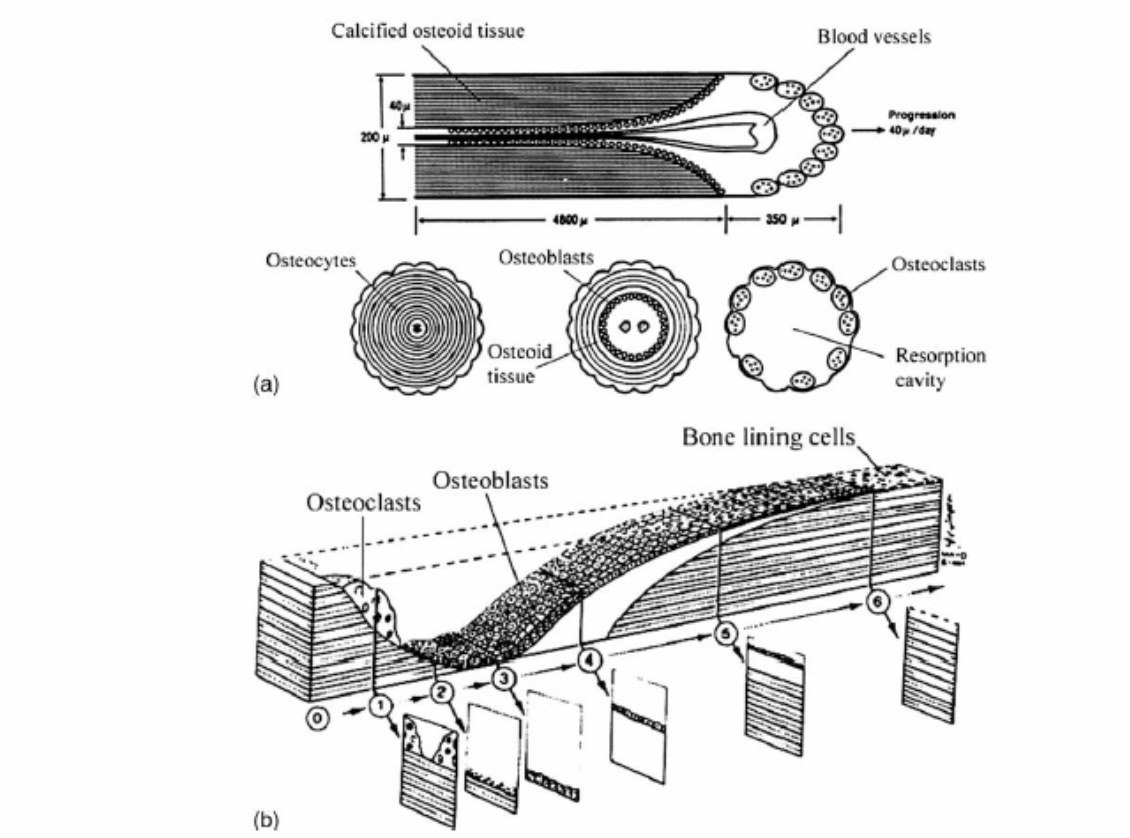

Figure 3.3 : A-R-F sequence in cortical bone (a) and in trabecular bone (b) [9]**.**

The details of BMU lifespan is such that; after activation, osteoclasts resolves the tissue matrix, by demineralizing it with acid and dissolving collagens with enzymes. This resorption period followed by reversal period in which the resoprtion process is

ended and none of the cell-type exist. After reversal period osteoblasts form new osteoids which known as formation period.

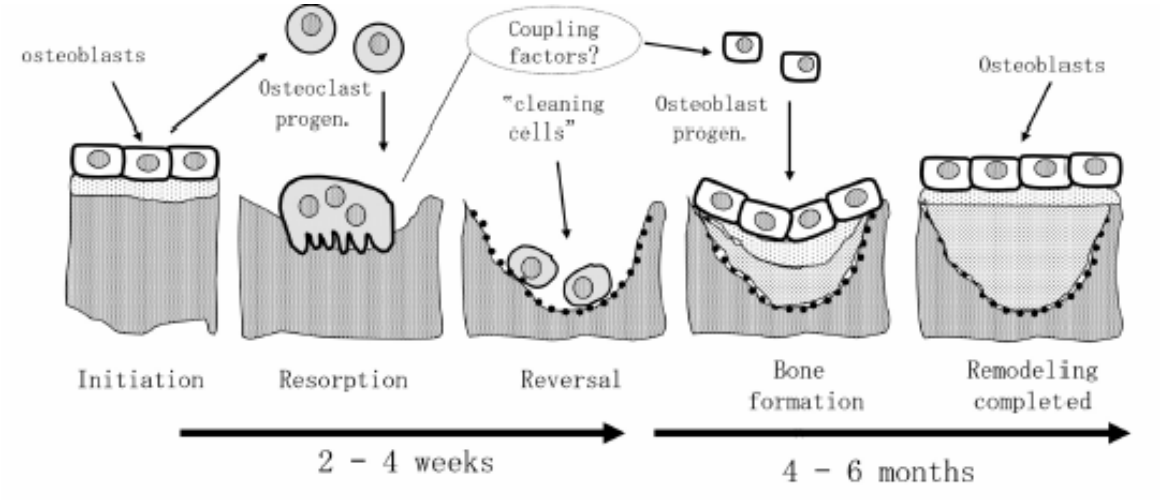

Figure 3.4 : Remodeling of bone tissue with BMUs [10]**.**

3.1.4 Mechanical behavior of bone

To be able to understand the evolution and results of bone remodeling, mechanical behaviour of bone have to be clarified. Bone is a porous, heterogenous, nonlinear, viscoelastic and anisotropic material with different properties in tension and compression, and being a living tissue makes it different from other materials. To obtain mechanical properties of bone some standard mechanical tests are done such as uniaxial tension and uniaxial compression, three point bending and four point bending. The table given below shows the result of experimental studies on cortical part of femur to determine the strength of bone. The first and second directions are radial and circumferential directions respectively while the third direction coincidence with the longitudinal axis of bone.

Even though by some standard and ultrasound tests the elasticity modulus of cortical bone in different directions are determined, it is difficult to find out specific values of elastic properties of trabecular bone. The reason is that, mechanical properties in trabecular bone are restrictively related to chemical composition, in other words the distribution of trabeculea, and as it mentioned before, the distibution of trabeculae depend on the metabolical, mechanical, physiological activities due to the adaptive behaviour of internal structure.

Table 3.1 : Material properties of cortical bone [11].

Investigators	Reilly, Burstein, Frankel (1974)	Yoon and Katz (1976)	Ashman, Cowin, Van Buskirk, Rise (1987)
Method	Mechanical	Ultrasound	Mechanical
E_1 (GPa)	11.5	18.8	12.0
E_2 (GPa)	11.5	18.8	13.4
E_3 (GPa)	17.0	27.4	20.0
G_{12} (GPa)	-	7.17	4.53
G_{13} (GPa)	3.3	8.71	5.61
G_{23} (GPa)	3.3	8.71	6.23
υ_{12}	0.58	0.312	0.376
υ_{13}	-	0.193	0.222
υ_{23}	-	0.193	0.235
υ_{21}	0.58	0.312	0.422
υ_{31}	0.46	0.281	0.371
υ_{32}	0.46	0.281	0.350

To be able to follow the principle of continuum mechanics in bone remodeling phenomen, properties in trabecular bone are averaged in a volume due to the discontinuous structure of trabeculea. The principles of continuum mechanics are explained in Appendix A. Before going further some descriptions have to be clarified. According to Garcia et al. [12] the formulations about internal scalar variables are defined as below.

Total volume is the volume of both tissue, marrow and voids.

$$V_T = V_B + V_V \tag{3.1}$$

where the indices T, B, V refer to total, tissue, void respectively.

Tissue volume is the volume of bone tissue that not include any marrow and void.

$$V_B = V_O + V_M + V_W \tag{3.2}$$

where the indices O, M, W refer to organic, mineral and water respectively.

Water has no significant effect on mechanical behaviour for bone, so tissue volume equation can be reduced as

$$V_B = V_O + V_M \tag{3.3}$$

which is the sum of osteoid and mineralize part in bone matrix.

Porosity is the proportion of void volume to total volume.

$$p = \frac{V_V}{V_T} = \frac{V_T - V_B}{V_T} = 1 - \frac{V_B}{V_T} \tag{3.4}$$

Apparent density is the quatient of total mass to total volume. As other words the averaged value of microstructural distribution of mass.

$$\rho = \frac{m_d}{V_T} = \frac{m_O + m_M}{V_T} \tag{3.5}$$

where total mass, m_T, is

$$m_T = m_O + m_M + m_W \tag{3.6}$$

and dry mass, m_d, is

$$m_d = m_O + m_M \tag{3.7}$$

Bone tissue density, ρ_t, is an imaginary density which represent bone without porosity.

$$\rho_t = \frac{m_d}{V_B} \tag{3.8}$$

so porosity, p, can be written as below

$$p = 1 - \frac{\rho}{\rho_t} \tag{3.9}$$

Ash fraction, a, is a feature that measure degree of mineralization.

$$a = \frac{m_M}{m_d} \tag{3.10}$$

The relation between mechanical properties and apparent density are established in different ways by researches. As stated in Doblare et al. [4] the relations that derived from different studies are given below. For example; according to Carter and Hayes (1977), one of the most cited works, the relation between elasticity modulus, E, and apparent density is

$$E = E(\rho) = c\rho^{\gamma} \tag{3.11}$$

where c is an constant and γ is the penalization power vary between 2 or 3. On the other hand; Lotz et al. (1991) determine the compressive strength and elastic modulus of femoral bone in axial and transversial directions. The elasticity modulus of trabecular bone was defined as

$$E = \begin{pmatrix} 1904\rho^{1.64} & for & axial \\ 1157\rho^{1.78} & for & transversial \end{pmatrix} \tag{3.12}$$

Also Jacobs (1994) stated the relation between elasticity modulus and apparent density as below.

$$E = B(\rho)\rho^{\beta(\rho)} = \begin{pmatrix} 2014\rho^{2.5} & for & \rho \le 1.2 \\ 1763\rho^{3.2} & for & \rho \ge 1.2 \end{pmatrix} \tag{3.13}$$

Beside these works some researhers shown the relation between mechanical properties and mineralization. The most representative compositional variable is the ash density with the following correlation. This expression covers over 96% of the statistical variation in the mechanical behaviour of combined vertebral and femoral data over the range of ash density (0.03–1.22)

$$E = 10500\rho_a^{\,2.47\pm0.04} \tag{3.14}$$

where ρ_a is ash density. Also Keyak et al. (1994) studied the relationship between mechanical properties and ash density for trabecular bone by obtaining the following expressions with 92% correlation. The relation of elastic modulus and density given as below.

$$E = 33900\rho_a^{2.2} \quad for \quad \rho_a \leq 0.27 \tag{3.15}$$

The disadvantage of this model is that, it is not considering the influence of bone volume fraction seperately from ash fraction which is modeled later by Hernandez et al. (2001) who express density as a function of both bone volume fraction and ash fraction.

$$\rho = \frac{V_B}{V_T}\rho_t = (1.41 + 1.29a) \tag{3.16}$$

They determine the elastic modulus and compressive strength with 97% correlation.

$$E = 84370\left(\frac{V_B}{V_T}\right)^{2.58\pm0.02} a^{2.74\pm0.13} \tag{3.17}$$

The unit of Young's modulus in the equations above is MPa while densities are g/cm^3.

As it is mentioned before, mechanical properties of bone is very complex to implement in computational bone remodeling models. Due to the complexity of mechanical features, some assumptions have to be made to make everything suitable for computational models.

First of all, on the contrary of soft tissues, the deformation of bone is small enough to ignore geometric nonlinearity. As a result of that the strain-displacement relation remains linear. Equation **(3.18)** shows general strain-displacement relation in index notation.

$$\varepsilon_{ij} = \frac{1}{2}\left(\frac{\partial u_i}{\partial x_j} + \frac{\partial u_j}{\partial x_i} - \frac{\partial u_k}{\partial x_i}\frac{\partial u_k}{\partial x_j}\right) \tag{3.18}$$

By neglecting the nonlinear part (the third term), equation is transformed to below.

$$\varepsilon_{ij} = \frac{1}{2}\left(\frac{\partial u_i}{\partial x_j} + \frac{\partial u_j}{\partial x_i}\right) \tag{3.19}$$

Although bone is a viscoelastic material due to the flow network, which is shaped by marrows and water flowing through canals, the contribution of marrows and water to the mechanical strength is inefficient which allows us to neglect the viscoelastic behaviour. Additionaly, the behaviour of bone remain almost linear in physiological strain, if it does not exceed 0.01 με (Cowin et al. 1987). The constitutive equation of linear elastic material given below.

$$\boldsymbol{\sigma} = \mathbf{c} : \boldsymbol{\varepsilon} \tag{3.20}$$

where **C** is 4th order tensor that refer to stiffness (elasticity) and **ε** represent strain tensor while **σ** is stress tensor.

Last assumption is taking bone as an isotropic material, eventhough the dependency of mechanical properties of bone to the directions is an obvious and significant parameter and in bone remodeling studies anisotropic character is preserved by a 2nd order fabric tensor, **H** [13, 14]**.**

In the equation below the stiffness tensor C_{ijkl} is given in matrix format while considering the isotropy.

$$C = \begin{bmatrix} 2\mu+\lambda & \lambda & \lambda & 0 & 0 & 0 \\ \lambda & 2\mu+\lambda & \lambda & 0 & 0 & 0 \\ \lambda & \lambda & 2\mu+\lambda & 0 & 0 & 0 \\ 0 & 0 & 0 & \mu & 0 & 0 \\ 0 & 0 & 0 & 0 & \mu & 0 \\ 0 & 0 & 0 & 0 & 0 & \mu \end{bmatrix} \tag{3.21}$$

where lame's constant are given below.

$$\mu = \frac{E}{2(1+\nu)} \qquad \lambda = \frac{\nu E}{(1+\nu)(1-2\nu)} \tag{3.22}$$

In our study, bone is going to be modeled as isotropic, linear, elastic material instead of anisotropic, nonlinear, viscoelastic material. Consequently, the constitutive equation of bone depend on only two parameters; Young's modulus, E, and poisson ratio, v. While Young's modulus is related with apparent density.

$$\begin{bmatrix} \sigma_{11} \\ \sigma_{22} \\ \sigma_{33} \\ \sigma_{23} \\ \sigma_{31} \\ \sigma_{12} \end{bmatrix} = \begin{bmatrix} 2\mu+\lambda & \lambda & \lambda & 0 & 0 & 0 \\ \lambda & 2\mu+\lambda & \lambda & 0 & 0 & 0 \\ \lambda & \lambda & 2\mu+\lambda & 0 & 0 & 0 \\ 0 & 0 & 0 & \mu & 0 & 0 \\ 0 & 0 & 0 & 0 & \mu & 0 \\ 0 & 0 & 0 & 0 & 0 & \mu \end{bmatrix} \begin{bmatrix} \varepsilon_{11} \\ \varepsilon_{22} \\ \varepsilon_{33} \\ 2\varepsilon_{23} \\ 2\varepsilon_{31} \\ 2\varepsilon_{12} \end{bmatrix} \quad \textbf{(3.23)}$$

Although this is a very superficial approach, it gives reasonable and valitated results.

3.2 Bone Remodeling Theories and Models

As it mentioned before, bone is capable of changing its internal structure and external shape to deal with metabolic, physiological and mechanical activities and consequently each bone microstructure is marvellously adapted to serve specific functions.

The purpose of this study was to understand bone remodeling concept first, then investigate theories and computational models and generate a algorithm based on previous studies with introduction of some original concepts.

Although the remodeling of bone is a very complex process includes a lot of parameters such as; sex, age, hormonal conditions, physilogical conditions, mechanical activities and building a computational model that connects bone remodeling with entire parameters considered above is impossible, it is believed that mechanical activities are one of the most influential factors during remodeling and a mechanical activity based bone remodeling algorithm is sufficient enough for most of the cases.

In the literature; there are many theories and computational models covering both internal and external remodeling processes utilizing different approaches.

The concept of bone remodeling known as Wolff’s Law claims that trabeculea alines in the principle stress trajectories. Although the loop behind remodeling action is not

known entirely, it is obvious that there is a mechanical feedback system which results in increase of bone mass with high loads and decrease of bone mass with reduced loads.

Even though there are a lot of phenomenological models investigate remodeling process by using different theories with either in macroscopic or microscopic levels, they have a common point: many apply a mechanical stimulus as a feedback system in forms of; stress [15,16] strain [17,18], strain energy density [6,7,18,19], strain energy density rate [20-22] or damage [4,13]. In these models generally the change in the interval parameters calculated depending on mechanical stimulus and consequently new properties estimated in both macroscopic levels [4,6,7,13,14,17,18,19] or in bone cell based which explains bone behaviour and morphology on the scale of individual trabeculea [21,22].

3.2.1 The model of Pauwels and Kummer

Pauwels worked on a mathematical formulation about bone remodeling in 1965. He proposed an optimal stress level, above which formation and below which resorption occurs.

$$\frac{dm}{dt} = c(\sigma - \sigma_u)(\sigma - \sigma_n)(\sigma - \sigma_o) \qquad \textbf{(3.24)}$$

where m is mass and σ is stress.

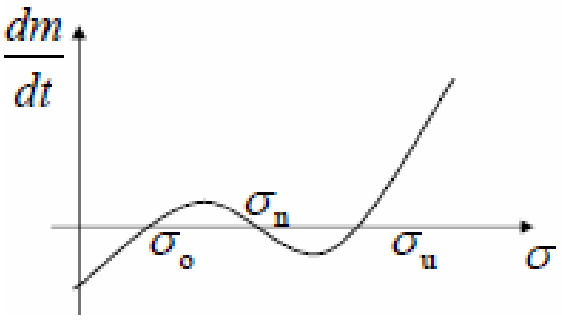

Figure 3.5 : Formation and resorption rate due to stress level.

His contemporary, Kummer ran the first computer simulation of internal remodeling by comparing it with a second order feedback system as stated in Jacobs (1994) [23].

3.2.2 The theory of self optimizing material

In the work of Fyhrie and Carter (1986), they assume bone tissue to be self optimizing material with the objective of aligning trabecular architecture with principle stress orientation, and adapting its apparent density ρ to an effective stress σ_{eff}. Based on strength or strain optimization the equation developed is

$$\rho = A\sigma_{eff}^{a} \tag{3.25}$$

where ρ is apparent density, A and a are constant and σ_{eff} is effective stress [22]**.** The effective stress is determined from either a failure or an elastic energy criteria. This unified theory can be used to quantitavely predict bone architecture and adaptive remodeling and coincidence with Wolff's Law and also with analytical/experimental findings which are reporter by Hayes and Snyder (1981).

In later publications (Carter et al., 1987; Fyrie and Carter, 1986b) they emphasize the application of the theory to predict the optimal density distribution of the proximal femur according to the above criterian, using a numerical formulation in combination with the FEM. They assume $a = 0.5$ and the effective stress to be derived from the apparent strain energy density (SED) in the form,

$$\sigma_{eff} = \sqrt{2EU} \tag{3.26}$$

where E is the average apparent Young's modulus and U is the apparent strain energy density [22].

Carter and Fyrie [17] proposed a daily stimulus, S*, to maintain bone mass. Stimulus, S*, can be directly associated with the stimulus to the mineralized tissue and is given by

$$S^{*} \propto \left(\sum_{day} n_i \left(U_{bi}\right)^{k} \right) \tag{3.27}$$

where n_i is the number of cycles of load type i, k is the energy exponent constant and U_b is the true SED in bone. Since true strain energy density is constant, equation **(3.28)** provided that cortical bone density, ρ_c, equals the true or bulk density of the trabeculae, ρ, bone itself.

$$U = U_b \frac{\rho}{\rho_c} \tag{3.28}$$

The stimulus above can be given in terms of continuum model strain energy density either.

$$S^* \propto \frac{1}{\rho^k} \left(\sum_{day} n_i (U_i)^k \right) \tag{3.29}$$

If bone maintenance stimulus is assumed constant again in everywhere, the local bone apparent density can be written as

$$\rho \propto \left(\sum n_i (U_i)^k \right)^{(1/k)} \tag{3.30}$$

In the case of a single load case, the analysis equation above degenerates

$$\rho \propto U \tag{3.31}$$

so the optimization function also can be transformed to

$$\rho = c' U \tag{3.32}$$

By integrating the equations **(3.11)**, **(3.26)** and **(3.32)** continuum strain energy density can be written as

$$U \propto \left(\bar{\sigma}_{eff} \right)^2 / \rho^3 \tag{3.33}$$

Substitution of equation **(3.33)** into the equation **(3.30)** yields

$$\rho \propto \left[\sum n_i \left(\bar{\sigma}_i \right)^{2k} / \rho^{3k} \right]^{1/k}$$

$$\rho \propto \left[\sum n_i \left(\bar{\sigma}_i \right)^{2k} \right]^{1/4k} \tag{3.34}$$

end if we let $m = 2k$

$$\rho \propto \left[\sum n_i \left(\bar{\sigma}_i\right)\right]^{1/2m} \tag{3.35}$$

where $\bar{\sigma}_i$, is the effective stress and the stress exponent *m* is an experimental parameter varying from 3 to 8 [24]**.** The most important contribution of this model is the consideration of the influence of different load cases and the number of load cycles for each case.

The model is also extended to include the effect of anisotropy by Carter et al. (1989); who proposed that trabeculae tend to orientate according to a directional quantity which is related to stresses, named as normal equivalent stress. This model considers the different contributions of different load cases.

$$\sigma_n^*(\mathbf{n}) = \left[\sum_{i=1}^{N} \left(\frac{n_i}{n_t}\right) (\mathbf{n} \bullet \boldsymbol{\sigma}_\mathbf{i} \bullet \mathbf{n})^m\right]^{1/m} \tag{3.36}$$

3.2.3 The theory of adaptive elasticity

With the increased capacity of computers, computer simulation of bone adaptations became popular in 1980s. The first continuum model is completed by Cowin and Hegedus in 1976 titled as Theory of Adaptive Elasticity [5]**.** The theory of adaptive elasticity was developed to describe the remodeling behaviour of cortical bone [25-27]. This theory primarily attempts to describe the adaptive remodeling behaviour of bone from one loading configuration to another, rather than predicting the optimal structure of normal bone, as in the theory of self optimization [17]**.** It is assumed that cortical bone is in a homeostatic equilibrium strain state and when a change of load or ubnormal strain state occur, bone is stimulated to adapt its mass to regain the equilibrium strain state. In the theory, the rate of adaptation is coupled to the difference between the equilibrium and the actual strain states.

Following the suggestion by Frost (1964), Cowin and associates separate internal and surface (external) remodeling [7].

$$\frac{dE}{dt} = A_{ij}(\varepsilon_{ij} - \varepsilon_{ij}^0) \tag{3.37}$$

where E is the local modulus of elasticity, ε_{ij} is the actual strain tensor, ε_{ij}^{0} is the equilibrium strain tensor and A_{ij} is the matrix of remodeling coefficients.

In the case of external remodeling the bone can only add or remove material on the periosteal and endosteal surfaces, stimulated by strain state at those surfaces, according to

$$\frac{dX}{dt} = B_{ij}(\varepsilon_{ij} - \varepsilon_{ij}^{0}) \qquad \textbf{(3.38)}$$

where X is a characteristic surface coordinate perpendicular to the surface, and B_{ij} again a matrix of remodeling coefficients.

Firoozbakhsh and Cowin [27] also considered a quadratic relation between strain and rate of adaptation and peformed a number of studies to determine possible values of the remodeling coefficients.

Cowin et al. [28] extended this theory to include anisotropy by introducing the fabric tensor, **H**, and reorientation of the trabecular architecture as a function of strain. The fabric tensor, **H,** is a numeric measure of the trabecular architecture and the directional arrangement of the microstructure of cancellous. **H** is a second-order positive definite tensor, whose principal directions are coincident with the principal directions of the microstructure and its principal values are proportional to the amount of bone mass along each principal direction. The internal parameters considered were the internal porosity and the fabric tensor, that was determined by Cowin by the mean interception length (MIL) method [14].

3.2.4 The model of Huiskes et al.

In the work of Huiskes et al. [7] a two dimensional computer model is developed in combination with an alternative formulation of the theory of adaptive elasticity. As a first difference, they use strain energy density as a feed back control variable instead of strain tensor.

$$U = \frac{1}{2}\varepsilon_{ij}\sigma_{ij} \qquad \textbf{(3.39)}$$

where σ_{ij} is the local stress tensor and ε_{ij} is the strain tensor. The difference between actual strain energy density (SED), U, and a site-specific homeostatic equilibrium SED, U_n, is assumed as the driving force for adaptive elasticity.

In the second place , a suggestion from Carter (1984) is followed ,which approve a lazy zone where bone is neither resorbed nor formed, instead of assuming a linear relation between adaptive rate and SED. It is assumed that a certain threshold level in over or underloading must be exceeded before bone reacts.

U(t,x) is the actual local SED and $U_n(x,t)$ is the homeostatic SED, where t is the the time and x is the localization vector. When $U > (1+s)U_n$ or $U < (1-s)U_n$, adaptive activity is initiated, where s is the thereshold level and the rate of adaptation, A, is the slope of curves. Thus; for internal remodeling equation of state can be written as

$$\frac{dE}{dt} = \begin{pmatrix} A_e(U-(1+s)U_n) & for & U > (1+s)U_n \\ 0 & for & (1-s)U_n \le U \le (1+s)U_n \\ A_e(U-(1-s)U_n) & for & U < (1-s)U_n \end{pmatrix} \quad \textbf{(3.40)}$$

A similar formula is used for external remodeling whereby , dX/dt, the rate of surface growth perpendecilar to the surface.

$$\frac{dX}{dt} = \begin{pmatrix} A_x(U-(1+s)U_n) & for & U > (1+s)U_n \\ 0 & for & (1-s)U_n \le U \le (1+s)U_n \\ A_x(U-(1-s)U_n) & for & U < (1-s)U_n \end{pmatrix} \quad \textbf{(3.41)}$$

To determine the geometrical or material changes, the remodeling rates are integrated, using Forward Euler integration with a constant time step Δt, whereby, for internal remodeling, the change is elastic modulus in each step follow from (s=0)

$$\Delta E^i = E^i(t+\Delta t) - E^i(t) = \Delta t A_e(U^i(t) - U_n^i) \quad \textbf{(3.42)}$$

where i is the number of elements. For external remodeling the relocations of the surface points perpendicular to the surface in each step follow from

$$\Delta X^j = X^j(t+\Delta t) - X^j(t) = \Delta t A_x(U^j(t) - U_n^j) \quad \textbf{(3.43)}$$

where j is the number of surface nodal points concerned.

Some problems are detected like negative values of the elastic modulus or excessive geometry distortion using this model, but several examples solved succesfully like external remodelling of a cantilever beam made of bone tissue and a simple model of a prosthesis in a bone predicting the effect of “stress shielding”. The density was calculated from the elastic modulus according to equation **(3.11)**. The results show similarity with actual proximal femur density distribution and also are very similar with one which obtained by Fyhrie and Carter (1986b) and Carter et al. (1987b), using their self optimization (SO) theory. Obviously, there are some distinct differences between self optimization and adaptive elasticity theory while SO theory predicting what value U_n should actually have, on the other hand AE describing the remodeling process of bone tissue towards a homestatic SED U_n.

In later works, Weinans et al. [6], Mullender et al. 1994), characterized the mechanical behaviour of bone tissue using the apparent density as internal variable like other authors [29-31].

In the work of Carter et al., (1989), a stimulus S was defined which considered the individual loading configurations by averaging their individual contributions.

$$S = \frac{1}{n}\frac{1}{\rho}\sum_{i=1}^{n} U_i \qquad \textbf{(3.44)}$$

where U_i is the SED values for loading case i, n is the total number of loading cases and ρ is the apparent density [6].

Consequently, the change of apparent density is written in terms of the strain energy density, taking into account the influence of different load cases.

$$\frac{d\rho}{dt} = B\left(\frac{U_a}{\rho} - k\right) \qquad \textbf{(3.45)}$$

$$0 < \rho \le \rho_{cb}$$

where $\rho = \rho(x, y, z)$ is the apparent density, ρ_{cb} is the density of cortical bone, B and k are constants. To determine the new density Forward Euler method is used which is mentioned earlier studies of Huiskes and Weinans [7]. The density

distribution show good resemblance with real proximal femur. The relation between density and Young modulus was taken from Carter and Hayes (1977) as

$$E = 3790\rho^3 \tag{3.46}$$

After calculating elastic modulus; the constitutive equation is updated. This incremental loop continues until model is convergenced. The objective function of convergence criteria is expressed as

$$\Theta = \frac{1}{m}\sum_{i=1}^{m}\left|\frac{U_a^i}{\rho^i} - k\right| \tag{3.47}$$

where m is the number of elements and U_a^i is the average SED for all loading cases considered in element i. The value of Θ is calculated after each iteration and indicates that if the objective $U_a/\rho = k$ is reached in the whole structure or not. It must be mentioned that the remodeling objective will not be met at the elements either formed or resorbed completely [6].

3.2.5 The isotropic Stanford model

The Isotropic Stanford Model based on works of Carter and co workers in the theory of self optimization. This model suggests that bone tissue need a certain level of mechanical stimulus and auto regulated to maintain that level. So, first of all; the distinction between continuum level and tissue level has to be made. Relation between the variables at continuum level (macro) and tissue level (micro) can be written as

$$Z = R(n)Z_t \tag{3.48}$$

where Z and Z_t respectively is any scalar function at continuum level and tissue level and n refer to porosity. For example if porosity taken as zero this means the complete mineralization of bone (R(0)=1) and consequently continuum level and tissue level become same. From experimental estimates Jacobs [23] gives the relation between the tissue and continuum level stress measure as below.

$$R(\rho) = \left(\frac{\rho}{\rho_t} \right)^2 \tag{3.49}$$

And by integrating equation **(3.48)** and **(3.49)** the tissue effective stress can be written as

$$\overline{\sigma_t} = \left(\frac{\rho_t}{\rho} \right)^2 \overline{\sigma} \tag{3.50}$$

while the effective stress, $\overline{\sigma}$, mentioned before in self optimizing material as

$$\overline{\sigma} = \sqrt{2EU} = \sqrt{E\varepsilon : C : \varepsilon} \tag{3.51}$$

where C is the constitutive tensor. So by integrating the equations **(3.50)** and daily stress stimulus, ψ, the stimulus in bone tissue level, ψ_t, can be written as

$$\Psi_t = \left(\sum_{i=1}^{N} n_i \overline{\sigma}_{ti}^{m} \right)^{1/m} = \sum_{i=1}^{N} n_i^{1/m} \overline{\sigma}_{ti} = \sum_{i=1}^{N} n_i^{1/m} \left(\frac{\rho_t}{\rho} \right)^2 \overline{\sigma} \tag{3.52}$$

There is a case of equilibrium, in which the bone mass is maintained. The condition for this equilibrium is given as

$$\Psi_t = \Psi_t^* \tag{3.53}$$

where ψ_t^* denotes the tissue equilibrium stimulus. The error from this equilibrium is assumed to be the driving force of remodeling [5].

$$e = \Psi_t - \Psi_t^* \tag{3.54}$$

The linear relationship between the surface remodeling rate, $\dot{r}$, and the error, e, is given as

$$\dot{r} = \begin{pmatrix} c((\Psi_t - \Psi_t^*) + w) & for & (\Psi_t - \Psi_t^*) < -w \\ 0 & for & -w \le (\Psi_t - \Psi_t^*) \le +w \\ -c((\Psi_t - \Psi_t^*) - w) & for & (\Psi_t - \Psi_t^*) > +w \end{pmatrix} \tag{3.55}$$

where c is a constant which can be changed for different cases, the value w denotes the half-width of dead zone no remodeling takes place. Next term is specific surface area, S_v, which is the internal surface area per referance volume and directly related to the porosity by the polynomial with coefficients in mm^2/mm^3.

$$S_v = 0.02876p^5 - 0.10104p^4 + 0.13396p^3 - 0.09304p^2 + 0.03226p \quad \textbf{(3.56)}$$

The approximation is taken from Martin (1984) who experimentally determined the available surface for each bone in term of porosity. The specific surface area is important because, the remodeling process occurs on internal tissue surfaces.

The density rate law given in the equation below.

$$\dot{\rho} = \dot{r} S_V \rho_t k \quad \textbf{(3.57)}$$

where k is the percentage of available surface for remodelling and taken 1 due to the simplificity of model and ρ_t is the density of completely mineralised bone with null porosity. In this model new bone assumed to be completely mineralised.

To determine the new density the Euler Forward method was implented with adequetly small time steps.

$$\rho_{t+\Delta t} = \rho_t + \dot{\rho}_t \, \Delta t \quad \textbf{(3.58)}$$

where i refer to the number of element.

The connection between elastic modulus, poisson ratio and apparent density is given in the equations **(3.59)** [14]**.**

$$E = B(\rho)\rho^{B(\rho)} = \begin{pmatrix} 2014\rho^{2.5} & for & \rho \le 1.2 \\ 1763\rho^{3.2} & for & \rho \ge 1.2 \end{pmatrix}$$
$$\upsilon = \upsilon(\rho) = \begin{pmatrix} 0.2 & for & \rho \le 1.2 \\ 0.32 & for & \rho \ge 1.2 \end{pmatrix} \quad \textbf{(3.59)}$$

After calculating Young's modulus and posisson ratio the constitutive equation, C, can be determined [5].

In the study of Beaupre et al. [29] the analysis converged when the change in apparent density for every element was less that 0.02 g/cm^3. However in the study of Thomas [5],who use same remodeling algorithm with different values of parameters, mentioned that the numerical results tends in a stable way to solution, but consistency is not proved, so a new parameter for convergence criteria is introduced **(3.60)**. This equation gives the average of the density change for the volume of the whole model. The value oscillates with an amplitude which indicates the unstability of the model.

$$\xi = \frac{\int_V \left| \dot{\rho} \right| dV}{\int_V dV} \tag{3.60}$$

3.2.6 Anisotropic extension of Stanford model

This model assumes that the bone structure adapts by minimising or maximising a certain “efficiency” defined as to the difference between the external power rate and the variation of the internal energy, constrained by the condition of remaining inside the dead-zone. [14] This is a constrained optimisation problem that is solved by optimising the associated Lagrangian, getting finally (Jacobs et al.,1997)

$$\dot{C} = \frac{\beta \dot{\rho}}{\rho} \frac{\boldsymbol{\sigma} \otimes \boldsymbol{\sigma}}{\boldsymbol{\sigma} : \boldsymbol{\varepsilon}} \tag{3.61}$$

where it is noted that the evolution of the elasticity tensor is directly coupled to the evolution of the density. The constitutive anisotropic relation reduced to the previous isotropic formulation when bone is permanently loaded by a spherical stress state.

3.2.7 Damaged based anisotropic model of Doblare and Garcia

To save these difficulties in the model Jacobs (1997) mentioned above, Doblare and Garcia (2002) propose a new remodelling model, by identifying the “internal variables” associated to the bone microstructure, follows the steps of the extension of the CDM for the anisotropic case introduced by Cordebois and Sideroff (1982).

Their concept of damage can be understood as a measure of the void volume inside the bone tissue, while directionality follows the idea suggested by Cowin for the fabric tensor. Therefore undamaged material is the ideal situation of bone with null porosity and perfectly isotropic. The process of bone resorption thus corresponds directly with the classical damage concept, since it increases the void ratio, while bone apposition produces damage reduction or bone repair that has to be adequately considered in this extended damage theory. This implies that, on the contrary to the standard case in which damage always has a positive evolution as a direct corollary of the second law of thermodynamics, in a "damage-repair" theory the damage evolution may also be negative (during the repairing process) due to the provision of metabolic energy not considered in a purely mechanical model [14].

Finally, it could mentioned that the bone resorption process is different from the standard Mechanical Damage problem for non-living materials. For the latter, damage increases in a certain region due to the appearance of a stress level higher than a predefined value, while in bone resorption this additional damage production occurs when the stress level is below a certain threshold. This difference will imply important thermodynamic differences. Damage tensor expressed as

$$D = 1 - \left(\frac{\rho}{\hat{\rho}} \right)^{\beta/2} \qquad \textbf{(3.62a)}$$

$$\sqrt{G}\,\hat{\mathbf{H}} = 1 - \mathbf{H}^2 \qquad \textbf{(3.62b)}$$

where $\hat{\rho}$ is the maximum density of ideal bone with null porosity, 1 is the identity second order tensor, β is the experimental parameter which relates the elastic modulus and the apparent density, G is an adjusting parameter that is obtained by particularising the general anisotropic model to the isotropic case and $\mathbf{H}\hat{}$ is the fabric tensor, which normalised such that $\det \mathbf{H}\hat{} = 1^3$ This damage tensor includes not only the microdirectionality of the bone structure through the fabric tensor, but also the porosity by means of ρ . In addition, and contrary to the Jacobs et al. (1997), both variables are independent due to the normalisation condition for $\mathbf{H}\hat{}$.

In order to simplify the formulation, the intermediate tensor **H** used as internal variable and called as the remodelling tensor and directly related to the damage

tensor **D** and includes both physical variables ρ and **Hˆ**. So effective stress can be written as

$$\tilde{\boldsymbol{\sigma}} = \mathbf{H}^{-1}\boldsymbol{\sigma}\mathbf{H}^{-1} \tag{3.63}$$

which leads to a constitutive tensor, whose orthotropy directions coincide with those of the principal axes of the damage tensor **D** and therefore of **H** and **Hˆ** . After that elasticity tensor is computed in the principle axes of fabric tensor, **Hˆ**.

Once the internal damage variable has been defined, the next step is to define the external mechanical stimulus of the problem. In analogy to Plasticity (Simo and Hughes, 1998), the stimulus is identified with the variable thermodynamically associated with the damage tensor or, even better, to the remodelling tensor **H**. However, in order to establish this stimulus, mechanical variable (strain or stress) that externally "drives" the process has to defined. In the study strain is used as the "external driving force", although exactly the same results can be obtained if stress is considered as earlier proposed by Wolff (1892). The stimulus is defined as

$$\mathbf{Y} = \frac{\partial \chi(\boldsymbol{\varepsilon}, \mathbf{H})}{\partial \mathbf{H}} = \frac{\partial \Psi}{\partial \boldsymbol{\sigma}} \frac{\partial \boldsymbol{\sigma}}{\partial \mathbf{H}} \perp_{\varepsilon = ct} \tag{3.64}$$

with χ being the free energy function and where the constancy of **ε** in the evalution of the partial derivative has been made explicit.

The model properly represents the limiting effect in density values close to that of compact bone, establishing a limit value for the hardening exponent in complete agreement with experimental results. Other qualitative corollaries of the model that agree with experimental tests are that the "fabric tensor" is aligned (equal principal directions) with the elasticity tensor, and that the material tends to align its principal directions with the ones of the stress tensor, reaching a directional equilibrium when the stress is aligned with the fabric tensor, although the density value can still change. Furthermore, resorption implies a faster evolution of the anisotropic character of the constitutive tensor than apposition. Finally, it is shown that the computed density and stiffness distributions both in average and directional are very close to reality when applied to the proximal femur.

3.2.8 Model of Hazelwood

Hazelwood et al. (2001) created a mechanistic computational model of a representative volume of bone for bone remodeling driven by the replacement and reinforcement of damaged bone with fresh bone and the removal of under loaded bone to streamline the mass/performance relationship. Their code was the first to incorporate an integrated disuse model by using common parameter variables of daily BMU activation frequency for both the damage and disuse removal portions of the code. Elastic modulus and porosity values are looped in a code circuit that changes based upon the alteration of independent variables, such as the loading conditions or the number of walking cycles per day experienced. The mathematical model outputs the changes in bone parameters during the calculation interval, such as porosity, activation frequency and mechanical stimulus for a representative volume of bone. The research found that damped oscillations occurred with each of the remodeling parameters, which concurs with the physiological process of bone remodeling to find an optimal equilibrium value for each parameter. The Hazelwood et al. (2001) code is easily portable, resulting in its use in finite element models in various bones, animals and loading conditions [32].

3.2.9 Model of Ruimermann et al.

The model of Weinans and Huiskes (1992) produced density distributions that showed good resemblance with those in a real proximal femur.However, only if these distributions were locally averaged from discontinuous density patterns in the femoral head, where the trabecular bone is located. It is the nature of the differential equations used to mathematically describe the adaptive remodeling process that the simulation produces discontinuous end configurations, known as “checker boarding” means that in the ongoing process the stiffer elements will even become stiffer, while the others loose density, until they are virtually empty. The reason of that is both sensation of the local mechanical stimulus and the actual adaptation of bone mass is in the same location, which result in elements only work for themselves that not fit the biology of remodeling process. So the sensation of mechanical stimuli and adaptation of material properties should be separated in the theory, as was done by Mullender et al. (1994) and Huiskes (1995). Osteocytes within the tissue matrix were assumed to be mechanosensitive and capable of translating signals to the bone

surface to attract so-called basic multicellular units BMU's which control the net apposition or removal of bone tissue. The separation of sensation and density adaptation into two different functions prevented the so-called checker-boarding phenomenon. The model was able to realign its trabeculae to alternative loads and so explained both modeling and adaptation. After the structure was optimized or adapted to the external loads the activity of the BMU's stopped.

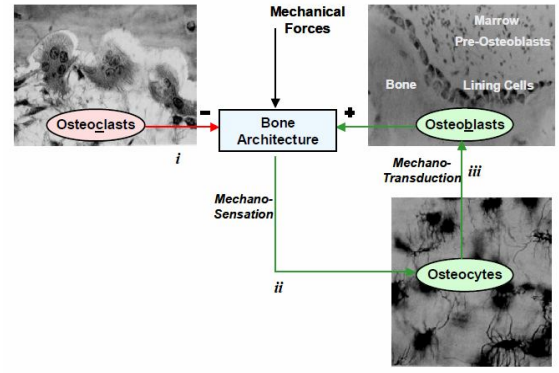

Figure 3.6 : Proposed regulation mechanism [22].

The differences between actual trabecular bone and the approach above is that the activity of both osteoclasts and osteoblasts continues throughout life and these separate activities incorporated in a theory which was developed by Huiskes and associates (Huiskes et al., 2000; Ruimerman et al., 2001). The new theory is based on that tissue adaptation on a specific location x at time t was supposed to be the result of osteoclastic bone resorption and osteoblastic bone formation [21,22].

$$\frac{dm_{tot}(x,t)}{dt} = \frac{dm_{bl}(x,t)}{dt} - \frac{dm_{cl}(x,t)}{dt} \qquad \textbf{(3.65)}$$

Osteoblast activity at the trabecular surface is controlled by osteocyctic bone formation stimuli. For a total stimulus P(mol mm^{-2} day^{-1}) that exceeds a certain threshold value k_{tr} osteoblast tissue formation is

$$\frac{dm_{bl}(x,t)}{dt} = \tau\left(P(x,t) - k_{kr}\right) \qquad \textbf{(3.66)}$$

where τ[MPa-1.s-1] is a rate constant.

The equation below shows that all osteocyctes located within the region have a contribution to the stimulus, P, depending on their mechanosensitivity μ_i (mol mm J^{-1}

s^{-1} day^{-1}) , where N is the total number of osteocycte located in that region, x_i is the location of osteocycte i, $R(x_i,t)$ is the mechanical signal that osteocycte senses and $f(x,x_i)$ describes the decay in signal intensity relative to distance d and decay parameter D.

$$P(x,t) = \sum_{i=1}^{N} f(x,x^i)\mu_i R(x_i,t) \text{ with } \quad f(x,x') = e^{-d(x,x')/D} \tag{3.67}$$

Osteoclast bone resorption is described as

$$\frac{dm_{cl}(x,t)}{dt} = -r_{cl} \tag{3.68}$$

where r_{cl} (mm^3 day^{-1}) represents a stochastic function.

Until now computational models of bone adaptation used static loads to evaluate the mechanical signals. It is, however, known that bone only reacts to dynamic loads. In the new theory the stimulus sensed by osteocytes is assumed to be a 'typical' strain energy density rate (SED-rate) R(x, t) in a recent loading history. Cyclic loading conditions, characterized by frequency and magnitude, were imposed and it was assumed that osteocytes react to the maximum SED-rate during the loading cycle. So the signal sensed by osteocytes is assumed to be a 'typical' strain energy density rate (SED-rate) R(x,t), calculated ısing FEA.

Ruibermann et al. [21] present a 3-D FEA model investigated its potential morphological predictability of metabolic reactions to mechanical loads. The computations simulated the development of trabecular morphological details during growth, relative to measurements in growing pigs, reasonably realistic. Alternative loading directions produced new trabecular orientations. Reduction of load reduced trabecular thickness, connectivity and mass in the simulation, as is seen in disuse osteoporosis. Simulating the effects of estrogen deficiency through increased osteoclast resorption frequencies produced osteoporotic morphologies as well, as seen in post-menopausal osteoporosis. The theory provides a suitable computational framework to investigate hypothetical relationships between bone loading and metabolic expressions.

3.2.10 Topology Optimization

Bone remodeling simulation was also improved by structural topology optimization. (Bagge, 2000; Fernandes and Rodrigues, 1999; Hollister et al., 1994). Hollister et al., (1994) used the homogenization method to obtain the architecture of microtrabecular bone, and Bagge (2000) used topology optimization with compliance minimization to determine the initial material distribution for a femur. Jang et al., (2008) compare strain energy density based bone remodeling with structural topology optimization and shown that both method produced equivalent solutions [33].

Topology optimization iteratively redistributes the material in a design domain determining an optimal material arrangment. The control mechanism for the conceptually characterized as self-enhancing system, in which more load attracts more mass. Jang an Kim, (2008) formulated the optimization problem for bone remodeling as below [34].

Minimize

$$f(\boldsymbol{\rho}) = \sum_{j=1}^{3} c_j \left(\frac{1}{2} \mathbf{u}_j^T \mathbf{K} \mathbf{u}_j \right) \tag{3.67a}$$

Subject to

$$g_1(\boldsymbol{\rho}) = M = \sum_{i=1}^{N} \rho_i v_i \le M_0$$

$$g_2(\boldsymbol{\rho}) = P = \sum_{j=0}^{n_2} \sum_{i=1}^{n_1} h_2 \left| \rho_{i,j} - \rho_{i-1,j} \right| + \sum_{j=0}^{n_2} \sum_{i=1}^{n_1} h_1 \left| \rho_{i,j} - \rho_{i,j-1} \right| \ge P_0 \tag{3.67b}$$

where $0.05 \le \rho_i \le 1.0$ and c_j is the normalized weighting factor for three load cases, u_j is the nodal displacement vector of the jth load case, K is the stiffness matrix, v_i is the volume of the ith element, h_1 and h_2 are lengths of a finite element and n_1 and n_2 are the division of domain.

The disadvantage of this model is that; SED based bone remodeling algorithm is formulated in the space, however topology optimization is directly derived in the density space. As a result of that, topology optimization is not proper to simulate the physiological remodeling process obtaining intermediate states, instead, it produces

the equivalent final state more quickly and effeciently. Although this negative sight, in topology optimization choosing a proper Δt is not one of the concerns. Jang and Kim (2008) used a two dimensional micro-FE model of proximal femur to perform topology optimization with daily loading cases and the result showed that the strain energy distribution of the trabecular architecture become more uniform during the optimization.

4. DEVELOPING A NEW MODEL

So far, the theories about bone remodeling have been introduced and the models that are related with theories have been demonstrated along with some applications. In this chapter the model that is developed in our study will be introduced, the parameters about load cases which have an influence on bone adaptation will be discussed and validation of the remodeling algorithm will be controlled by observing some applications in femur and around dental implant. Lastly, the remodeling algorithm will be applied to a lumbar model to show bone resorption and formation around a pedical screw due to loading conditions.

4.1 The Remodeling Algorithm

In our study, a model that based on adaptive elasticity theory is proposed which claims that when a change of load or abnormal strain state occure, bone is stimulated to adapt its mass to regain the equilibrium state. So the main idea is the adaptation of internal structure in macroscopic level based on the distribution of strain energy density (SED) per mass (J/kg) which is arranged by parameters of daily mechanical loads that affect remodeling process until it reachs an equilibrium state where no stimulation is observed.

As it mentioned before the feed back control variable of our model is strain energy density per unit mass, M, is given below in equation **(4.1a)**.

$$M(\mathbf{x},t) = \frac{U(\mathbf{x},t)}{\rho(\mathbf{x},t)} \qquad \textbf{(4.2a)}$$

$$K(\mathbf{x},t) = \frac{U_n(\mathbf{x},t)}{\rho(\mathbf{x},t)} \qquad \textbf{(4.1b)}$$

where ρ is the apparent density, U_n and U are the homeostatic equilibrium state SED and actual SED respectively. The strain energy density (SED) can be shown as

$$U = \int_0^{\varepsilon} \boldsymbol{\sigma} d\boldsymbol{\varepsilon} \tag{4.2}$$

where **σ** is the local stress tensor and **ε** is the strain tensor.

Although the difference between homeostatic state, K, and actual state, M, is the driving force of remodeling, there is a zone, s, where neither formation nor resorption is occured called lazy zone. So the driving force, ψ, in other words mechanical stimulus error can be written as below.

$$\Psi = \begin{pmatrix} M-(1+s)K & for & M > (1+s)K \\ 0 & for & (1+s)K \geq M \geq (1-s)K \\ M-(1-s)K & for & (1-s)K > M \end{pmatrix} \tag{4.3}$$

As a result of that the change of apparent density with respect to time is

$$\frac{d\rho}{dt} = \begin{pmatrix} A_f\left[M-(1+s)K\right]^a & for & M > (1+s)K \\ 0 & for & (1+s)K \geq M \geq (1-s)K \\ A_r\left[M-(1-s)K\right]^\beta & for & (1-s)K > M \end{pmatrix} \tag{4.4}$$

where A_f and A_r are the remodeling constants for formation and resorption respectively and α, β show the relation between the change of density and mechanical stimulus error. In our study the remodeling relation between density and stimulus is taken to be linear and same remodeling constant is used for both formation and resportion.

Although up to this point, it can be said that the positive values of mechanical stimulus lead to increasing in bone mass as a result of raised apparent density while negative values cause decreasing in bone mass, this approach is not completely true and does not represent all the observed states. Beside the case of underloading, also tremendous overloading of bone tissue may lead to absorption either [12,35]**.** So the relation stated above has to be improved by adding a "necrosis parameter" due to overloading. In some studies the relation between apparent density change and

resorption due to overloading is taken to be parabolic [35] while some of the other studies show this relation with sudden reduction [36]. We institute a relation when the value SED per mass due to overloading is exceeded, formation is stopped immediately and resorption takes place with a progressive linear rate. This assumption is shown in equation 4.5,

$$\frac{d\rho}{dt} = \begin{bmatrix} -C - D_2[M - N_2] & for & M \geq N_2 \\ -D_1[M - N_1] & for & N_2 > M \geq N_1 \\ A[M - (1+s)K] & for & N_1 > M > (1+s)K \\ 0 & for & (1+s)K \geq M \geq (1-s)K \\ A[M - (1-s)K] & for & (1-s)K > M \end{bmatrix} \quad \textbf{(4.5)}$$

where D_1 and D_2 are resorption constants due to overloading while N_1 and N_2 are the necrosis limit value of SED per mass beyond which resorption takes place with different rates. And C is a constant that connect different overloading resorption region with each other.

Finally, apparent density value according to the change can be written as below

$$\rho_{t+1} = \rho_t + \left(\frac{d\rho}{dt}\right)_t \Delta t \qquad 0 < \rho \leq \rho_{cb} \quad \textbf{(4.6)}$$

where ρ_{cb} represent the density of cortical bone.

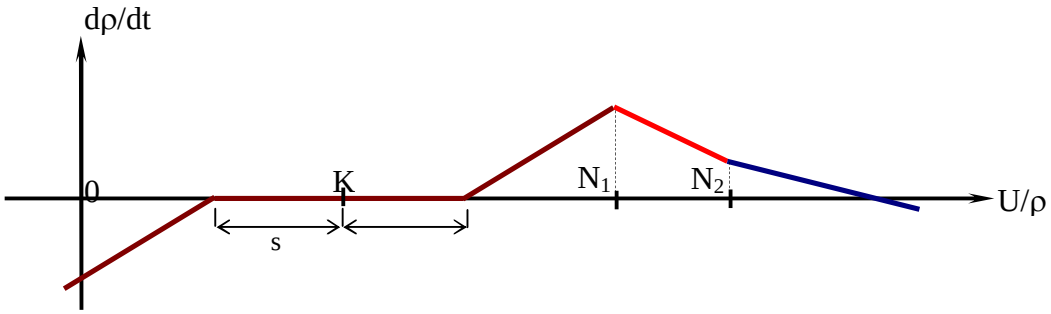

Figure 4.1 : Example figure.

4.2 Characterization of Load Cases

The characterization problem of load histories is one of the most significant issues due to the different time scales of load and apparent response. Load history can be summarized as a small number of similar activities that conform load groups. Only the most important scenarios for remodelling are considered; the rest are disregarded. This approach assumes that the order of load application has no influence on the adaptive response of the bone. This seems reasonable due to the difference between the time scales of causes (scenario frequencies) and effects (remodeling process) as was proved by Jacobs (1994). Although this assumption gives reasonable results, it will be more adequate to generate a general case where all loads that actually act on bone during one period (i.e; day) and their effects according to their importance in period take into account. Thus the starting point is the extraction of whole parameters from a loading history which have an influence on remodeling process. According to Turner (1998) there are three fundamental rules that govern the bone adaptation process [37].

First of all, instead of static loads bone adaptation is mainly driven by dynamic loads. It is first notice by Hert and coworkers (1971) who observe that dynamic, but not static strains increased bone formation in rabbits. Thus dynamic strains appeared to be the primary stimulus of bone adaptation. Lanyon and Rubin (1984) demonstrated that bone adaptation was directly proportional to the peak applied strain in the isolated avian ulna model. And Rubin and Mucleod (1994), show that frequency of the loading waveform was an important factor on bone adaptation. By experiments Turner (1998) confirmed that strain rate also is an important parameter in bone adaptation. In brief, it can be said that dynamic strains drive bone adaptation, the strain stimulus is increased if the magnitude or frequency of the dynamic signal is increased and increasing strain rate enhances the strain stimulus. According to topics that mentioned above strain stimulus can be written as

$$P \propto k_1 \varepsilon f \tag{4.7}$$

where P is the strain stimulus, k_1 is a proportionality constant, ε is peak to peak strain magnitude (or for our case strain energy density per mass (M)) and f is loading frequency in cycles per second. The equation can be generalized using the Fourier

method, that allows to any periodic loading waveform to be expanded into a series of sine waves at different amplitudes and frequencies. So the equation above can be improved to equation below

$$P \propto k_1 \sum_{i=1}^{n} \varepsilon_i f_i \qquad \textbf{(4.8)}$$

where n represents the number of frequency components for each loading conditions.

By this formulation; static case can be recovered: if loading is static, frequency will vanish and consequently strain stimulus, which overlap with experiments. Also it is obvious that a load with high frequency and low magnitude and a load with low frequency and high magnitude approximately have same effect on bone adaptation.

Second rule that has a significant effect on bone adaptation is that increased duration of skeletal loading does not yield proportional increase in bone mass. As loading duration is increased the bone formation response tends to saturate. It is proved by experimental studies of Rubin and Lanyon (1984) and Umemura (1997). The data from these studies can be characterized mathematically using a logarithmic function. Also as it mentioned before a mathematical approach that explains this phenomeon was derived by Carter et. al, (1987) which is expressed as;

$$S \propto \left[\sum_{j=1}^{k} N_j \sigma_j^m \right]^{1/m} \qquad \textbf{(4.9)}$$

where S is the stimulus, k is the number of different daily loading cases, N is the number of loading cycles per day for each loading condition and σ is the effective stress (or strain or for our case strain energy density per mass (M)) for each loading condition and m is a constant. The value of m is a weighting factor for the relative importance of stress or loading cycles on stimulus. For example; if m is taken 1, the effects of stress magnitude and loading cycles would be equal. However, by experimental data it is clearly shown that the value of m must be greater than 1. Carter and coworkers estimated this value as 4, based on the experimental data of Rubin and Lanyon (1984), and from a curve fit to Umerman's (1997) experimental study the value of m become 3.5.

The formulation above has to be improved because it does not include the effects of loading frequency. So by taking account the relation between loading frequency (f), strain magnitude (ε or σ or M=U/ρ) and duration of loading (number of loading cycles per day, N), bone adaptation stimulus can be written as either

$$S \propto \sum_{j=1}^{k} \log(1+N_j)P_j \qquad \textbf{(4.10a)}$$

or

$$S \propto \left[\sum_{j=1}^{k} N_j P_j^m \right]^{1/m} \qquad \textbf{(4.10b)}$$

Last rule about bone adaptation due to loads is the accommodation of bone cells to routine loading. As it mentioned before, adaptation is an error driven activity, so numerous cycles of normal strain change during the predominant activity has no effect on remodeling while just a few cycle of abnormal strain changes stimulate bone adaptation.

4.3 The Finite Element Model

Remodeling algorithm is merged with finite element method to generate a computational model that give the internal structure adaptation according to density with respect to time due to daily load cases. An implicit finite element analysis is performed by software package ABAQUS. The flow chart from the start of an ABAQUS/Standard analysis to the end is shown in Figure 4.2. The remodeling algorithm is implemented by writing FORTRAN codes to Abaqus subroutines; UMAT, SDVINI, USDFLD and URDFIL. In Appendix B, a brief information about Abaqus subroutines is given and the validation of umat code is shown.

Although an implicit finite element analysis is performed, according to equation **(4.6)** the updating scheme of density is in explicit form; where the material properties of next increment are calculated based on the result of current increment. So the updating scheme of density for every integration point can be written by integrating equations **(4.5)** and **(4.6)**

$$\rho_m^{(j+1)} = \begin{bmatrix} \rho_m^{(j)} + (-C - D_2)\Delta t\left[S_m^{(j)} - N_2\right] & for & S_m^{(j)} \geq N_2 \\ \rho_m^{(j)} + (-D_1)\Delta t\left[S_m^{(j)} - N_1\right] & for & N_2 > S_m^{(j)} \geq N_1 \\ \rho_m^{(j)} + A\Delta t\left[S_m^{(j)} - (1+s)K\right] & for & N_1 > S_m^{(j)} > (1+s)K \\ 0 & for & (1+s)K \geq S_m^{(j)} \geq (1-s)K \\ \rho_m^{(j)} + A\Delta t\left[S_m^{(j)} - (1-s)K\right] & for & (1-s)K > S_m^{(j)} \end{bmatrix} \quad \textbf{(4.11)}$$

where m and j represent the number of integration point and increment respectively and Δt is the incremental time and S is the final form of stimulus that was given in equation **(4.10b)**. The remodeling constants are choosen by considering the remodeling rate in a day. After the estimation of density, Young's modulus is calculated at each integration point with the formulea given below by Carter and Hayes (1977).

$$E_m^{(j+1)} = 3.790\left(\rho_m^{(j+1)}\right)^3 \quad \textbf{(4.12)}$$

where the unit of E and ρ are Pa and kg/m^3 respectively.

Although the density updating algorithm is similar with Weinans et al. models **[6]**, the approach developed herein to daily assamble load cases and their consequences become more realistic by take into account frequency, f, daily loading cycles, N and weight factor, m. Also due to the different time scale of load and response, it is more convenient to generate an algorithm that includes two different phase; loading, and remodeling, which is updated sequentially in a loop. Although until now whole studies that simulate remodeling process, implement loading and remodeling in the same scheme, in this study loading and remodeling cases are seperated from each other.

4.3.1 Loading sequence

First of all, all load cases that act on the bone in the scope due to different activities were investigated. Secondly the coefficients that reflect the importance of loads according to their frequency, duration and influence are estimated. An analysis within seconds is performed with the whole possible load cases. The strain energy density per mass which will be used in remodeling process is calculated and peak-holded at each integration point. A simulation of holding the strain energy density according to influence of load cases is shown in Appendix B.

4.3.2 Remodeling sequence

Following the analysis of all the cycles that represent daily load cases is performed and required strain energy density per mass values according to characteristic of load cases is obtained, the second scheme of analysis starts where only material properties are updated. At this stage, no load is applied on bone. This scheme simulates days of bone progress so the incremental time is in order of days. After the estimation of new material properties according to mechanical stimulus that is calculated for each integration point with respect to strain energy density, the loading analyses take place again. This process continues until the model is converged according to a convergence criteria or iteration is manually terminated. The block diagram of loading and remodeling processes is shown in the Figure 4.3.

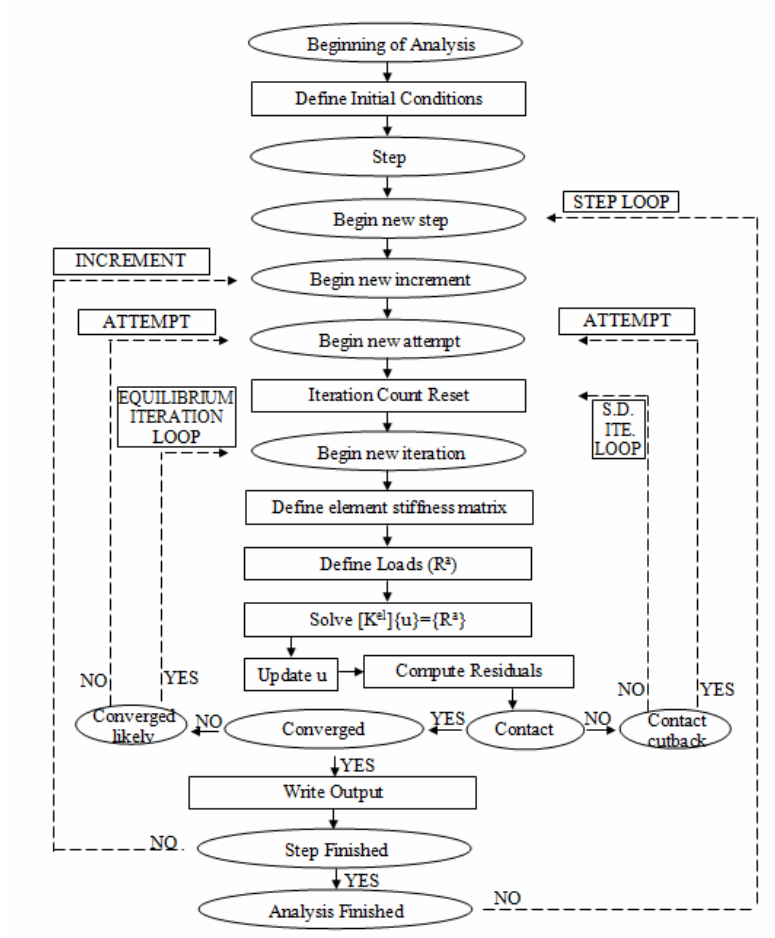

Figure 4.2 : The flow chart of an ABAQUS/Standard analysis.

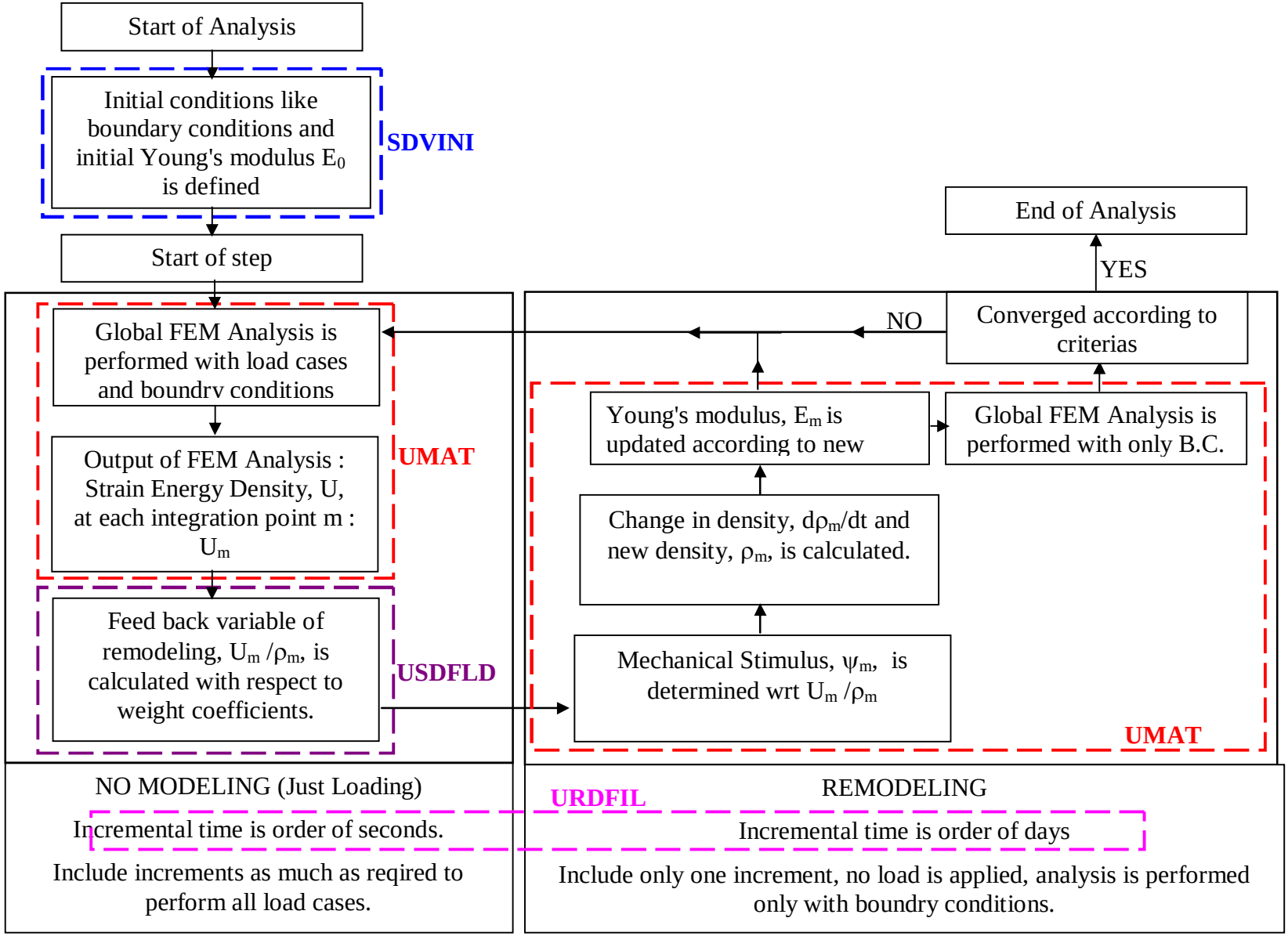

Figure 4.3 : The block diagram of loading and remodeling process.

4.4 Validation of the Model

After proving that ABAQUS subroutines are working properly, which is shown in Appendix B, the accuracy of remodeling algorithm with respect to clinical outcomes is investigated. First of all, an analysis is performed using a femur model which is subjected to the loads of gait cycle. As a second example, the remodeling of bone tissue around a dental implant during mastication is examined.

4.4.1 Bone remodeling in proximal femur model

A proximal femur model is used for this study. The initial material properties of bone constitutents is given in table 4.1. Between spongious and cortical parts tie constraint is given. Femur is fixed from the bottom surfaces. The magnitude and position of loads that are subjected to femur during gait cycle is given in Table 4.2 and Figure 4.4.

Table 4.1 : Initial material properties of cortical and spongious bone.

	Material properties	
	Young's modulus (GPa)	Poisson ratio
Cortical Bone	20	0.3
Spongious Bone	2	0.3

Table 4.2 : Features of loads acting to femur during gait cycle [38].

Load Cases	Cycles per day	Load over the femoral head		Reaction at the abductor	
		(N)	(°)	(N)	(°)
1	6000	2317	24	703	28
2	2000	1158	-15	351	-8
3	2000	1548	56	468	35

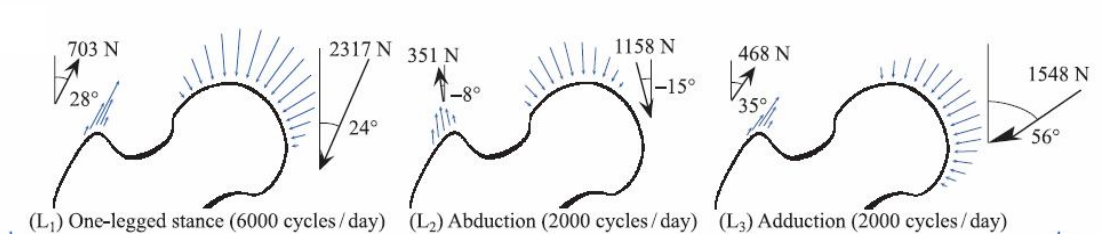

Figure 4.4 : Load cases and applied regions [39].

The load sequence of gait cycle is given Figure 4.5. As it has ben mentioned before the order of load application is assumed to have no influence on the adaptive response of the bone and only the most important scenarios for remodelling are considered; the rest are disregarded. Thus; gait cycle can be divided into four subregions which is shown in Figure 4.6. These subregions are accepted as different scenarios, whose weights over remodeling differ due to different number of daily repetitions. The weight of load cases are given in Table 4.2.

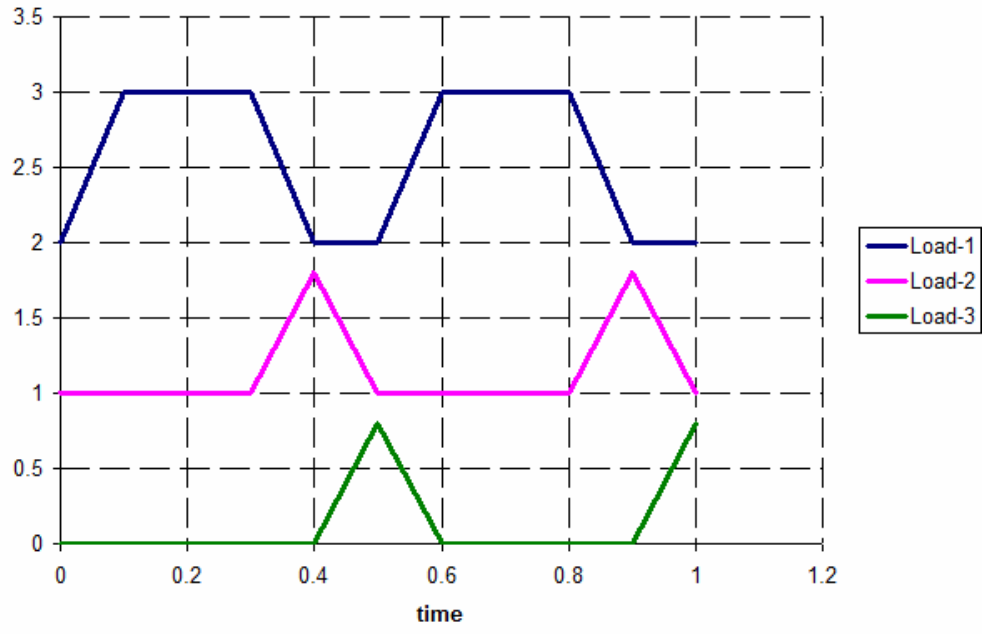

Figure 4.5 : Load sequence during gait cycle

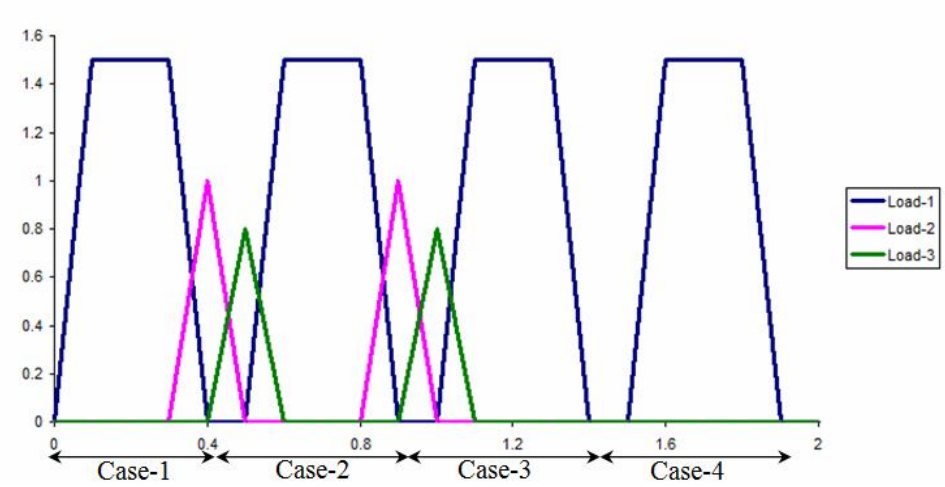

Figure 4.6 : Subregions of gait cycle.

Table 4.3 : Characterization of load cases

Cases	Load duration (sec)	Number of daily cycles	Weight of number of daily cycles
Case 1	0.0-0.4	1000	0.75
Case 2	0.4-0.9	1000	0.75
Case 3	0.9-1.4	1000	0.75
Case 4	1.4-1.9	3000	1.00

Remodeling analysis is only applied to spongious bone. Thus; in loading sequence, the maximum value of strain energy density per mass is peak-holded at each integration point of spongious bone. During remodeling, only formation and resorption due to loading and underloading are taking into account by neglecting the overloading outcomes. The remodeling constants are settled by repeating the analysis with different values of constants until the actual trabeculea alignment and density distribution of proximal femur is approximately observed. The final remodeling constants are given in the Table 4.4 and as a result, changing density distribution of proximal femur from the first to sixth month is shown in Figure 4.7 from a to f. The computational results show similarity with real proximal femur density distribution [40] and with the works availabe in the literature [6-7,29,40-42].

The convergence of model is ensured when the density distribution settled in a band through months. As it seen from Figure 4.7 between (e) and (f) density distribution does not change where whole values of stimulus at integration points are either drop to dead zone or fixed at maximum or minimum values. The maximum value of spongious bone density is equal to cortical bone density. In addition, a minimum value is given to aviod the numerical singularities in the computational model.

Table 4.4 : Remodeling constants of femur model.

K : homeostatic state reference stimulus (J/kg)	2.75
A : bone remodeling constant (kg.day/m^5)	30
m : exponents of daily stimulus	4
s : half wide of dead zone	0.45
Δt : remodeling time (day)	3

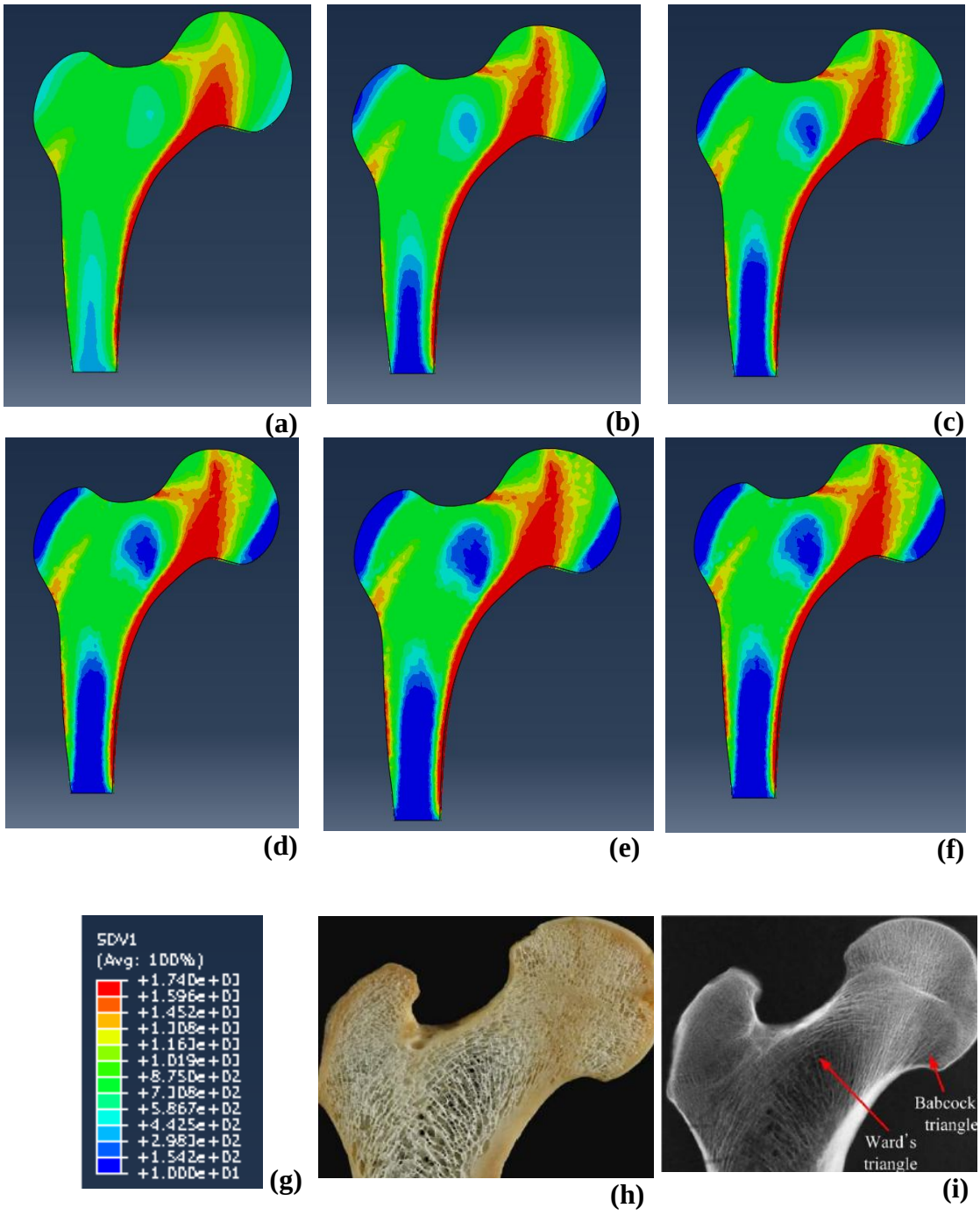

Figure 4.7 : Density distribution of proximal femur (a-f) by computational simulation and (h,i) Photograph and radiograph [40].

4.4.2 Bone remodeling around a dental implant

In the second verification model, bone remodeling around a dental implant is simulated. Between bones tie constraint is given and to simulate the behaviour between the surfaces of implant and bones, surface to surface interaction is given by defining the normal behaviour as hard contact and tangential behaviour with tangent friction, having a 0.1 friction coefficient. No stabilization is assigned for this model and clerance for damping is taken as 0.0001. Model is fixed from sliced surfaces of mandibula and a concentrated force, F=100N, is applied to the top of implant in the x-y plane with 11° incline which is shown in Figure 4.8. The amplitude of load is given Figure 4.9. The initial material properties of bones and the material property of titanium implant is given in Table 4.5.

Table 4.5 : Material properties of dental model.

	Material properties	
	Young's modulus (GPa)	Poisson ratio
Cortical Bone	20	0.3
Spongious Bone	2	0.3
Implant	110	0.3

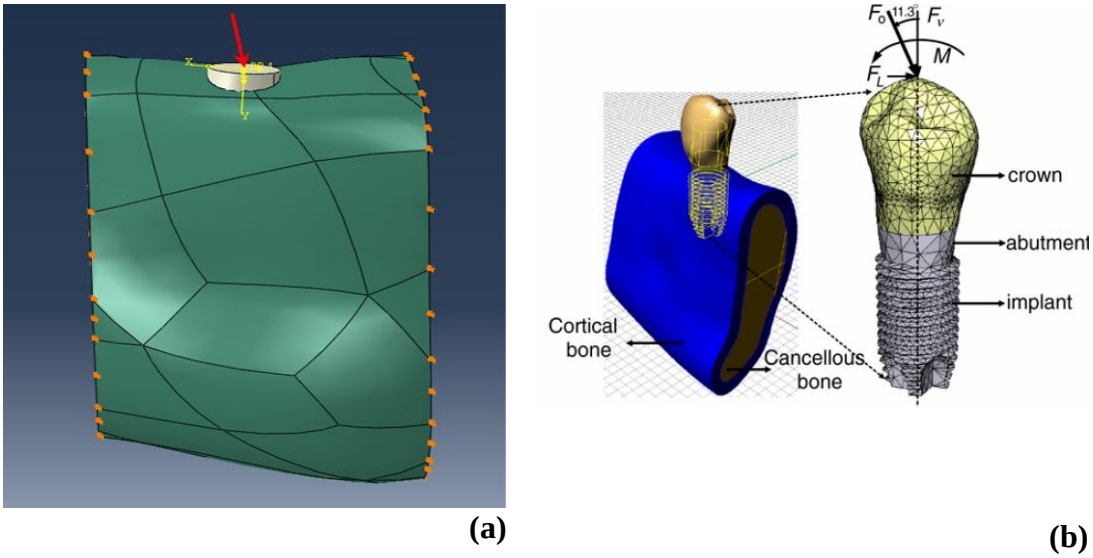

(a) **(b)**

Figure 4.8 : (a)Dental implant model. (b)Position of concentrated load [35].

In loading sequence, the maximum value of strain energy density per mass is reached when force is applied completely. As distinct from femur model, cortical bone remodeling is also included and resorption due to overloading is taking into account.

In the spongious bone, formation and resorption occurred due to loading and underloading respectively, while in cortical bone only the resorption activity due to overloading is taken into account. The remodeling constants are given in Table 4.6. In the table, necrosis limit for cortical bone represents the limit, above which resorption because of overloading is observed. As a result of single load case, there is no need to the exponent of daily stimulus, m. The results of density distribution around a dental implant from the first to fifth month are shown in Figure 4.10. As seen from the results, it can be said that, because of the direction of load, resorption due to overloading is observed in tiny regions. The output of simulation is consistent with the results in litterateur [35,43,44].

Table 4.6 : Remodeling constants of implant induced dental model.

	Spon. B.	Cort. B.
K : homeostatic state reference stimulus (J/kg)	0.1	-
N : necrosis limit (J/kg)	-	0.8
A : bone remodeling constant (kg.day/m^5)	200	-
D : bone remodeling constant due to overloading (kg.day/m^5)	0	0.6
s : half wide of dead zone	0	-
Δt : remodeling time (day)	2	2

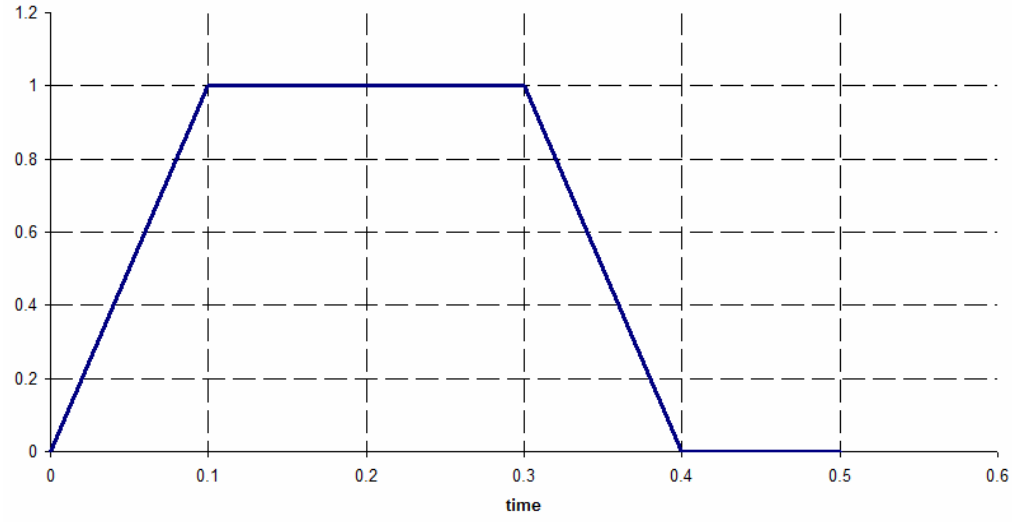

Figure 4.9 : Amplitude of concentrated force.

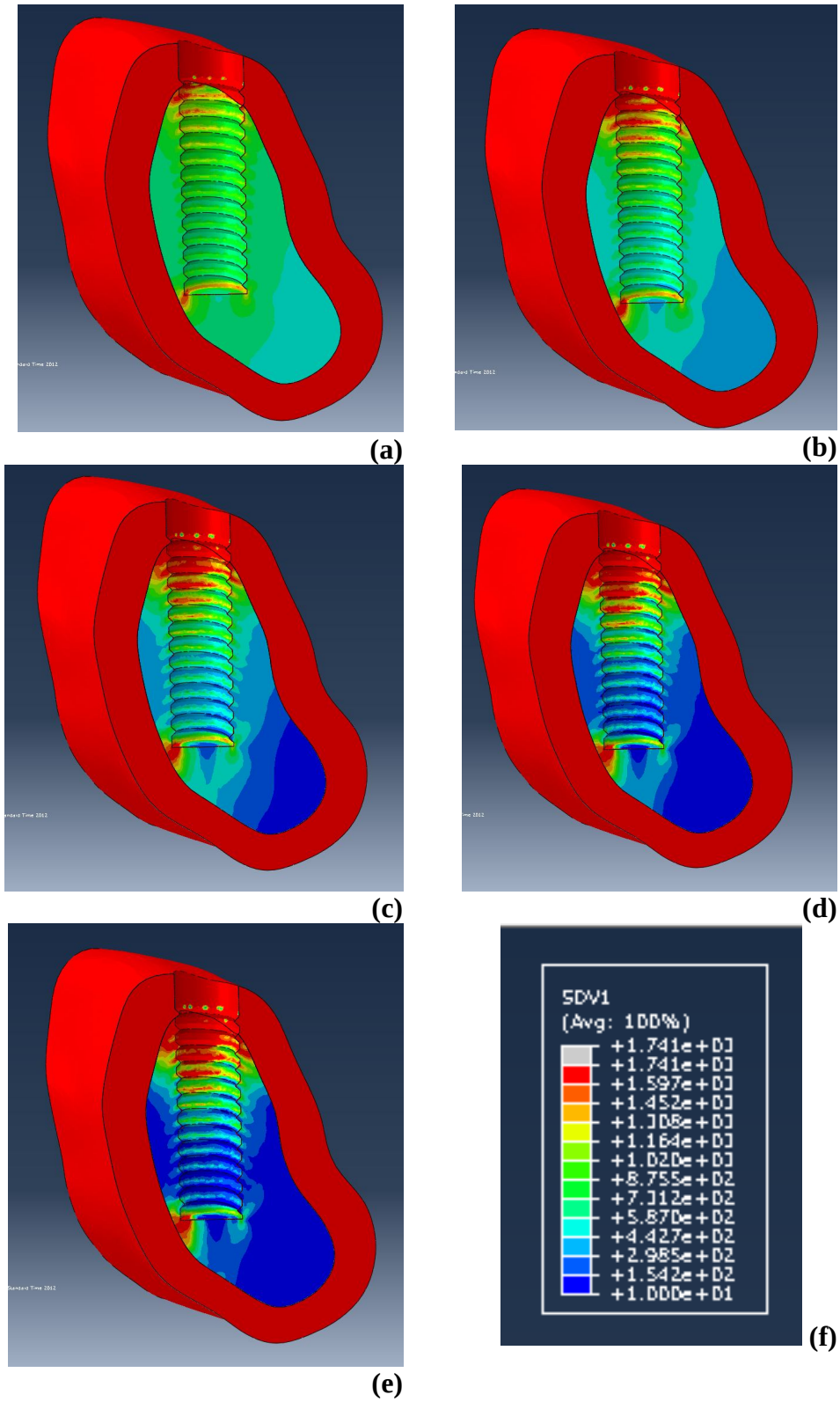

Figure 4.10 : (a-e) Density distribution around dental implant from the first to fifth month respectively.

4.5 Bone Remodeling Around Lumbar Pedicle Screw

In the third model, implant induced lumbar vertebrae (L3) is simulated. For whole surfaces in the contact, except the interface between implant and bones, tie constraint is given. For interface between implant and bones node to surface interaction is given by defining the normal behaviour as hard contact and tangential behaviour with 0.1 friction coefficient. No stabilization is assigned for this model and clerance for damping is taken as 0.0001. Model is fixed from the bottom surfaces of annulus fibrosis and nucleus fibrosis (disc) to avoid local singularities as it can be seen in Figure 4.11 (a). The initial material properties of bones and the material properties of implant, annulus and nucleus fibrosis is given in Table 4.7.

Table 4.7 : Material properties of lumbar model.

	Material properties	
	Young's modulus (GPa)	Poisson ratio
Cortical Bone	10	0.3
Spongious Bone	0.1	0.2
Annulus and nucleus fib.	0.8	0.48
Implant	114	0.3

To simulate compressive load [45,46] a displacement boundary condition is given during the whole process. A concantrated force, F=450N, is applied to the head of the implant which is shown in Figure 4.11 (b). Force is applied in this order: First of all, implant is enforced in -y direction by a load and then system is discharged by removing the load, an identical load is applied to the exact point in the opposite direction. The loading sequence is given in the Figure 4.12.

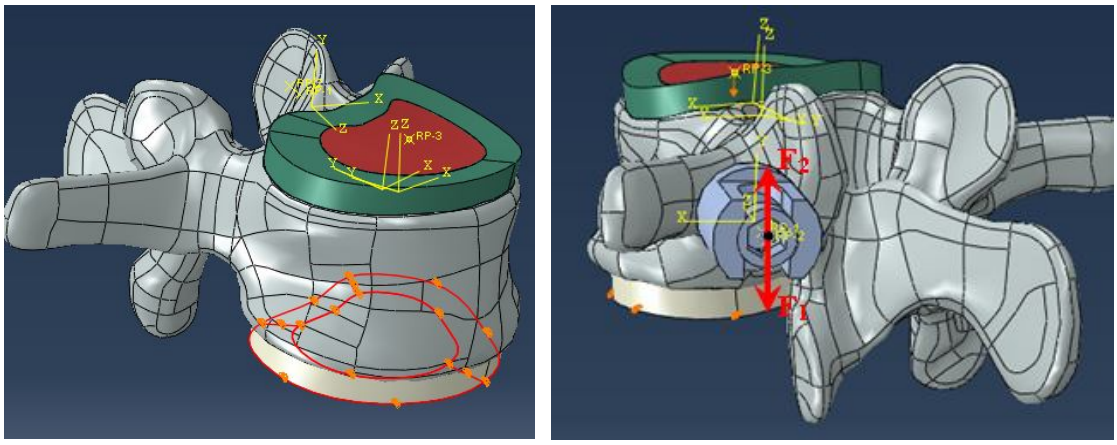

(a) **(b)**

Figure 4.11 : Implant induced lumbar vertebrae (L3) model.

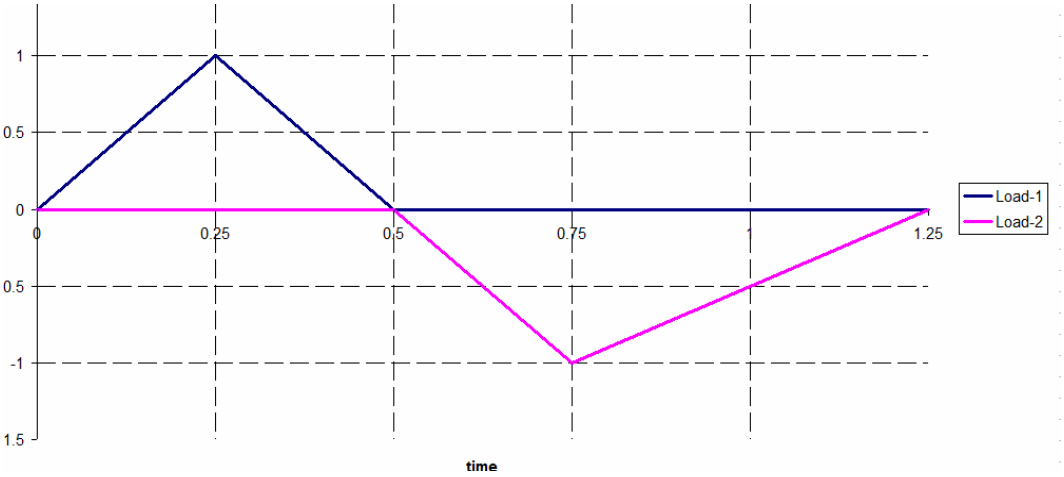

Figure 4.12 : Load sequence during loading

During these loading and unloading processes maximum strain energy density values are peak-holded at each integration point. By this method, whole values required for remodeling process is obtained. Two different remodeling process with different constants are performed on both cortical and spongeous bone. In cortical bone, during remodeling process, resorption due to overloading is taking into account only. As different from dental model, instead of one overloading limit, four different limits with different resorption remodeling constants are assigned to the bone. The reason of using a method like this in necrosis, is the huge amount of stimulus difference between the limits of overloading band. In spongious bone, beside forming and absorbing due to loading and underloading, resorption due to overloading is also taken into account. Like cortical bone, for overloading situation, different remodeling constants are given to different regions according to the stimulus value. In the Table 4.8 the remodeling parameters for two different remodeling case is given. Also it has to be mentioned that in the second case resorption due to underloading is not taking into account for spongious bone. In the Figure 4.13 and 4. 14 density distribution due to case 1 and 2 is shown respectively. A more detail figure of resorbed and formed areas of spongious and cortical bone is given in Figure 4.15. Also CT scan of a patient is given in Figure 4.15.

Table 4.8 : Remodeling constants of implant induced lumbar model.

CASE -1	**Spongious B.**	**Cortical B.**
K : homeostatic state reference stimulus (J/kg)	0.09741	2.89
N_1 : first necrosis limit (J/kg)	2.015	4.34
N_2 : second necrosis limit	6.72	14.47
N_3 : third necrosis limit	-	28.94
N_4 : fourth necrosis limit	-	50.65
A : bone remodeling constant (kg.day/m^5)	10	-
D_1 : 1st bone remodeling constant due to overloading (kg.day/m^5)	0.213	0.214
D_2 : 2nd bone remodeling constant due to overloading	0.02	0.14
D_3 : 3rd bone remodeling constant due to overloading	-	0.08
D_4 : 4st bone remodeling constant due to overloading	-	0.005
C_1: 1st connection constant between different overloading regions (kg.day/m^5)	1.00	2.17
C_2: 2nd connection constant between different overloading regions	-	4.1958
C_3 : 3rd connection constant between different overloading regions	-	5.93
s : half wide of dead zone	0.724	-
t : remodeling time (day)	10	10
CASE -2	**Spongious B.**	**Cortical B.**
K : homeostatic state reference stimulus (J/kg)	0.1	2.89
N_1 : first necrosis limit (J/kg)	1.34	2.89
N_2 : second necrosis limit	2.015	14.47
N_3 : third necrosis limit	6.72	28.94
N_4 : fourth necrosis limit	-	50.65
A : bone remodeling constant (kg.day/m^5)	20	-
D_1 : 1st bone remodeling constant due to overloading (kg.day/m^5)	1	0.4
D_2 : 2nd bone remodeling constant due to overloading	0.85	0.14
D_3 : 3rd bone remodeling constant due to overloading	0.01	0.08
D_4 : 4st bone remodeling constant due to overloading	-	0.005
C_1: 1st connection constant between different overloading regions (kg.day/m^5)	0.675	4.632
C_2: 2nd connection constant between different overloading regions	4.674	6.6578
C_3 : 3rd connection constant between different overloading regions	-	8.3946
s : half wide of dead zone	0.2	-
t : remodeling time (day)	10	10

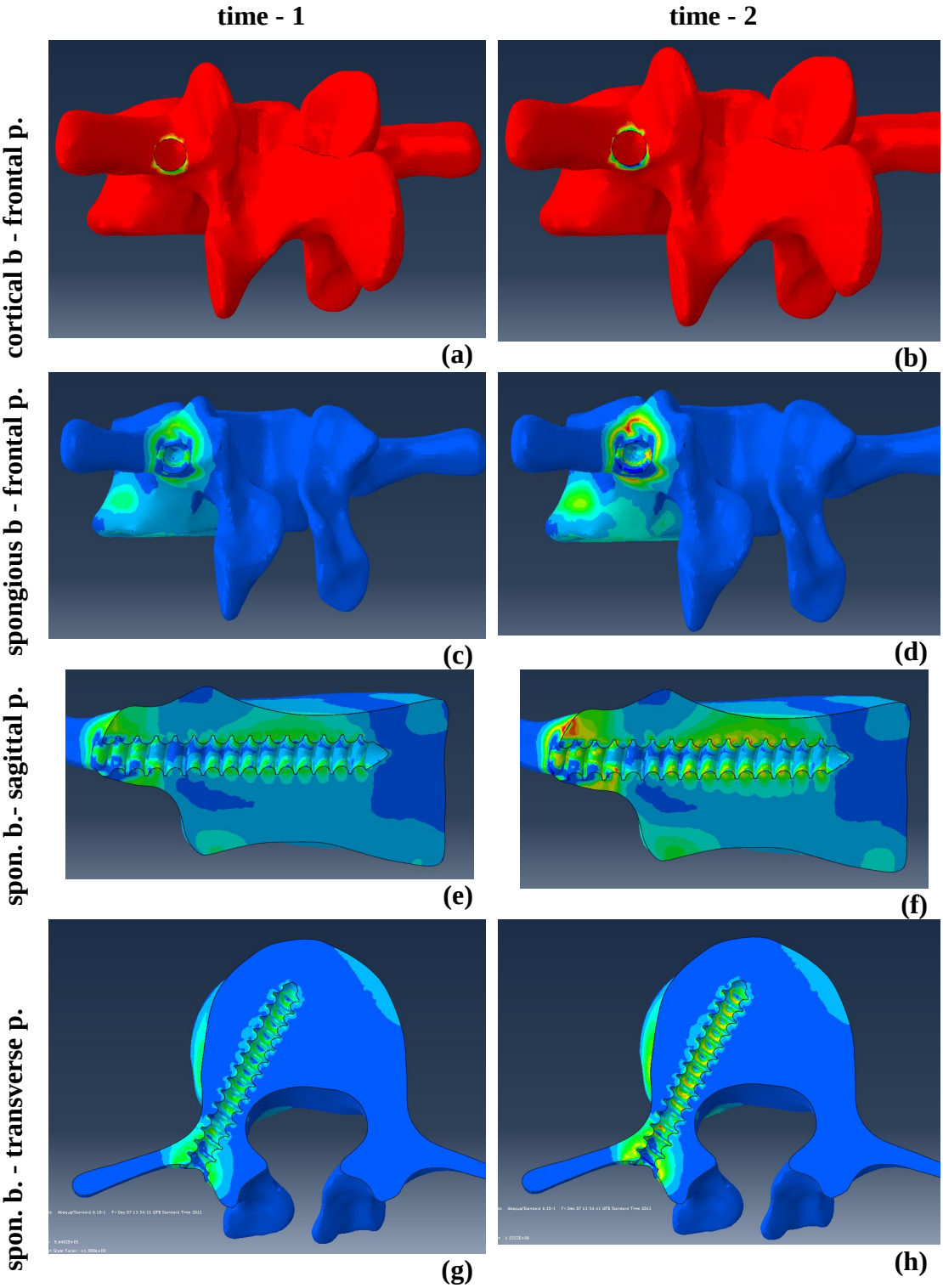

Figure 4.13 : Density distribution of lumbar vertebra for case – 1 at (a,c,e,f) 3th month and (b,d,f,h) 6th month.

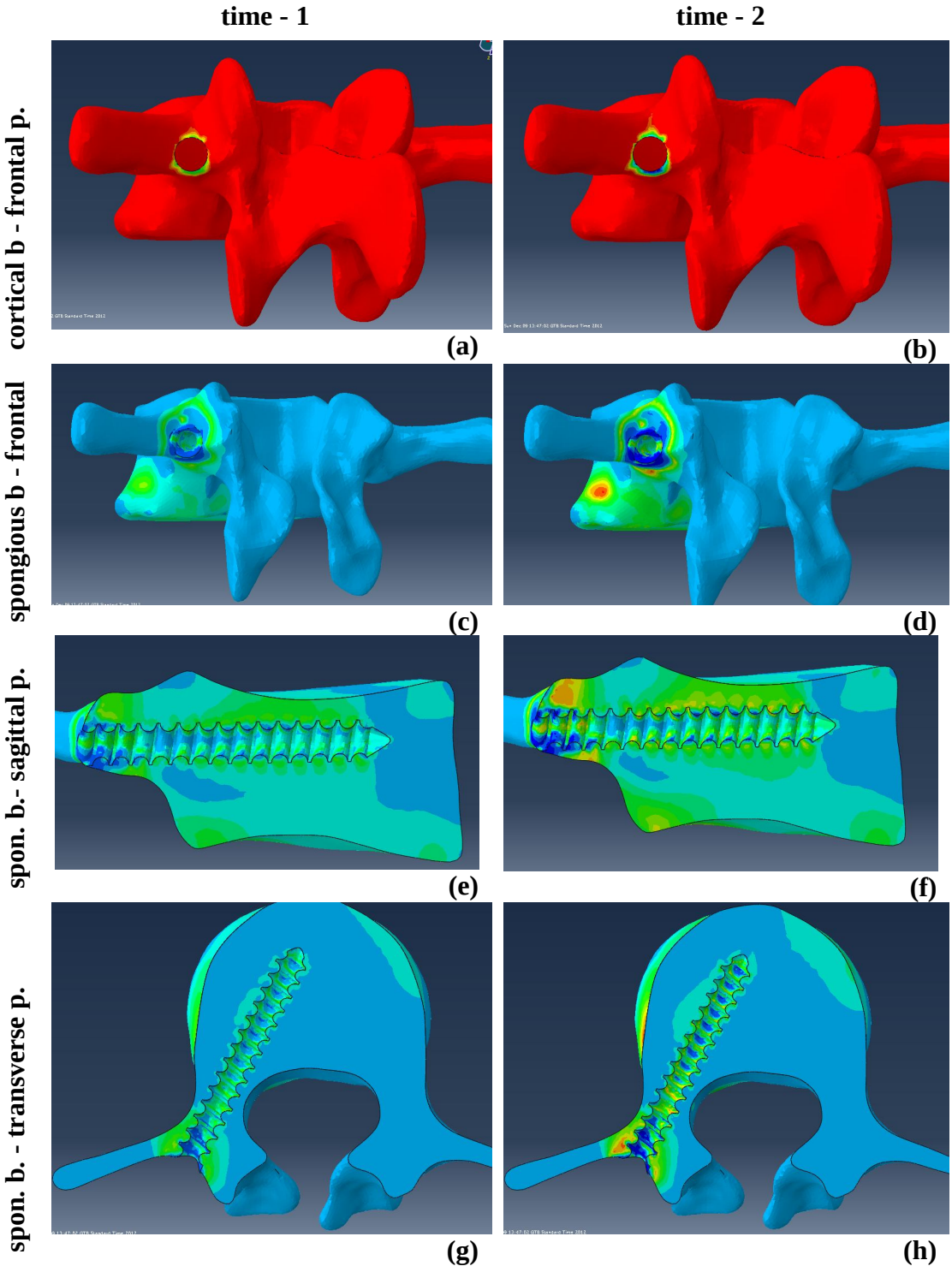

Figure 4.14 : Density distribution of lumbar vertebra for case – 2 at (a,c,e,f) 3th month and (b,d,f,h) 6th month.

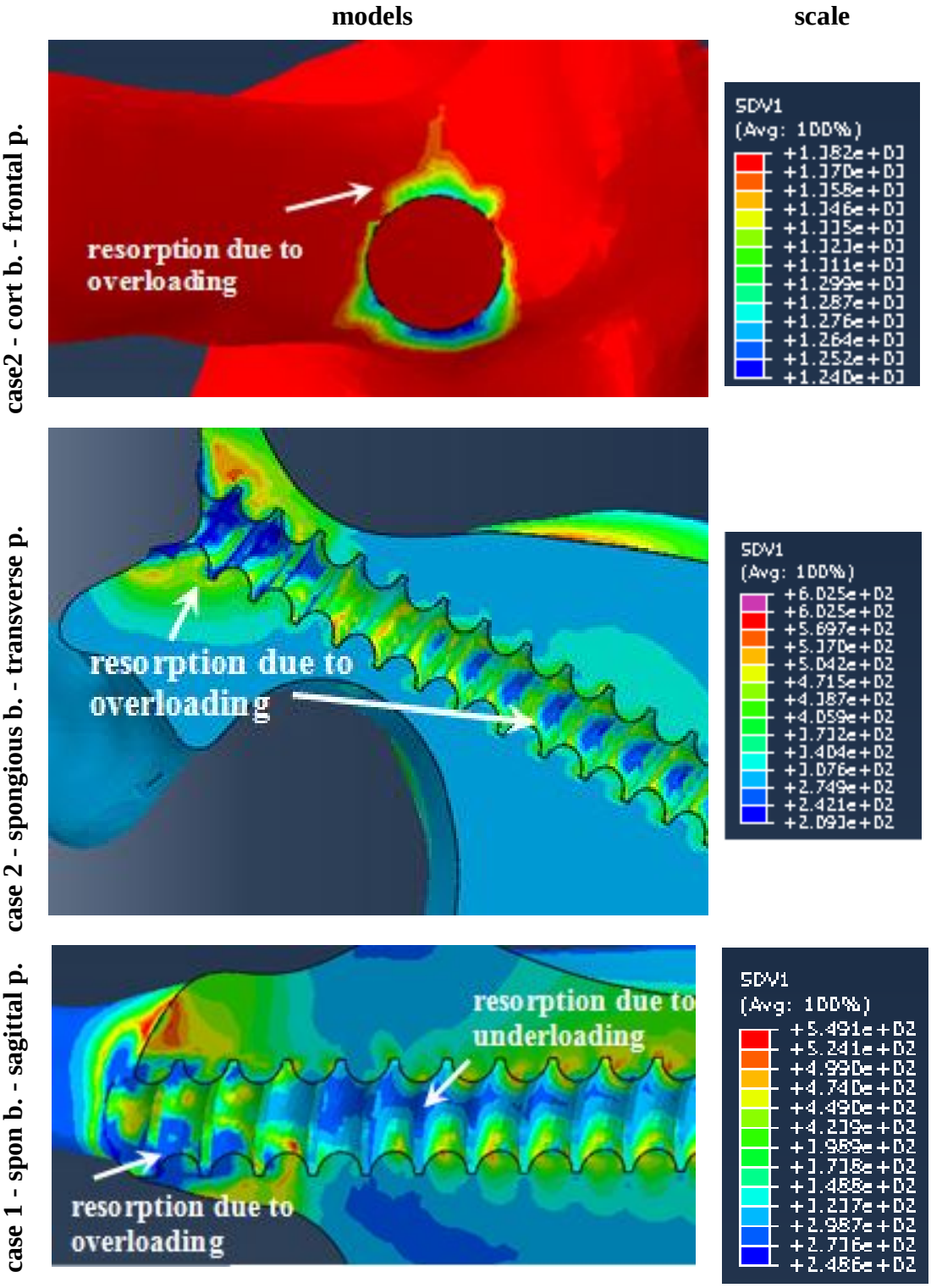

Figure 4.15 : A more detailed look to resorbed and formed areas of bones.

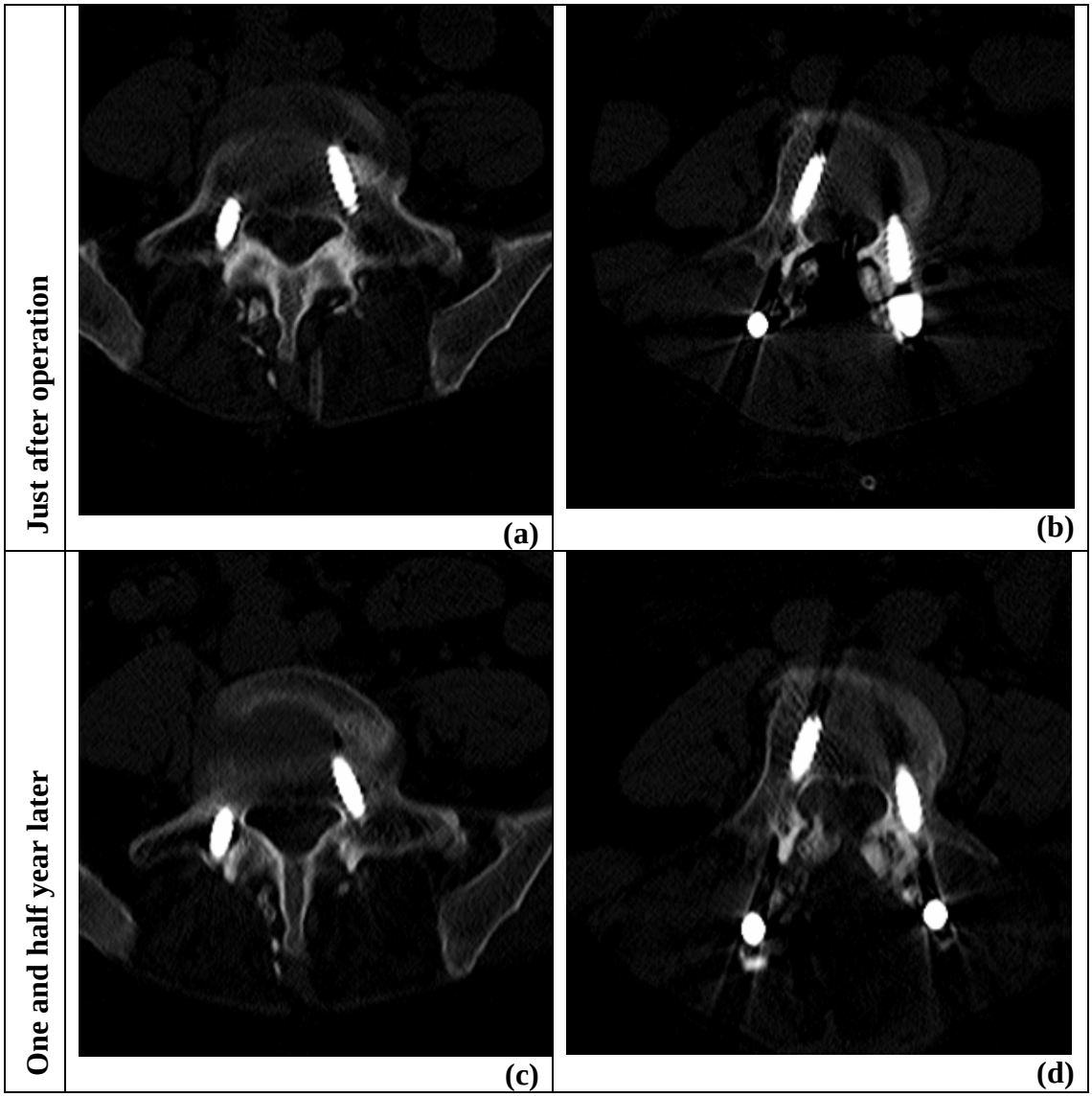

Figure 4.16 : Radiograph of density distribution of pedicle screw lumbar vetrebrae. (a,b) Just after operation. (c,d) One and half year later.

5. CONCLUSION AND RECOMMENDATIONS

In the study, a new approach to the bone adaptation process is introduced which decouples the loading cycles (short term events which occur in cycles in order of seconds) and the remodeling process (long term events which occur in order of days). Until now whole studies that simulate remodeling process, implement loading and remodeling concepts in the same scheme. In this study loading and remodeling cases were performed apart from each other. First of all, all load cases that act on the bone in the scope due to different activities were investigated. Secondly, the coefficients that reflect the importance of loads according to their frequency, duration and influence were estimated based on literature data and an analysis within seconds is performed representing all the possible load cases. After whole cycles that represent daily load cases was analyzed and required mechanical stimulus distribution in the bone according to weight of load cases were calculated, the second step of analysis, remodeling, takes place where material properties were updated according to mechanical stimulus.

The model and algorithms have been validated against density distribution of proximal femur during gait cycle and density distribution of mandibula during mastication. Good agreement has been observed with the results available in the literature. Also the accuracy of model is proven accroding to the results of analysis that performed with different mesh refinements.

After validation, new method is applied to investigate bone remodeling around lumbar pedicle screw and results are found to be consistent with clinical observations.

In future studies, it will become possible to optimize required daily physical activities to take advantage from applied implants for longer times by decoupling loads into different weighted individual cases. Also the existing model may be improved by adding the fabric tensor, **H**, to simulate the anisotropic behaviour of bone. Additionaly; by writing a new multifield element model the diminishing rate of

remodeling signal due to the distance between sensing and forming-resorbing cells can be taking into account.

REFERENCES

[1] **Marieb, E. N., and Hoehn, K.** (2006). *Human Anatomy & Physiology*. (Seventh Edition). United States of America: Pearson Education Inc.

[2] **Seeley, S. T.** (2004). *Anatomy and Physiology*. (Sixth Edition). Unites States of America: The McGraw-Hill Companies.

[3] **Miller, S. C., and Jee, W. S. S.** (1992). Bone lining cells. In *Bone* (B. K. Hall, ed.) (Vol. 4, pp.1-19.). CRC Press, Boca Raton, FL.

[4] **Doblare, M., Garcia, J. M., and Gomez, M. J.** (2004). Modeling Bone Tissue Fracture and Healing: A Review. *Engineering Fracture Mechanics.* Vol. ***71***, no. 13-14, pp. 1809-1840.

[5] **Rüberg, T.** (2004). Computer simulation of adaptive bone remodeling, *MS Thesis*, Technische Universitat Braunschweig, Centro Policteсnico Superior Zaragoza

[6] **Weinans, H., Huiskes,R., and Grootenboer H. J.** (1992). The Behavior of Adaptive Bone-Remodeling Simulation Models. *Journal of Biomechanics.* Vol. ***25***, no. 12, pp. 1424-1441.

[7] **Huiskes, R., Weinans, H., Grootenboer H. J., Dalstra, M., Fudala, B., and Slooff, T. J.** (1987). Adaptive Bone-Remodeling Theory Applied to Prothetic-Design Analysis. *Journal of Biomechanics.* Vol. ***20***, no. 11-12, pp. 1135-1150.

[8] **Fratzl, P., Weinkamer, R.** (2007). Nature's Hierarchical Materials. *Progress in Materials Science.* Vol. ***52***, no. 8, pp. 1263-1334.

[9] **Fridez, P.** (1996). Modelisation De L'adaption Osseuse Externa, *PhD Thesis*, EPFL, Lausanne.

[10] **Martin, R. B., Burr D. B., and Sharkey N. A.** (1998). *Skeletal tissue mechanics.* New York: Springer-Verlang.

[11] **Cowin, S. C.** (2010). Bone Cell and Tissue Mechanics. *International Centre for Mechanical Sciences*, Palazzo Del Torso, Italy, 19–23 July.

[12] **Garcia, A., Rueberg, T., Doblare, M.** (2010). Bone Cell and Tissue Mechanics: Mechanistics Models of Bone Remodelling. *International Centre for Mechanical Sciences*, Palazzo Del Torso, Italy, 19–23 July.

[13] **Doblare, M., and Garcia, J. M.** (2001). Application of an Anisotropic Bone Remodeling Model Based on a Damage-Repair Theory to the Analysis of the Proximal Femur Before and After Total Hip Replacement. *Journal of Biomechanics.* Vol. ***34***, pp. 1157-1170.

[14] **Doblare, M., and Garcia, J. M.** (2002). Anisotropic Bone Remodeling Model Based on a Continuum Damage-Repair Theory. *Journal of Biomechanics.* Vol. ***35***, no. 1, pp. 1-17.

[15] **Tsubota, K., and Adachi, T., and Tomita, Y.** (2002). Functional Adaptation of Cancellous Bone in Human Proximal Femur Predicted by Trabecular Surface Remodelling Simulation Toward Uniform Stress State. *Journal of Biomechanics.* Vol. ***35***, no. 12, pp. 1541-1551.

[16] **Garcia, A., Rueberg, T., Doblare, M.** (2010). Bone Cell and Tissue Mechanics: Phenomenological Models. *International Centre for Mechanical Sciences,* Palazzo Del Torso, Italy, 19–23 July.

[17] **Carter, D. R., Fyhrie D. P., and Whalen, R. T.** (1987). Trabecular Bone Density and Loading History: Regulation of Connective Tissue Biology by Mechanical Energy. *Journal of Biomechanics.* Vol. ***20***, no. 8, pp. 785-794.

[18] **Cowin, S. C., and Hegedus, D. H.** (1976). Bone Remodeling: A Theory of Adaptive Elasticty. *Journal of Biomechanics.* Vol. ***6***, pp. 313-326.

[19] **Gwun, J., and Yong, K.,** (2008). Computational Study of Wolff's Law with Trabecular Architecture in the Human Proximal Femur Using Topology Optimization. *Journal of Biomechanics.* Vol. ***41***, no. 11, pp. 2353-2361.

[20] **Huiskes, R., Ruimerman, G. H., and Janssen J. D.** (2000). Effects of Mechanical Forces on Maintenance and Adaptation of Form in Trabecular Bone. *Nature.* Vol. ***405***, pp. 704-706.

[21] **Ruimerman, R., Hilbers, P., Rietbergen, B., Huiskes, R.** (2005). A Theoretical Framework for Strain-Related Trabecular Bone Maintenance and Adaptation. *Journal of Biomechanics.* Vol. ***38***, pp. 931-941.

[22] **Ruimerman, R.** (2005). Modeling and remodeling in bone tissue. *MS Thesis*, Technische Universiteit Eindhoven.

[23] **Jacobs, C. R.** (1994). Numerical Simulation of Bone Adaptation to Mechanical Loading. Dissertation for the Degree of Doctor of Philosophy, Stanford University.

[24] **Whalen, R. T., Carter, D. R.** (1998). Influence of Physical Activity on the Regulation of Bone Density. *Journal of Biomechanics.* Vol. ***21***, no 10, pp. 825-837.

[25] **Cowin, S. C., and Hegedus, D. H.** (1976). Bone Remodeling I: Theory of Adaptive Elasticity. *Journal of Elasticity.* Vol. ***6***, pp. 313-326.

[26] **Hegedus, D. H., and Cowin, S. C.** (1976). Bone remodeling II: Small Strain Adaptive Elasticity. *Journal of Elasticity.* Vol. ***6***, pp. 337-352.

[27] **Cowin, S. C., and Firoozbakhsh, K.** (1981). Bone Remodeling of Diaphyseal Surfaces Under Constant Load: Theoretical Predictions. *Journal of Biomechanics.* Vol. ***14***, pp. 471-484.

[28] **Cowin, S.C., Sadegh, A.M., and Luo, G.M.** (1992). An Evolutionary Wolff's Law for Trabecular Architecture. *Journal of Biomechanical Engineering*. Vol. 114, pp. 129-136.

[29] **Beaupre, G. S., Orr, T. E., and Carter, D. R.** (1990). An Approach for Time-Dependent Bone Modeling and Remodeling Applications: A Preliminary Remodeling Simulation. *Journal of Orthopaedic Research.* Vol. ***8***, no. 5, pp. 662-670.

[30] **Carter, D. R., Orr, T. E., and Fyhrie D. P.** (1989). Relationships Between Loading History and Femoral Cancellous Bone Architecture. *Journal of Biomechanics.* Vol. ***22***, pp. 231-244.

[31] **Fyhrie D. P., and Carter, D. R.** (1986). A Unifying Principle Relating Stress to Trabecular Bone Morphology. *Journal of Orthopaedic Research.* Vol. ***4***, pp. 304-317.

[32] **Alexander M. S.** (2009). A Computational Model of Apoptotic Osteocycte Correlation to Cortical Bone Remodelling Parameters. *MS Thesis*, California Polytechnic State University.

[33] **Jang, I. G., Kim, I. Y., and Byung, M. K.** (2009). Analogy of Strain Energy Density Based Bone Remodeling Algorithm and Structural Topology Optimization. *ASME Journal of Biomedical Engineering.* Vol. ***131***, Issue 1, Article 011012.

[34] **Jang, I. G., and Kim, I. Y.,** (2009). Computational Simulation of Trabecular Adaptation Progress In Human Proximal Femur During Growth. *Journal of Biomechanics.* Vol. ***42***, Issue 5, pp. 573-580.

[35] **Lin, D., Li, Q., Li, W., and Swain, M.,** (2009). Dental Implant Induced Bone Remodelling And Associated Algorithms. *Journal of the Mechanical Behavior of Biomedical Materials.* Vol. **2**, pp. 410-432.

[36] **Behrens, B. A., Nolte, I., Wefstaedt, P., Stukenborg-Colsmon, C., and Bouguecha, A.** (2009). Numerical Investigations on the Strain-Adaptive Bone Remodeling in the Periprosthetic Femur: Influence of the Boundary Conditions. *Biomedical Engineering, **8**,* doi:10.1186/1475-925X-8-7.

[37] **Turner, C. H.** (1998). Three Rules for Bone Adaptation to Mechanical Stimuli. *Bone.* Vol. ***23***, no. 5, pp. 399-407.

[38] **Hambli, R., Lespessailees, E., and Benhamou, C. L.** (in pres). Integrated Remodeling to Fracture Finite Element Model Of Human Proximal Femur Behaviour. *Journal of the Mechanical Behavior of Biomedical Materials.*

[39] **Tsubota, K., Suzuki, Y., Yamada, T., Hojo, M., Makinouchi, A., and Adachi, T.** (2009). Computer Simulation of Trabecular Remodeling in Human Proximal Femur Using Large-Scale Voxel FE Models: Approach to Understanding Wolff's Law. *Journal of Biomechanics.* Vol. ***42***, pp. 1088-1094.

[40] **Jang, I. G., and Kim, I. Y.** (2010). Application of Design Space Optimization to Bone Remodeling Simulation of Trabecular Architecture in Human Proximal Femur For Higher Computational Efficiency. *Finite Elements in Analysis and Design.* Vol. ***46***, pp. 311-319.

[41] **Miller, Z., Fuchs, B. M., Arcan, M.** (2002). Trabecular Bone Adaptation with an Orthotropic Material Model. *Journal of Biomechanics.* Vol. ***35***, Issue 2, pp. 247-256.

[42] **Garcia, J. M., Doblare, M., and Cegonino, J.** (2002). Bone Remodeling Simulation: A Tool for Implant Design. *Computational Materials Science*. Vol. ***25***, Issue 1-2, pp. 100-114.

[43] **Chou, H. Y., Jagodnik, J. J., and Müftü, S.** (2008). Predictions of Bone Remodeling Around Dental Implant Systems. *Journal of Biomechanics.* Vol. ***41***, no. 6, pp. 1365-1373.

[44] **Lin, D., Li, Q., Li, W., Duckmanton, N., and Swain, M.** (2010). Mandibular Bone Remodeling Induced by Dental Implant. *Journal of Biomechanics.* Vol. ***43***, no. 2, pp. 287-293.

[45] **Jang, I. G., and Kim, I. Y.** (2010). Computational Study on the Effect of Loading Alteration Caused by Disc Degeneration on the Trabecular Architecture in Human Lumbar Spine. *Journal of Biomechanics.* Vol. ***43***, Issue 3, pp. 492-499.

[46] **Schmidt, H., Shirazi, A., Galbusera, F., and Wilke, H. J.** (2010). Response Analysis of Lumbar Spine During Regular Daily Activities - A Finite Element Analysis. *Journal of Biomechanics.* Vol. ***43***, no. 10, pp. 1849-1856.

[47] **Sadd, M. H.** (2005). *Elasticity Book: Theory, Applications, and Numerics.* United States of America: The McGraw-Hill Companies.

[48] **Url-1** < http://www.colorado.edu/engineering/cas/courses.d/IFEM.d/>, date retrieved 01.11.2012

[49] **Stress (Mechanics.)**. (n.d.). In *Wikipedia*. Date retrieved: 01.11.2012, adress: *http://en.wikipedia.org/wiki/Stress_(mechanics)*

APPENDICES

APPENDIX A: Continuum Mechanics

APPENDIX B: ABAQUS Subroutines

APPENDIX A

Since this study is based on macroscopic level formulations; where microstructure is homogenized by phenomelogical averaging, model is suitable for continuum mechanics approaches.

As we mentioned before, for sake of simplicity, few assumptions is made by taking bone as a heterogenous, isotropic, linear, elastic material where plasticity effects can be neglected due to small strain and displacement values.

The basic relations of continuum mechanics for three-dimensional linear elastic solid are summarized below which include strain-displacement, constitutive and equilibrium equations [47,48].

APPENDIX A.1 The Strain-Displacement Equations

By ignoring the nonlinear part due to small strain and displacement values, strain can be written as

$$\varepsilon_{ij} = \frac{1}{2}\left(\frac{\partial u_i}{\partial x_j} + \frac{\partial u_j}{\partial x_i}\right) \qquad \textbf{(A 1.1)}$$

where $u_i(x_j)$ denote the components of the displacement vector field $\mathbf{u}(x_j)$ and ε_{ij} are the components of the strain tensor $\boldsymbol{\varepsilon}$. The whole components of strain tensor can be written as below.

$$\varepsilon_{11} = \frac{\partial u_1}{\partial x_1} \qquad \textbf{(A 1.2a)}$$

$$\varepsilon_{22} = \frac{\partial u_2}{\partial x_2} \qquad \textbf{(A 1.2b)}$$

$$\varepsilon_{33} = \frac{\partial u_3}{\partial x_3} \qquad \textbf{(A 1.2c)}$$

$$\varepsilon_{12} = \frac{1}{2}\left(\frac{\partial u_1}{\partial x_2} + \frac{\partial u_2}{\partial x_1}\right) \qquad \textbf{(A 1.2d)}$$

$$\varepsilon_{23} = \frac{1}{2}\left(\frac{\partial u_2}{\partial x_3} + \frac{\partial u_3}{\partial x_2}\right) \qquad \textbf{(A 1.2e)}$$

$$\varepsilon_{23} = \frac{1}{2}\left(\frac{\partial u_2}{\partial x_3} + \frac{\partial u_3}{\partial x_2}\right) \qquad \textbf{(A 1.2f)}$$

The linear strain tensor in matrix format is shown below.

$$\underline{\boldsymbol{\varepsilon}} = \left[\varepsilon_{ij}\right] = \begin{bmatrix} \varepsilon_{11} & \varepsilon_{12} & \varepsilon_{13} \\ & \varepsilon_{22} & \varepsilon_{23} \\ sym & & \varepsilon_{33} \end{bmatrix} \qquad \textbf{(A 1.3)}$$

The strain components in another coordinate system x'_j which is related to x_i can be written by transformation

$$\varepsilon'_{ij} = a_{im} a_{jn} \varepsilon_{mn} \qquad \textbf{(A 1.4)}$$

where a represents the transformation tensor and the relation between coordinate systems are shown below.

$$x_i = a_{ij} x'_j \qquad \textbf{(A 1.5)}$$

APPENDIX A.2 Compatibility Equations

The strain tensor **ε** has six independent components while the displacement field has three independent components. It shows that there must be three independent conditions between ε_{ij}. These expressions arise from the condition of compatibility of deformation. In the three-dimensional case and under small strain assumption these compatibility equations can be written as below.

$$\varepsilon_{ij,kl} + \varepsilon_{kl,ij} = \varepsilon_{ik,jl} + \varepsilon_{jl,ik} \qquad \textbf{(A 2.1)}$$

For instance, for two dimensional case only one equation survives which can be written as both tensor and standard notation as below respectively.

$$\frac{\partial^2 \varepsilon_{11}}{\partial x_2{}^2} + \frac{\partial^2 \varepsilon_{22}}{\partial x_1{}^2} = 2\frac{\partial^2 \varepsilon_{12}}{\partial x_1 \partial x_2} \qquad \textbf{(A 2.2)}$$

APPENDIX A.3 Traction Vector and Stress Tensor

Consider a continuum body and an interior point P(x_i). Make a cut through P with a plane who has an exterior normal **n**, which is illustrated in Figure A.1.

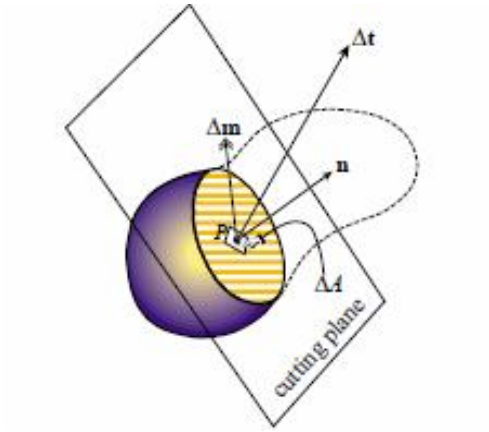

Figure A.1 : Plane cut through a body for defining interior force at point P [48].

The stress (traction) vector at P for direction n is defined as

$$\mathbf{T}^n = \lim_{\Delta A \to 0} \frac{\Delta \mathbf{t}}{\Delta A} \qquad \textbf{(A 3.1)}$$

where ΔA is a differential area surrounding point *P* on the cutting plane and Δ**t** is resultant force. Also the couple stress vector for direction n can be written as

$$\mathbf{M}^n = \lim_{\Delta A \to 0} \frac{\Delta \mathbf{m}}{\Delta A} \qquad \textbf{(A 3.2)}$$

where Δ**m** is resultant moment. It is optional to include $\mathbf{M}^n$ in the theory of stress. In classical continuum mechanics it is generally assumed that $\mathbf{M}^n$ =0 which corresponds

to non-polar materials. Polar material models are generally considered only when continua are subjected to strong electromagnetic fields.

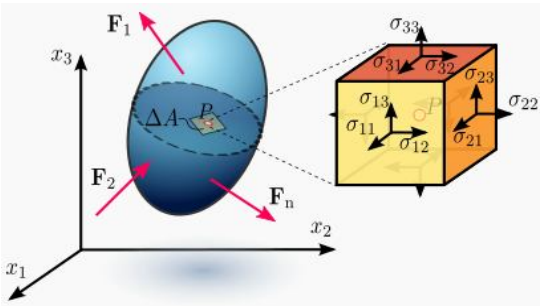

Figure A.2 : Shows stress in a loaded deformable material body [49].

From equation (A 3.2) it can be seen that traction vector depends on both the spatial location and the unit normal vector to the surface under study. Thus, even though we may be investigating the same point, the traction vector still varies as a function of the orientation of the surface normal. Because the traction is defined as force per unit area, the total surface force is determined through integration as per relation.

$$\mathbf{T}^{\mathbf{n}}(\mathbf{x},\mathbf{n}) = -\mathbf{T}^{\mathbf{n}}(\mathbf{x},-\mathbf{n}) \qquad \textbf{(A 3.3)}$$

If a special case is considered where ΔA coincides with each of the three coordinate planes with the unit normal vector pointing along the positive coordinate axes that is shown in the Figure A.2. The traction vector on each case can be written as

$$\begin{aligned}
\mathbf{T}^{\mathbf{n}}(\mathbf{x},\mathbf{n}=\mathbf{e_1}) &= \sigma_{11}\mathbf{e_1} + \sigma_{12}\mathbf{e}_2 + \sigma_{13}\mathbf{e}_3 \\
\mathbf{T}^{\mathbf{n}}(\mathbf{x},\mathbf{n}=\mathbf{e_2}) &= \sigma_{21}\mathbf{e_1} + \sigma_{22}\mathbf{e}_2 + \sigma_{23}\mathbf{e}_3 \\
\mathbf{T}^{\mathbf{n}}(\mathbf{x},\mathbf{n}=\mathbf{e_3}) &= \sigma_{31}\mathbf{e_1} + \sigma_{32}\mathbf{e}_2 + \sigma_{33}\mathbf{e}_3
\end{aligned} \qquad \textbf{(A 3.4)}$$

where e_1, e_2, e_3 are the unit vectors along each coordinate direction, and the nine values of σ_{ij} , $\{\sigma_{11}, \sigma_{22}, \sigma_{33}, \sigma_{12}, \sigma_{13}, \sigma_{21}, \sigma_{31}, \sigma_{23}, \sigma_{32}\}$, are the components of the Cauchy stress tensor which is shown below in matrix format.

$$\underline{\boldsymbol{\sigma}} = [\sigma_{ij}] = \begin{bmatrix} \sigma_{11} & \sigma_{12} & \sigma_{13} \\ \sigma_{21} & \sigma_{22} & \sigma_{23} \\ \sigma_{31} & \sigma_{32} & \sigma_{33} \end{bmatrix} = \begin{bmatrix} \sigma_{xx} & \sigma_{xy} & \sigma_{xz} \\ \sigma_{yx} & \sigma_{yy} & \sigma_{yz} \\ \sigma_{zx} & \sigma_{zy} & \sigma_{zz} \end{bmatrix} = \begin{bmatrix} \sigma_{xx} & \tau_{xy} & \tau_{xz} \\ \tau_{yx} & \sigma_{yy} & \tau_{yz} \\ \tau_{zx} & \tau_{zy} & \sigma_{zz} \end{bmatrix} \quad \textbf{(A 3.5)}$$

where x,y,z used to write expression in engineering format and σ and τ represents the normal and shear stress respectively. For non polar materials stress tensor is symmetric.

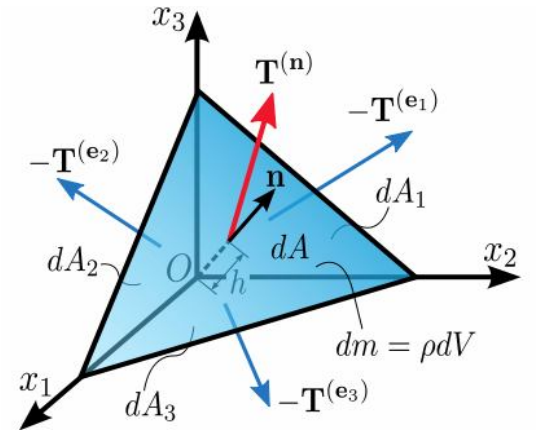

Figure A.3 : Stress vector acting on plane with normal unit vector **n**[49].

If the traction vector on an oblique plane with arbitrary orientation is considered where faces are normal to x_1, x_2, x_3, consequently n can be written as below.

$$\mathbf{n} = n_{x1}\mathbf{e_1} + n_{x2}\mathbf{e_2} + n_{x3}\mathbf{e_3} \quad \textbf{(A 3.6)}$$

The equilibrium of that tetrahedron elemental between tractions on the oblique and coordinate faces give the equation below.

$$\mathbf{T^n} = n_{x1}\mathbf{T^n}(\mathbf{n} = \mathbf{e_1}) + n_{x2}\mathbf{T^n}(\mathbf{n} = \mathbf{e_2}) + n_{x3}\mathbf{T^n}(\mathbf{n} = \mathbf{e_3}) \quad \textbf{(A 3.7)}$$

If the expression above integrate with equation (A 3.4), the relation can be written as

$$\begin{aligned} \mathbf{T^n} = &\left(\sigma_{11}n_{x1} + \sigma_{21}n_{x1} + \sigma_{31}n_{x1}\right)\mathbf{e_1} \\ &+ \left(\sigma_{12}n_{x1} + \sigma_{22}n_{x1} + \sigma_{32}n_{x1}\right)\mathbf{e_2} \\ &+ \left(\sigma_{13}n_{x1} + \sigma_{23}n_{x1} + \sigma_{33}n_{x1}\right)\mathbf{e}_3 \end{aligned} \quad \textbf{(A 3.8)}$$

or in index notation

$$T_i^n = \sigma_{ij} n_j \qquad \textbf{(A 3.9)}$$

Following the principles of small deformation theory, the previous definitions for the stress tensor and traction vector do not make a distinction between the deformed and undeformed configurations of the body. Such a distinction only leads to small modifications that are considered higher order effects and are normally neglected.

APPENDIX A.4 Equilibrium Equations

The stress field in an elastic solid is continuously distributed within the body determined from the applied loadings. The applied loadings satisfy the equations of static equilibrium; that is, the summation of forces and moments is zero. If the entire body is in equilibrium, then all parts must be in equilibrium.

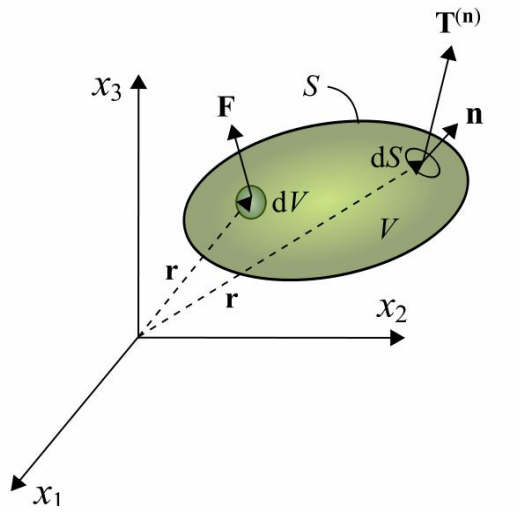

Figure A.4 : Continuum body in equilibrium [49].

We consider a closed subdomain with volume V and surface S within a body in equilibrium. For static equilibrium, conservation of linear momentum implies that the forces acting on this region are balanced and thus the resultant force must vanish. This concept can be written in index notation as below

$$\int\int_S T_i^n dS + \int\int\int_V F_i dV = \int_V \rho a_i dV = 0 \qquad \textbf{(A 4.1)}$$

where ρ is the body density, F_i is the applied force. If we substitute $T_i^n = \sigma_{ij} n_j$ in the surface integral, we get the equation below.

$$\iint_S \sigma_{ij} n_j dS + \iiint_V F_i dV = 0 \qquad \textbf{(A 4.2)}$$

To transform the surface integral to a volume integral Gauss' divergence theorem is used. For any vector field **a**:

$$\int_S \mathbf{a.n} dS = \int_V \mathbf{div.a} dV \qquad \textbf{(A 4.3)}$$

Consequently the equilibrium integral can be reduced to equation below for an arbitrary volume.

$$\iiint_V \left[\sigma_{ij,j} + F_i\right] dV = 0 \qquad \textbf{(A 4.4)}$$

Because the region V is arbitrary and the integrand above is continuous, zero-value theorem can be used which is represented as below.

$$\iiint_V f_{ij.....k} dV = 0 \Rightarrow f_{ij....k} = 0 \in V \qquad \textbf{(A 4.5)}$$

So according to zero-value theorem, the integrand must vanish as equation below.

$$\sigma_{ij,j} + F_i = 0 \qquad \textbf{(A 4.6)}$$

This result represents three differential equations of equilibrium which must be satisfied if the medium is at rest or moving uniformly with respect to an inertial frame, the accelerations vanish. The there equilibrium equations are written below.

$$\begin{aligned}
&\frac{\partial \sigma_{11}}{\partial x_1} + \frac{\partial \sigma_{21}}{\partial x_2} + \frac{\partial \sigma_{31}}{\partial x_3} + F_1 = 0 \\
&\frac{\partial \sigma_{12}}{\partial x_1} + \frac{\partial \sigma_{22}}{\partial x_2} + \frac{\partial \sigma_{32}}{\partial x_3} + F_2 = 0 \\
&\frac{\partial \sigma_{13}}{\partial x_1} + \frac{\partial \sigma_{23}}{\partial x_2} + \frac{\partial \sigma_{33}}{\partial x_3} + F_3 = 0
\end{aligned} \qquad \textbf{(A 4.7)}$$

APPENDIX A.5 Constitutive Equations

Constitutive equations characterize the behavior of the material of mechanical bodies. These equations are relations that constrain the space of deformations of a body (as defined by the strain tensor) and the state of internal forces (as defined by the stress tensor). The relations hold at each point of the body. They are generally partial differential equations, or even integrodifferential equations, in space and time.

The simplest type of constitutive equations are homogeneous linear algebraic relations that connect the stress and strain tensors at each point. This type of constitutive equation characterize the linear elastic solids, which is the only type we used in our study.

APPENDIX A.5.1 Elastic Solids

An elastic solid is characterized by either natural (undeformed) or the deformed state. The undeformed state is occured in the absence of applied forces while deformed state is occured by any reversible process.

These concepts are closely associated with the idea of stored energy, strain energy or stress energy. This expresses mathematically that the behavior of an elastic solid is independent of the preceding history of the material. In other words, the state of stress depends only on the state of strain, and not on the path followed to get to that strain.

APPENDIX A.5.2 The Strain Energy

U is the strain energy per unit of deformed volume which is also called strain energy density (SED). SED is generally a function of position (x_i) and the deformation of the body at that position. Since in linear elasticity the deformation may be characterized by the strain tensor ε_{ij} the expression of SED can be written as below.

$$U = U(x_i, \varepsilon_{ij}) \qquad \textbf{(A 5.1)}$$

Additional features about SED is listed below.

- U is a scalar invariant that means it is unaffected by rigid body displacements and by the orientation of the global rectangular cartesian coordinate (RCC) system.

- If U is independent of x_i over a volume V, the material is said to be homogeneous in V.
- If the stress-strain law is independent of directions in the material, the material is said to be isotropic and in isotropic materials, the strain energy density must be a function of the invariants of the strain tensor.

APPENDIX A.5.3 Principle of Virtual Work

If a body is considered in static equilibrium, the principle of virtuel work (PVW) states that work done by all forces acting on that body during a virtuel displacement δu must be zero. Mathematically it can be represent as

$$\delta W_i + \delta W = 0 \qquad \textbf{(A 5.2)}$$

where W_i and W are the virtual work done by the internal and external forces, respectively.

The principle can be derived mathematically by multiply the equilibrium equations with δu_i, integrate over V and apply the divergence theorem and stress boundary conditions.

$$\int_V \left(\sigma_{ij,j} + F_i\right)\delta\bar{u} = \int_V \left[-\sigma_{ij,j}\delta\frac{1}{2}\left(u_{i,j} + u_{j,i}\right) + F_i\delta u_i \right] dV + \int_S \sigma_{ij} n_j \delta u_i dS = 0 \qquad \textbf{(A 5.3)}$$

Split the surface integral over $S_t \cup S_u$. The integral over the second term vanishes. The former can be transformed using the second of weighted by δu_i and integrated over S_t to produce

$$\int_V \sigma_{ij}\delta\varepsilon_{ij} dV = \int_V F_i \delta u_i + \int_{S_t} T_i^n \delta u_i dS \qquad \textbf{(A 5.4)}$$

But $\delta W_i = -\delta U$, where U is the total stored strain energy that represent as below

$$U = \int_V U dV \qquad \textbf{(A 5.5)}$$

Finally the equation is transferred to

$$\delta U = \int_V \sigma_{ij} \delta \varepsilon_{ij} dV \qquad \textbf{(A 5.6)}$$

APPENDIX A.5.4 Linear Elastic Constitutive Equations

An elastic material is defined as one in which the total internal energy is equal to the potential energy of the internal forces (also called elastic strain energy). Therefore the strain energy density is a function of strains, $U_0 = U_0(\varepsilon)$ and the variation of the internal energy can be expressed as

$$\delta U_0 = \frac{\partial U_0}{\partial \varepsilon_{ij}} \delta \varepsilon_{ij} \qquad \textbf{(A 5.7)}$$

Since the variation of strain is arbitrary, the stress-strain relation of an elastic material is given by

$$\boldsymbol{\sigma} = \frac{\partial U_0}{\partial \boldsymbol{\varepsilon}} \qquad \textbf{(A 5.8)}$$

For a linear elastic material, the quantity $\partial U_0 / \partial \varepsilon$ is a linear function of ε and therefore can be expressed as

$$\boldsymbol{\sigma} = \mathbf{c} : \boldsymbol{\varepsilon} \qquad \textbf{(A 5.9)}$$

or in index notation

$$\sigma_{ij} = c_{ijkl} \varepsilon_{kl} \qquad \textbf{(A 5.10)}$$

where c is fourth rank tensor of that include material constants, and also called as stiffness tensor, which is shown below in matrix format.

$$c = \frac{E(\rho)}{(1+\nu)(1-2\nu)} \begin{bmatrix} 1-\nu & \nu & \nu & 0 & 0 & 0 \\ \nu & 1-\nu & \nu & 0 & 0 & 0 \\ \nu & \nu & 1-\nu & 0 & 0 & 0 \\ 0 & 0 & 0 & \frac{(1-2\nu)}{2} & 0 & 0 \\ 0 & 0 & 0 & 0 & \frac{(1-2\nu)}{2} & 0 \\ 0 & 0 & 0 & 0 & 0 & \frac{(1-2\nu)}{2} \end{bmatrix} \qquad \textbf{(A 5.11)}$$

APPENDIX B

ABAQUS/Standard provides users with an extensive array of user subroutines that allow them to adapt ABAQUS to their particular analysis requirements. Some brief informations about subroutines UMAT, URDFIL, USDFLD, SDVINI which are used in our study is given.

- UMAT: Use this subroutine to define any complex, constitutive models for materials that cannot be modeled with the available ABAQUS material models.
- URDFIL: Use this subroutine to read the data from the results (.fil) file at the end of an increment. The information can be used to make decisions such as when to terminate the analysis or whether to overwrite the results of the previous increment.
- USDFLD: Use this subroutine to define the values of field variables directly at the integration points of elements. The field variable values can be functions of element variables such as stress or strain.
- SDVINI: Use this subroutine to define initial solution-dependent state variable fields at particular material points, shell section points, contact slave nodes, or for user elements or initialize solution-dependent state variables allocated.

APPENDIX B.1 Introduction to our code

In this section, we prove that ABAQUS/Standard and the code we developed give exactly same results with different load cases, boundary conditions, element types, constraints and geometries. Also the determination of strain energy density according to weight of load cases and the regulation of incremental time is shown.

As mentioned before our code contains UMAT, URDFIL, USDFLD and SDVINI subroutines. The information about for which purposes those subroutines are chosen and the specific features that is used in the code is explained below.

UMAT is used to determine constitutive behavior of material and Jacobian matrix. In this study, bones are taken as linear elastic materials. During analysis updating

process of apparent density is also fulfilled by UMAT. Another subroutine, SDVINI, is used in defining the initial values of state variables that correspond to density and Young's modulus. URDFIL is used in determining incremental time values which is refer to seconds (loading) or days (remodeling). URDFIL also used in opening the required files during analysis where the weight of load cases were entered. Lastly, USDFLD is used in the calculation of mechanical stimulus according to the weights of loads scenarios.

APPENDIX B.2 Validation of code

The integrity of code is proven by performing different analysis with distinct boundary conditions, load cases, constraints, element types and geometries. For validation, four different models are prepared and each one is performed both with and without code. In figure B.1, three different cases that includes different loads and boundary conditions is shown. In case a, a concentrated force is applied instantaneously to the top surface of system in y-z plane and the system is fixed at x-y-z directions from the bottom surfaces. In case b, same boundary condition and same force with opposite direction are applied to different surfaces of system. In case c, distinct from previous cases, the load is applied with a tabular amplitude where maximum value of magnitude is reached at the end of first increment and begin to diminish by time.

For first model, case a is assigned. Between parts tie constraint is given and for mesh hexahedral element are chosen. In the second model, case b is taking into account with the same constraint type and instead of hex, tet elements is used. For the third model, case c is choosen. Like other models between big cubic parts tie constraint is given while at the interface surfaces of thin cubic part and other parts surface to surface interaction is assigned where normal behavior is simulated by default hard contact and for tangential behavior, penalty friction formulation with 0.1 friction coefficient is given. In the fourth model all conditions are taken same as the third one except element type which is tetrahedral.

The results of analyses both with and without code is compared. The displacement, stress, strain energy density outputs of models with and without code is represented in the Figures B.2-B.5. As it seen from figures there isn’t any difference between classical and subroutine analysis.

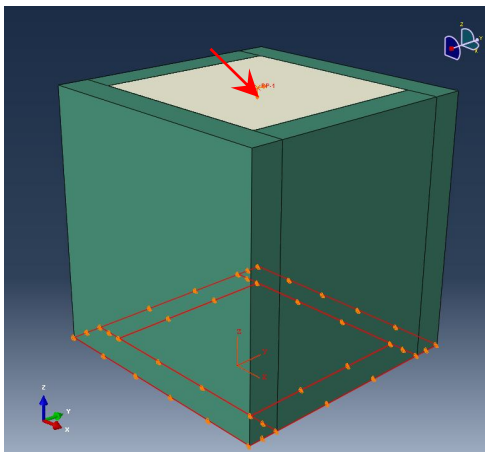

(a)

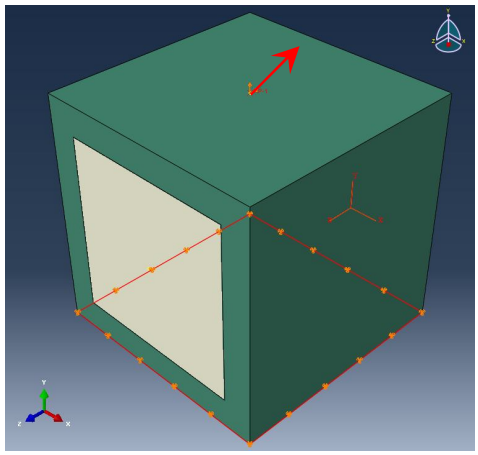

(b)

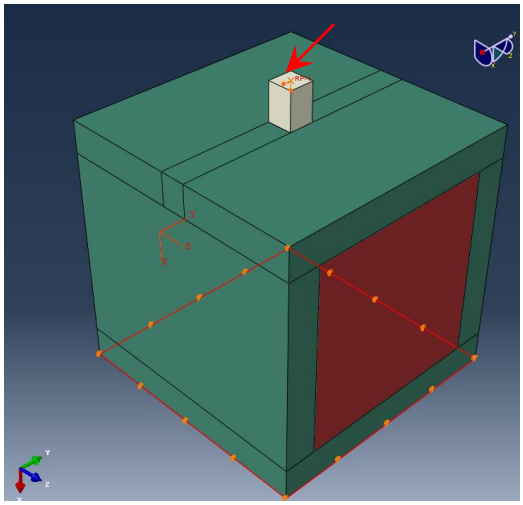

(c)

Figure B.1 : Boundary conditions and load cases.

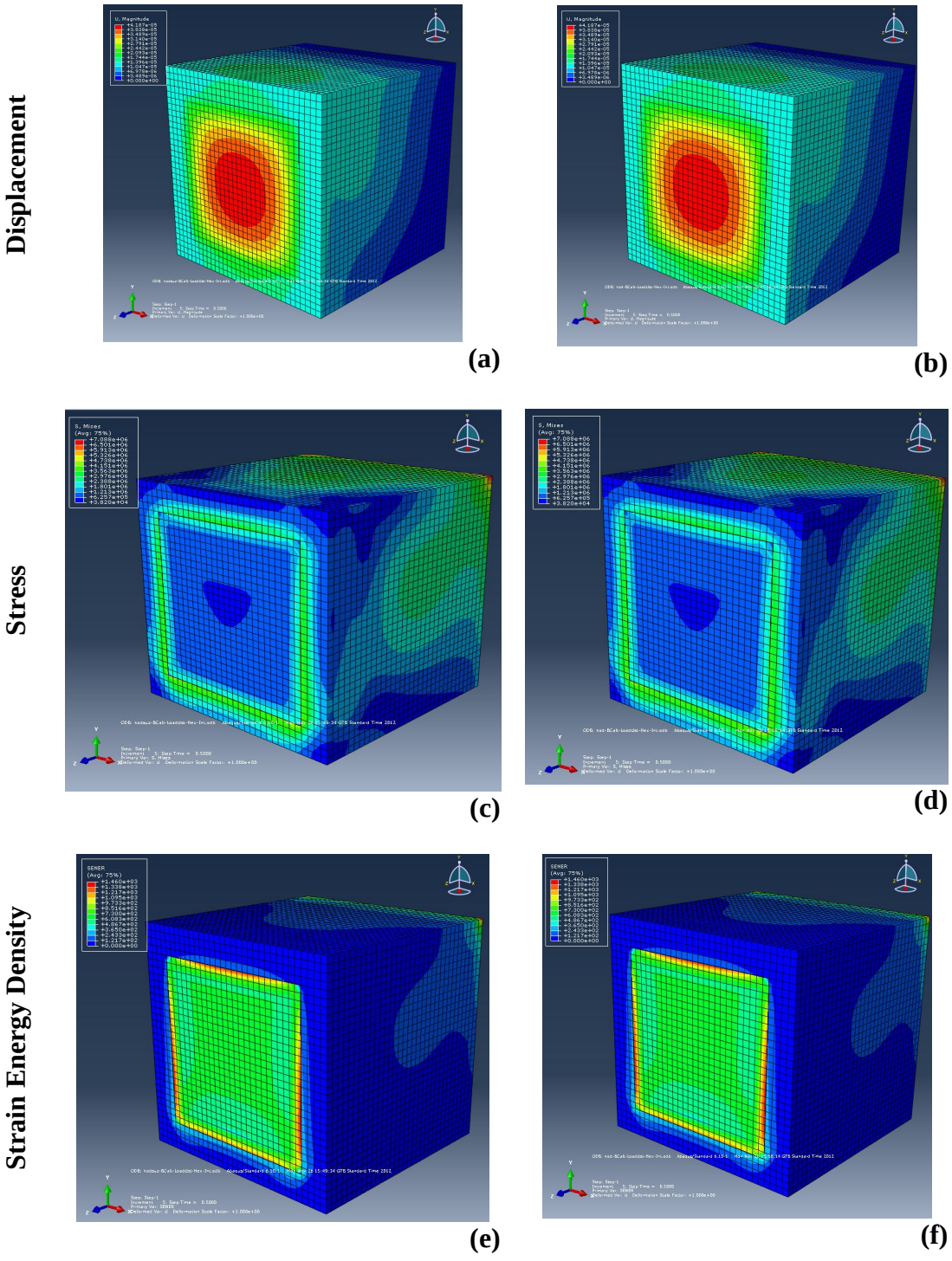

Figure B.2 : The comparative outputs of the first model for validation. (a,c,e) Without code. (b,d,f) With code.

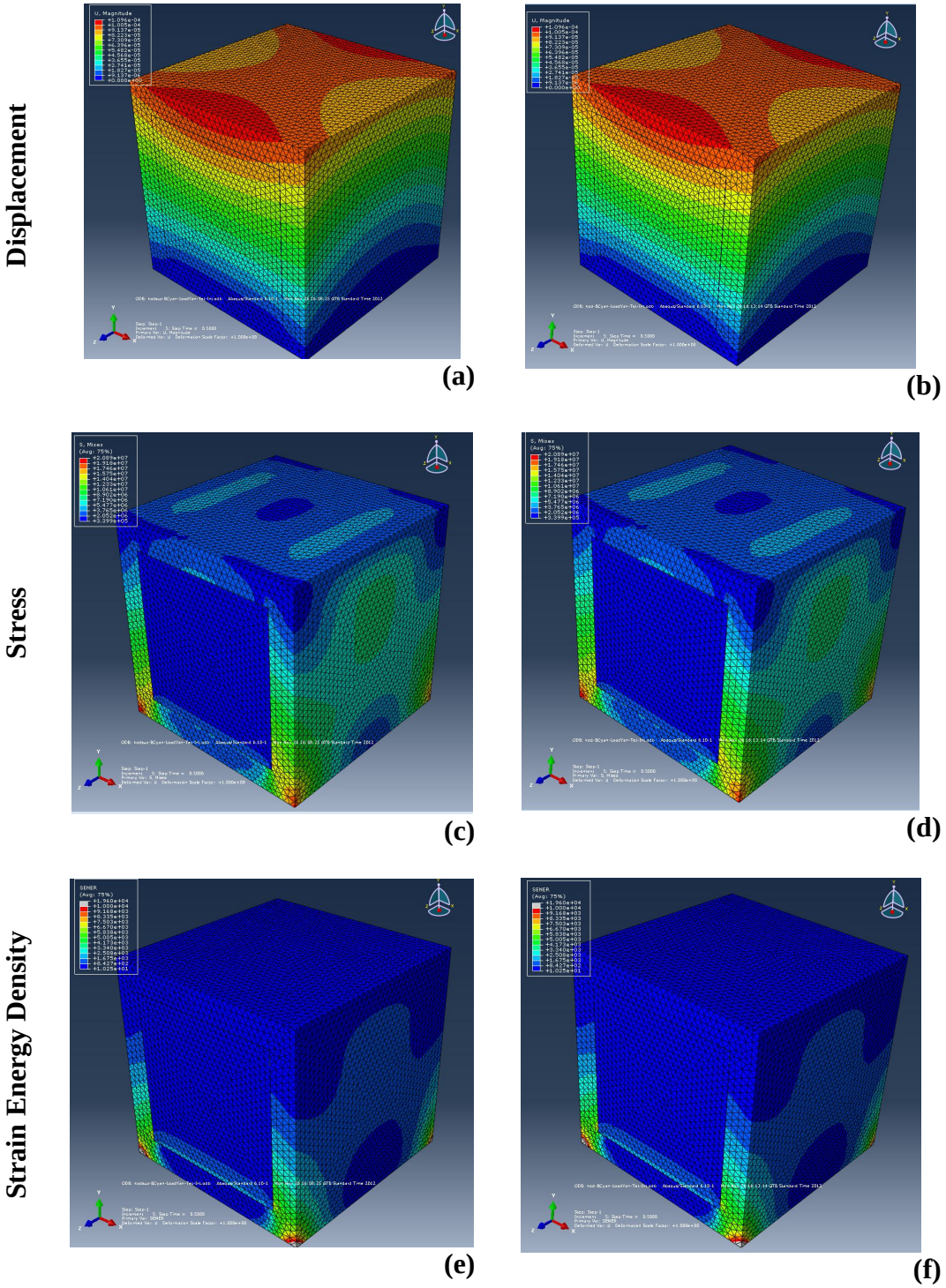

Figure B.3 : The comparative outputs of the second model for validation. (a,c,e) Without code. (b,d,f) With code.

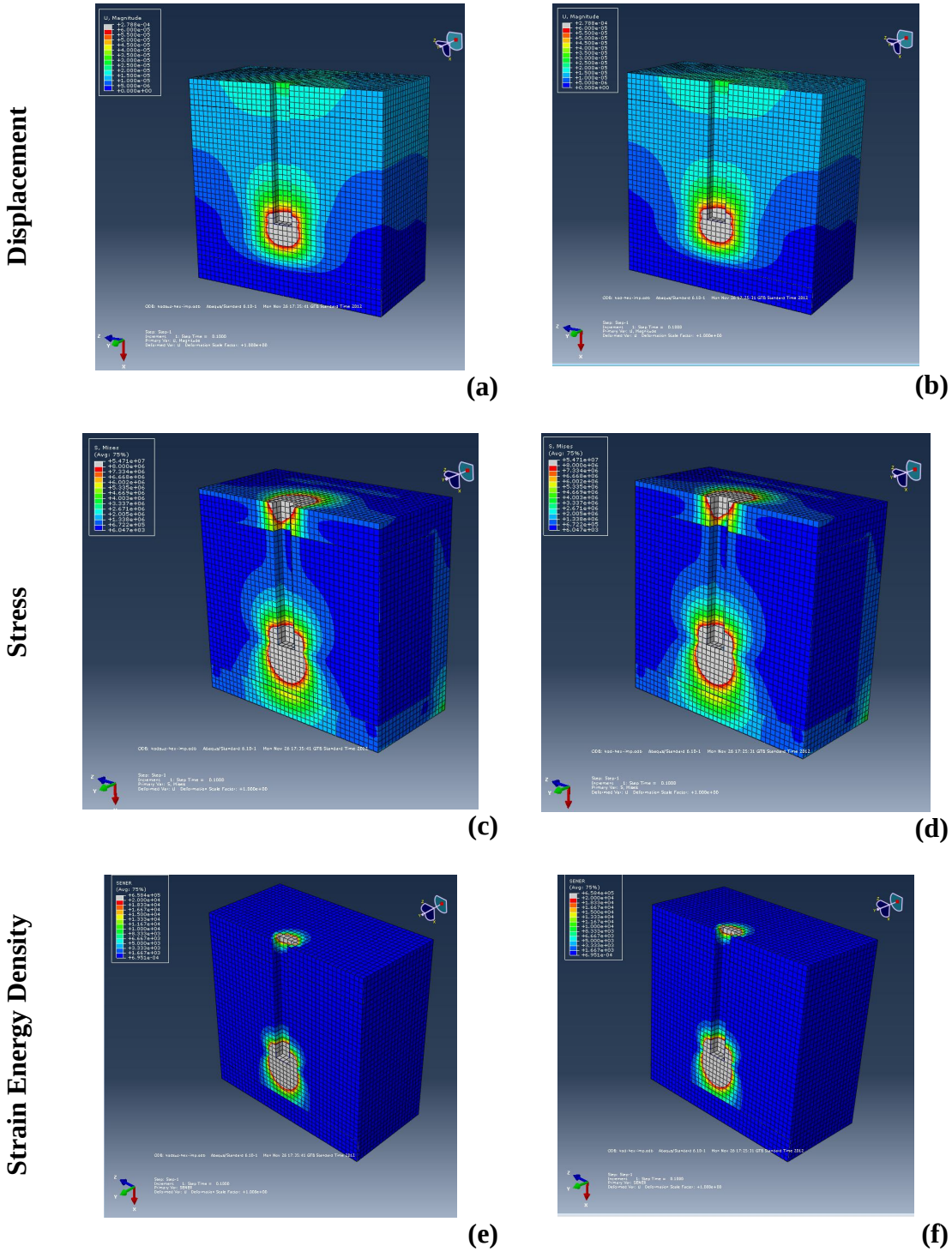

Figure B.4 : The comparative outputs of the third model for validation. (a,c,e) Without code. (b,d,f) With code.

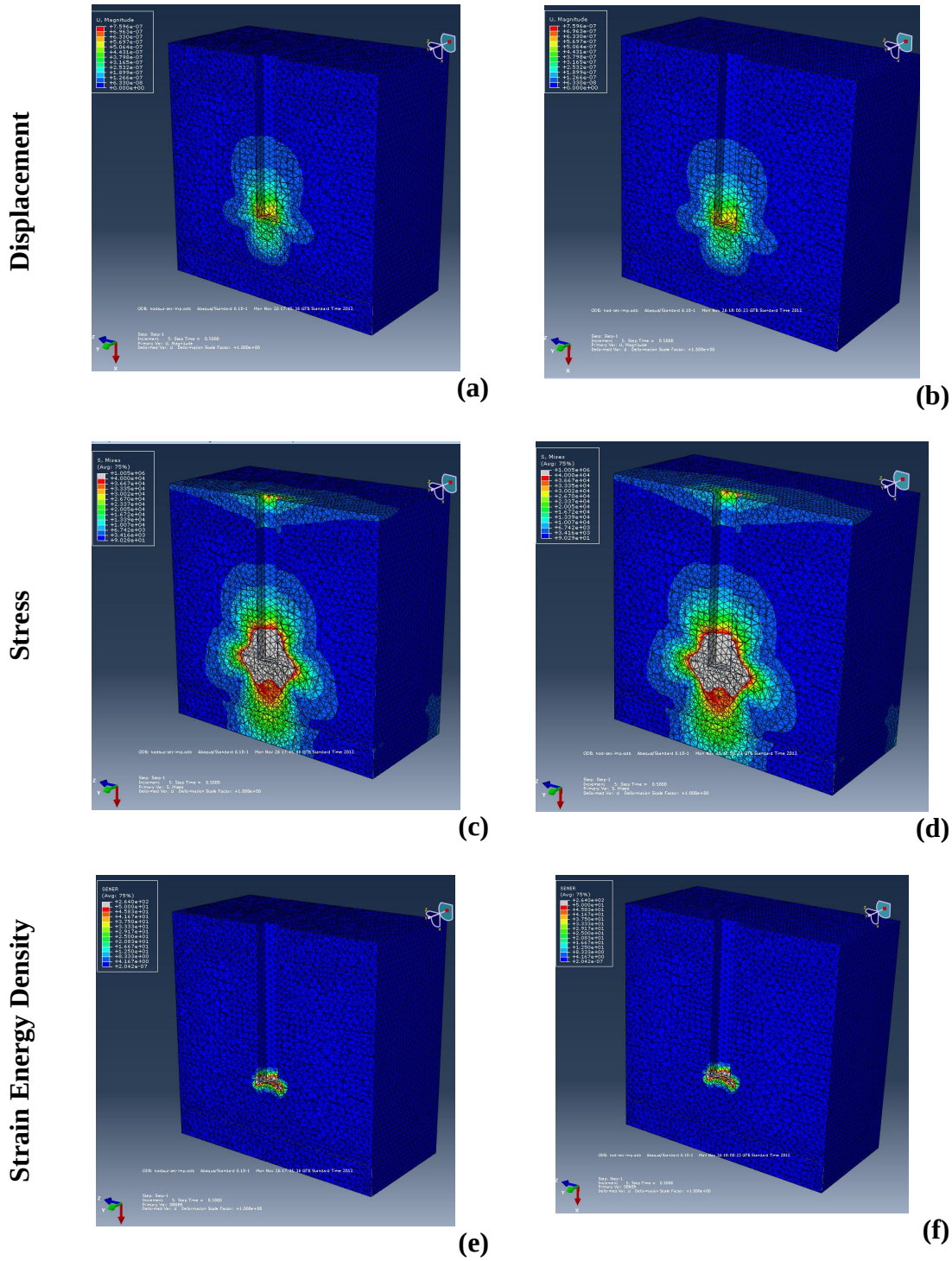

Figure B.5 : The comparative outputs of the fourth model for validation. (a,c,e) Without code. (b,d,f) With code.

APPENDIX B.3 Determination of driven strain energy density per mass

As it is mentioned before whole loads that act on bone has different effects on remodeling according to their features. To simulate this difference the result obtained from each load case is multiply with required coefficients according to their weight. We able to do those necessary calculations at each integration point by defining the value of strain energy density per mass as a field variable in USDFLD subrouine.

An application of USDFLD together with UMAT, SDVINI and URDFIL subroutines is shown below. In this example; we apply five different loads to five different points of model at different times. The locations of applied loads, boundary conditions and coupling surfaces are shown in the Figure B.6. Also the characteristic's of each load is given in the table B.1. The maximum value of strain energy density (SED) at each integration point is hold during analysis. The results of process is shown in the Figure B.7. Even though the value of SED changes at each increment due to the amplitude of applied loads, it is clearly seen that the maximum value is hold by defining it as a field variable in USDFLD and transferring to UMAT as a state variable with a proper algorithm. The manipulation of SED is a very significant issue because SED per mass taking as the mechanical stimulus of bone remodeling algorithm.

(a) **(b)**

Figure B.6 : Model of the USDFLD example.

Table B.1 : Load cases of USDFLD example.

Increment	Time (second)	Location (number of point)	Magnitude of Load
0	0	1	0,-5000,0
1	0.1	2	0,0,-2500
2	0.2	3	-3500,0,0
3	0.3	4	0,0,1800
4	0.4	5	4000,0,0

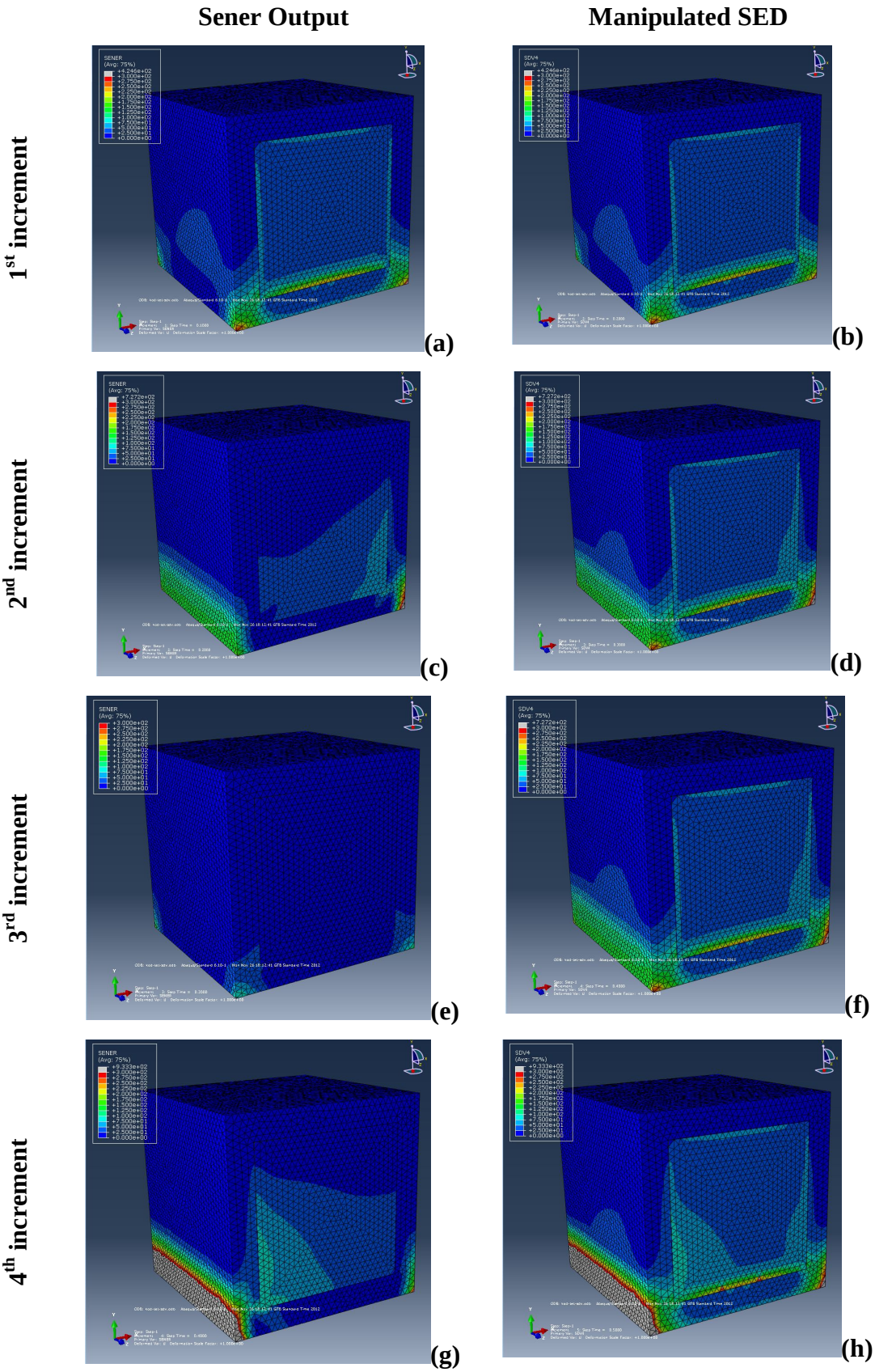

Figure B.7 : Results of manipulation process of SED by USDFLD subroutine.

APPENDIX B.4 Results obtained from implementation of remodeling algorithm

So far, it is proven that abaqus subroutines worked properly and strain energy density or mechanical stimulus can be manipulated as desired. In this session the accuracy of remodeling algorithm is proven, by implementing it to a 3D cubic model. Model is fixed from the bottom surface and concentrated loads are applied to the top and side surfaces with 45° incline. Concentrated loads are applied instantenously and simultaneously at the beginning of the analysis. As it seen from the results, system is optimize its internal structure by increasing and decreasing the apparent density in the required regions according to mechanical stimulus value.

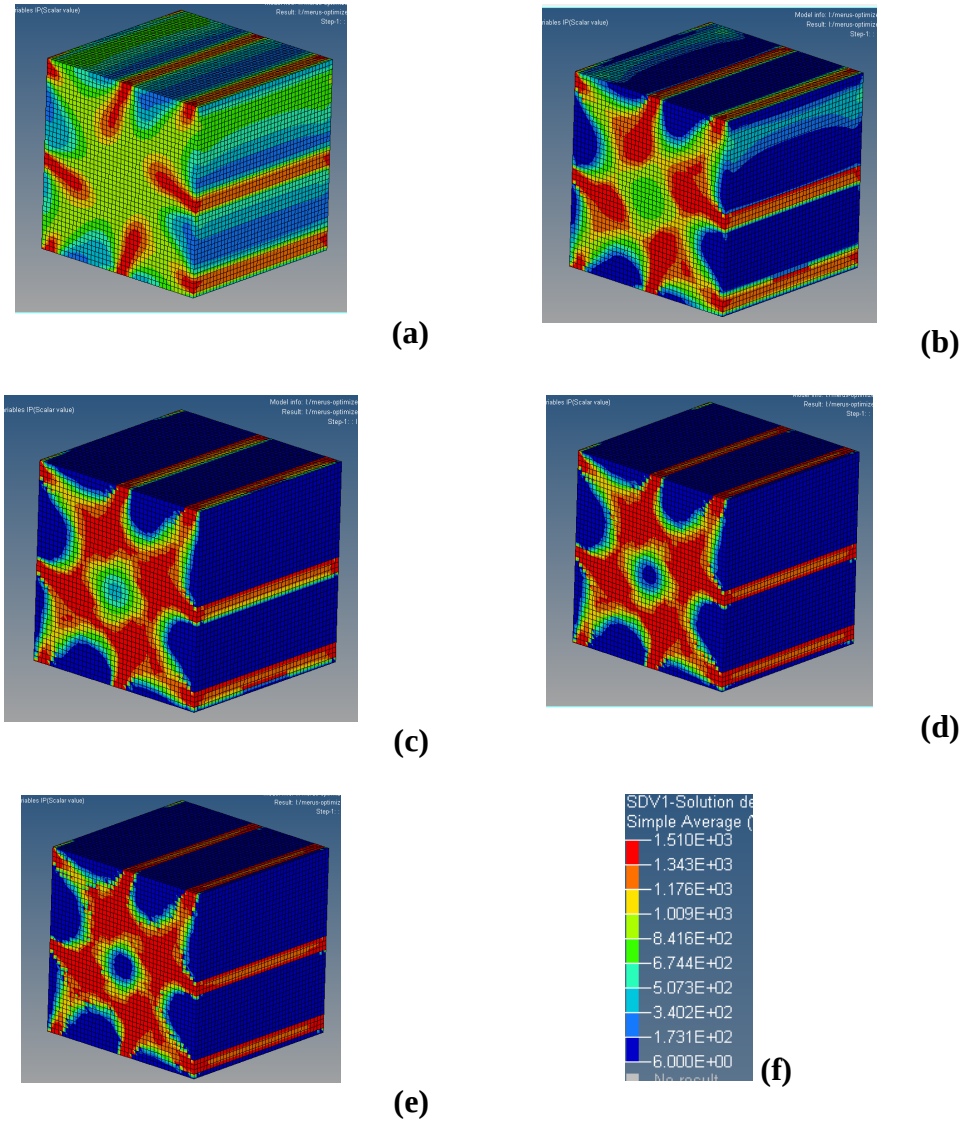

Figure B.8 : (a-e) Results of density distribution obtained after implementation of remodeling algorithm to a model.

CURRICULUM VITAE

Name Surname: **Meral TUNA**

Place and Date of Birth: **Tahran, 12.12.1987**

E-Mail: **tunamer@itu.edu.tr**

meraltuna87@gmail.com

Professional Experience and Rewards: Research Assistant

List of Publications and Patents:

International Publication:

Biomechanical Comparison of Dynamic Hip Screw, Proximal Femoral Nail, Cannulated Screw, and Monoaxial Fractures.
Imren, Y., Gürkan, V., Bilsel, K., Erdil, M., Tuna, M., Gürcan, C., Tuncay, T., Sen, C.
The Bone and Joint Journal (in review)

International Conference:

Effect on the stress distribution of laminate veneer design and materials in a maxillary central incisor: A 3D-finite element analysis
M.C. Balkaya, S. Baloglu, M. Tuna, S.C. Gurcan, B. Bekler
EPA 2011, Bern

Biomechanical Comparison of Dynamic Hip Screw, Proximal Femoral Nail, Cannulated Screw, and Monoaxial External Fixation in the Treatment of Basicervical Femoral Neck Fractures.
Y. Imren, V. Gurkan, K. Bilsel, M. Erdil, M. Tuna, C. Gürcan, I. Tuncay, C. Sen
Osteosynthese International 2013

Biomechanical Comparison of Dynamic Hip Screw, Proximal Femoral Nail, Cannulated Screw, and Monoaxial External Fixation in the Treatment of Basicervical Femoral Neck Fractures.
Y. Imren, V. Gurkan, K. Bilsel, M. Erdil, M. Tuna, C. Gürcan, I. Tuncay, C. Sen
14th EFORT Congress (14. Avrupa Ortopedi ve Travmatoloji Kongresi, İstanbul, 2013), Trauma

Correlation between chondral defect size, pressure distribution and condylar size.
G. Dikmen, O. I. Kilicoglu, F. Yıldız, K. Sariyilmaz, E. Bozdag, E. Sunbuloglu, M. Tuna
14th EFORT Congress (14. Avrupa Ortopedi ve Travmatoloji Kongresi, İstanbul, 2013), General Orthopaedics

Correlation between chondral defect size, pressure distribution and condylar size.
G. Dikmen, O. I. Kilicoglu, F. Yıldız, K. Sariyilmaz, E. Bozdag, E. Sunbuloglu, M. Tuna
ISOKOS Congress, 12-16 May 2013, Toronto, Canada

Biomechanical comparison of oblique and step-cut osteotomies of the femur in total hip arthroplasty with femoral shortening.
F. Yildiz, O. I. Kilicoglu, G. Dikmen, K. Sariyilmaz, E. Bozdag, E. Sunbuloglu, M. Tuna, O. Yazicioglu
14th EFORT Congress (14. Avrupa Ortopedi ve Travmatoloji Kongresi, İstanbul, 2013), Lower limb

National Conference:

Ostaokondral Defektlerde Defekt Çapı ve Lokal Kontakt Anatominin Eklem Basınç Dağılımı Üzerine Etkileri.
Göksel Dikmen, Önder İsmet Kılıçoğlu, Fatih Yıldız, Kerim Sarıyılmaz, Emin Sünbüloğlu, Ergün Bozdağ, Meral Tuna
Ortopedi ve Travmatoloji İstanbul Buluşması 2012

Kisaltmali total kalca artroplastilerinde uygulanan oblik ve basamakli femur osteotomilerinin biyomekanik olarak karsilastirilmasi
Fatih Yildiz, onder Kilicoglu, Kerim Sariyilmaz, Goksel Dikmen, onder Yazicioglu, Ergun Bozdag, Emin Sunbuloglu, Meral Tuna
Ortopedi ve Travmatoloji İstanbul Buluşması 2012

Kalca artroplastileri sonrasi gelisen Vancouver tip B1 periprostetik femur kiriklarinda plak-vida ve strut allogreftler ile yapilan farkli tespit yontemlerinin karsilastirilmasi(Biyomekanik calisma)
Kerim Sariyilmaz, Fatih Dikici, Fatih Yildiz, Goksel Dikmen, Ergun Bozdag, Emin Sunbuloglu, Meral Tuna, Onder Yazicioglu
Ortopedi ve Travmatoloji İstanbul Bulusmasi 2012, istanbul, Turkiye